

DESIGN AND QUANTITATION OF MEMBRANE BINDING LIPID  
ANCHORS-EXPLORING PRION-PRION INTERACTIONS

By

Manasa Gangula

(Under the direction of Dr. Colin Burns)

June, 2011

Department of Chemistry

The prion protein (PrP) is an endogenous, metal binding protein present in the neuronal cells of the central nervous system. Prion is associated with a class of neurodegenerative diseases known as transmissible spongiform encephalopathies. The C-terminal region of the prion protein is anchored to the cell surface by means of a glycosylphosphatidylinositol (GPI) anchor<sup>19</sup>. Studies indicate that PrP self-recognition may be an important factor in both the normal function and malfunction of PrP. Elucidating the molecular basis for PrP-PrP interactions in the context of its membrane bound state will help in understanding the normal function of PrP, such as the signaling mechanism for endocytosis, and the factors that influence disease causing structural changes. Fluorescently labeled models of prion protein were previously developed to investigate PrP-PrP interactions and metal binding at molecular level. Peptides constituting the metal binding region were anchored to small unilamellar vesicles (liposomes) and PrP-PrP interactions were studied as a function of added metal<sup>45</sup>. Anchoring the peptides is an essential step to understand the protein interactions in the context of a cell surface. The main objective of this research is to prepare a molecule capable of anchoring the majority of a PrP sample to a liposome and develop a spin-label based assay to

determine the percentage of molecules anchored to the liposome surface. Four lipophilic molecules containing a nitroxide spin-label have been synthesized and their electron paramagnetic resonance (EPR) spectra collected in the presence and absence of liposomes. The EPR spectrum of the nitroxide is very sensitive to the motion of the spin label and the proximity to other spin labeled molecules. The anchor with a linear chain of sixteen carbon atoms showed the most dramatic changes in the EPR spectrum and is likely the best anchor. We are planning to use a paramagnetic relaxation agent that aids in the quantitation and fluorescent compounds which aid in determining where the spin-labeled molecules localize. The spin-label methodology will allow us to conduct more quantitative experiments on PrP interactions with respect to metal binding, change in temperature, pH etc.

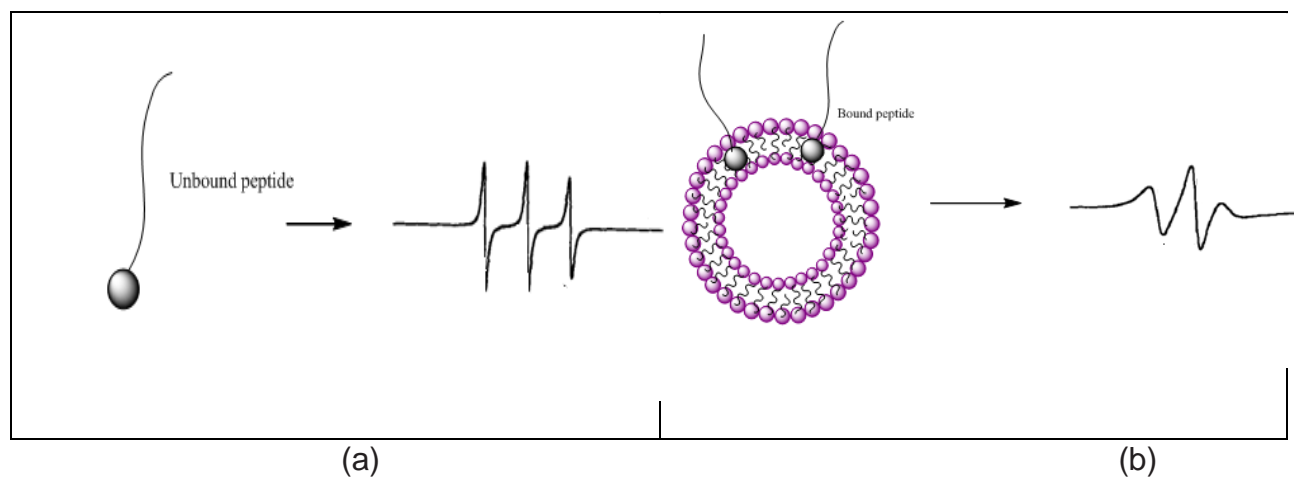


**Figure 1:** (a) Hypothetical EPR spectrum of unbound spin-labeled molecule (b) Hypothetical EPR spectrum of bound spin-labeled molecule

**DESIGN AND QUANTITATION OF MEMBRANE BINDING LIPID  
ANCHORS-EXPLORING PRION-PRION INTERACTIONS ON  
MEMBRANE SURFACES**

A Thesis

Presented to

The Faculty of the Department of Chemistry  
East Carolina University

In Partial Fulfillment

of the Requirements for the Degree  
Master of Science in Chemistry

By:

Manasa Gangula

June 2011

© 2011

Manasa Gangula

All Rights Reserved

**DESIGN AND QUANTITATION OF MEMBRANE BINDING LIPID  
ANCHORS: EXPLORING PRION-PRION INTERACTIONS ON  
MEMBRANES SURFACES**

By:

Manasa Gangula

Approved By:

DIRECTOR:

---

Dr. Colin S. Burns

COMMITTEE MEMBER:

---

Dr. William E. Allen

COMMITTEE MEMBER:

---

Dr. Anthony Kennedy

COMMITTEE MEMBER:

---

Dr. Yu Yang

COMMITTEE MEMBER:

---

Dr. Thomas Fink

CHAIR OF THE DEPARTMENT

OF CHEMISTRY:

---

Dr. Rickey P. Hicks

DEAN OF THE GRADUATE SCHOOL:

---

Dr. Paul J. Gemperl

## ***My dedication***

This work in its entirety is dedicated to my family at a distant land whose memories and affection never seem to fade away.

*... Mom & Dad,*

It has been an overwhelming conviction that I am always dumb-founded when it comes to expressing my gratitude to both of you and I don't feel any different writing this. Mom, thank you for being the best critic and for your deepest faith in me. Dad, thank you for your support and constant encouragement which has always strengthened my confidence in whatever I pursue. Your love and affection have always made me feel lively. Love you mom and dad.

*... Sisters Shailaja and Radhika*

Life wouldn't have been the same without you guys. Growing up with you has always been fun and adventurous. Your constant guidance has made me what I am today. Your pranks and witty remarks about life have always been cheering. Thank you so much for being there for me.

## **Acknowledgements**

This work would not have been possible without the guidance and ideas of Dr. Colin S. Burns. I would like to whole heartedly thank Dr. Burns for being so patient and helpful throughout the course of my masters program. Working with Dr. Burns has been a rewarding experience.

I would like to thank Praneetha Gogineni for all her support and love and for being there for me no matter what. I couldn't have asked for a more encouraging and caring friend in my life. I would like to thank Ramya Garapati for all help and support. It was fun sharing the lab with you guys.

I would like to thank my friends Dilip, Brahmam, Harita, Keerthi, Bhargavi, Sindhuri, Girish, Jaya, Abhinav, Venu, Ankit for always being by my side in their own special ways. Thanks for all the fun and support guys.

I would like to thank the Chemistry department for supporting me financially with teaching assistantship. I also thank all my committee members for their suggestions and for being very supportive. I thank all the teaching and non-teaching staff at the Chemistry department for creating such a friendly ambience for the students. I thank all the graduate students at the Chemistry department for their support.

## TABLE OF CONTENTS

LIST OF TABLES

LIST OF FIGURES

LIST OF ABBREVIATIONS

CHAPTER 1: INTRODUCTION TO PRION.....	1
1.1: Overview.....	1
1.2: Physiological Functions of PrP.....	3
1.3: PrP Self-Recognition.....	5
1.4: Importance of Membrane Location of PrP.....	9
1.5: Importance of Quantification of the Bound Peptide.....	15
CHAPTER 2: ELECTRON PARAMAGNETIC RESONANCE.....	17
2.1: Introduction to EPR.....	17
2.2: Spin Labels.....	26
2.3: EPR Instrumentation.....	28
CHAPTER 3: MATERIALS AND METHODS.....	31
3.1: Experimental Design.....	31
3.2: Synthesis and Purification of the Spin-labeled Anchors.....	36
3.3: Characterization of the Anchor Molecules.....	45
CHAPTER 4: LIPOSOMES.....	50
4.1: Preparation of Liposomes.....	50
4.2: Fluorescence Instrumentation.....	52
4.3: Dye Release Assay.....	53
CHAPTER 5: QUANTIFICATION OF THE LIPOPHILIC ANCHORS BY EPR.....	61
5.1: Control Experiments.....	61

5.2: Lipophilic Anchors.....	67
5.3: Quantification of the Membrane Bound Anchor Using Relaxation Agent...70	
5.4: Solid Phase Peptide Synthesis.....	79
5.5: Synthesis of Peptide Model.....	84
CHAPTER 6: FINAL CONCLUSIONS AND FUTURE STUDIES.....	89
REFERENCES.....	92
APPENDIX: SPECTROSCOPIC DATA.....	96

## LIST OF TABLES

3.1: Percentage yields of the synthesized anchor molecules.....	42
5.1: Values for percent bound anchors to the liposomes.....	78
5.2: Representative values for triplicate run of percent bound anchor of HDT.....	78
5.3: The peptide fragments and their corresponding m/z values.....	88

## LIST OF FIGURES

- 1.1: Cartoon of the three-dimensional structure of the intact human prion protein.....2
- 1.2: Plausible model for the tertiary structure of human huPrP<sup>Sc</sup>.<sup>9</sup> Note the increase in  $\beta$  sheet content shown in the secondary structure of huPrP<sup>Sc</sup>.....3
- 1.3: AFM analysis of the morphology of copper-bound  $\alpha$ BoPrP (24-242) insoluble complexes. (A) AFM image. (B) Distance profile of the selected region represented by the white bar on part (A).....7
- 1.4: Intra-repeat and inter-repeat Cu(II) site geometries and its macroscopic relevance in the PrP Cu(II) binding process. The atomic model depicts the intra-repeat (upper part) and inter-repeat (bottom part) Cu(II) site geometries observed for Cu(II) bound to PrP octarepeat region. The thick green and pink lines represent the polypeptide chain backbones. On the right-hand side, the macroscopic process of Cu(II) binding to this region is summarized.....8
- 1.5: Concentration-dependent secondary structure changes upon membrane anchoring. (A) PrP<sup>C</sup> bound to the raft-like lipid bilayer exhibits the same secondary structure (at lower concentrations) as anchorless recPrP in solution in NMR studies. (B) An increased concentration of PrP<sup>C</sup> at the membrane leads to a structural transition toward intermolecular beta sheet. (C) Schematic illustration of intermolecular  $\beta$ -sheet.....10
- 1.6: General illustration of pyrene-labeled peptides anchored to the outer surface of a SUV. When pyrene fluorophores (colored blue at the left) come into the proximity of one another, they form excimers (colored red at the right) which produce a distinct fluorescence signal at a longer wavelength.....13
- 1.7: (a) Fluorescence spectra of the native PrP peptide (4.15  $\mu$ M) at three different Cu<sup>2+</sup> loadings in a liposomal solution. (b) E/M ratio for the native PrP peptide as a function of titrated Cu<sup>2+</sup> (O) and Zn<sup>2+</sup> (■). The percent of interacting fluorophores presented at the right, y-axis, was calculated using eq 1. The metal ion concentration is reported in equivalents per peptide.....14
- 2.1: Pictorial representation of a population of free electrons in an external magnetic field ( $H_0$ ).....18
- 2.2: The  $M_s=+1/2$  and  $-1/2$  states have different energies in the presence of a magr field.....
- 2.3: Absorbance spectrum is converted into the first derivative spectrum in EPR.....19

2.4: Affect of impingement of the microwave radiation on the distribution of the spin states and relaxation back to the equilibrium.....	21
2.5: Energy diagram and the corresponding spectrum of a spin system with the value of $I = \frac{1}{2}$ ( $2I+1 = 2$ ).....	22
2.6: Variation of g-value with the magnetic field for an axially symmetric system.....	23
2.7: The molecular coordinate system of the nitroxide spin label used to define the direction of the applied magnetic field. The z-axis is parallel to the nitrogen 2p-orbital associated with the unpaired electron.....	25
2.8: Structures of 3-carboxy PROXYL and 4-aminoTEMPO.....	26
2.9: Simulated nitroxide spin label spectra for different $\tau_r$ values.....	28
2.10: Block Diagram of a typical Electron Spin Resonance Spectrometer.....	29
3.1: Structure of a unilamellar palmitoyl-oleyl-sn-glycero phosphatidylcholine (POPC) liposome consisting of polar and non-polar groups. The phosphatidylcholine head groups constitute the polar region and the lipid chains constitute the non-polar region of the liposome.....	32
3.2: Illustration of one of the ways by which the spin-labeled lipophilic molecule is anchored to the liposome. The nine carbon lipophilic hydrocarbon chain of Nonanoic acid-TEMPO is inserted into the liposome membrane whereas the hydrophilic nitroxide moiety is sticking out of the membrane.....	33
3.3: The lipophilic anchor completely inserts into the liposome or it might completely remain outside the liposome in the aqueous solvent. The lipophilic anchor shown in the figure is Nonanoic acid-TEMPO.....	34
3.4: Hypothetical EPR spectrum of a bound spin-labeled molecule. The peptide is bound to the liposome through the lipophilic anchor and its motion is somewhat restricted so the spin-label will give a characteristic EPR signal for the bound peptide.....	35
3.5: Hypothetical EPR spectrum of an unbound spin-labeled molecule. The peptide containing the spin-label and the lipophilic molecule is free in solution and gives a characteristic EPR signal which is significantly different from the bound peptide.....	35
3.6: Reaction scheme for the general method of synthesis of the anchor molecules using amide coupling reaction.....	37

3.7: Lipophilic molecules (1-3) and a hydrophilic molecule (4) were coupled to the spin label 4-amino-TEMPO via an amide bond. Molecule 4 serves as control for 3, as they are essentially isosteric.....	38
3.8: Pictorial representation of the extraction technique used to purify the lipophilic anchors and EMEAT.....	40
3.9: Representative HPLC Spectra for spin-labeled molecule HDT. The retention time of the molecule was 28 min.....	43
3.10: Representative ESI-MS spectrum of one of the lipophilic anchors, HDT. The molecular weight of the compound was 423.46 Da. A common observation of the mass spectra of the spin-labeled anchor molecules was the presence of $(M+2H)^+$ peak. The possible structure of the ion which corresponds to that $m/z$ value is shown in the figure (circled compound).....	45
3.11: Schematic representation of the mechanism involved in disproportionation reaction between two spin-labeled nitroxide molecules. (A) represents the nitroxide radical.....	46
3.12: Representative Proton NMR spectrum of HDT. The assigned peaks represent the protons corresponding to the structure of the compound.....	47
3.13: Expanded version of the Proton NMR spectrum of HDT in deuterated chloroform ( $CDCl_3$ ) for proton e.....	48
4.1: (a) Structure of POPC; (b) Structure of DMPC. Both contain a polar head group and a non-polar acyl lipid chain.....	49
4.2: Structure of a Liposome showing the alignment of the non-polar lipid chains and polar head groups of the lipid in a unilamellar vesicle.....	51
4.3: Structure of Calcein.....	53
4.4: Pictorial representation of calcein leakage assay. The blue circle depicts the liposome and the red circle depicts the calcein fluorophore.....	54
4.5: Fluorescence spectra of calcein encapsulated in DMPC liposomes in the presence (red squares) and absence of (blue diamonds) of Triton X. The fluorescence spectrum of the blank buffer solution (green triangles) is also shown in the figure. The fluorescence intensity is plotted against the emission wavelength of calcein.....	56

4.6: Fluorescence spectra of encapsulated calcein in POPC liposomes in the presence (red squares) and absence (blue diamonds) of Triton X. The blank spectrum of the buffer solution (green triangles) is also shown in the figure. The fluorescence intensity of the encapsulated is increased by several folds upon addition of Triton X.....	57
4.7: Fluorescence spectra of encapsulated calcein in POPC liposomes upon addition of anchor molecules. The blue line depicts the spectrum of the encapsulated liposomes after the addition of Triton X. The anchor to liposome ratio was maintained at 1:100...58	58
5.1: Calibration curves of 4-AT in water and methanol. The known concentrations of the spin-label molecule are plotted against the area under the curve of the corresponding concentration.....	61
5.2: EPR spectra of EMEAT vs NAT in methanol. Magnetic field (B) is plotted on the x-axis and arbitrary intensity on y-axis. The EPR spectra of both the compounds have been measured for the same concentrations.....	63
5.3: EPR spectra of EMEAT in the presence and absence of liposomes. EMEAT showed same behavior both in the solvent water as well as in the presence of the liposomes. The concentration of EMEAT was the same both in the liposomes and the solvent.....	64
5.4: EPR spectra of NAT in the presence and absence of liposomes. Both the spectra are area normalized. There is a subtle change in the line shape of the hyperfine lines for NAT in liposomes and the signal to noise ratio is a bit low (noisy signal: NAT-POPC).....	65
5.5: EPR spectra of HDT in the presence and absence of liposomes. In this case HDT was added to the liposomes after extrusion. Also, among the synthesized anchors, HDT has the longest hydrocarbon chain which imparts high lipophilicity to the anchor. In the figure the magnetic field is plotted against the arbitrary intensity.....	67
5.6: Comparison of the EPR spectra of HDT added to the liposomes during extrusion to HDT in solvent methanol.....	68
5.7: Scheme for separating the signals of bound from unbound spin-label using Chromium oxalate $[\text{Cr}(\text{C}_2\text{O}_4)_3]$ . Chromium oxalate is a polar relaxation agent soluble in water.....	70
5.8: Diagrammatic representation of the method used for calculating the percentage of bound spin-labeled anchor using the kaleidagraph software.....	71

5.9: Pictorial representation of the experimental design used to obtain uniform and reproducible results with minimum errors possible.....	72
5.10: EPR spectra of EMEAT in liposomes with (blue) and without (red) chromium. EMEAT was added to the liposome solution after extrusion. The concentration of chromium oxalate in solution was 20 mM.....	73
5.11: Representative EPR spectra of HDT in liposomes with (red) and without (blue) chromium. The anchor was added to the liposome after extrusion.....	74
5.12: Representative absorption spectra of HDT in liposomes with (red) and without (blue) chromium. X-axis represents the magnetic field in gauss (units).....	74
5.13: EPR spectra of PT in liposomes with (red) and without (blue) chromium oxalate.....	75
5.14: Representative EPR spectra of HDT in solvent methanol with (red) and without (blue) chromium. The signal from HDT with chromium can be seen as a flat line which is a result of broadening. It is very clear that the unbound HDT collides with the chromium resulting in total relaxation of the spin-label.....	76
5.16: Attachment of First Amino Acid (Fmoc-Lys(Mtt)-OH) to a resin in SPPS.....	80
5.17: Removal of Fmoc protecting group from the peptide chain.....	81
5.18: Removal of methytrityl protecting group from lysine.....	81
5.19: Reaction showing the attachment of the anchor 1-pyrenebutyric acid to the lysine amino acid.....	82
5.20: Model peptide with HDA and CP attached to the side chain of the lysine amino acid. Glycine spacers were used to reduce the steric hindrance from the resin and the rest of the amino acids.....	83
5.21: An ESI-MS spectrum in positive ion mode of RPLC purified peptide containing PBA and CP attached to the lysine residues of the C-terminus. The m/z values 883, 669, and 529.8 correspond to different fragments of the peptide containing either one or both of the molecules attached to the lysine residues.....	85
5.22: EPR spectra of the peptide model in liposomes with (green) and without (red) chromium.....	87

## LIST OF ABBREVIATIONS AND SYMBOLS

A: hyperfine coupling constant

AFM: Atomic force microscopy

4-AT: 4-amino TEMPO

AU: absorption units

BoPrP: Bovine Prion protein

$\beta$ : Bohr magneton for electron which is a collection of constants

C: Carbon

CP: 3-(Carboxy)-2,2,5,5-tetramethyl-1-pyrrolidinyloxy

Cu: copper

CW: continuous wave

DIC: Diisopropylcarbodiimide

DIPEA: N, N-Diisopropylethylamine

DMF: N, N-dimethylformamide

DMPC: 1,2-Dimyristoyl-*sn*-Glycero-3-Phosphocholine

DPPC: 1,2-dipalmitoyl-*sn*-glycero-3-phosphocholine

E/M: excimer/monomer

EDTA: Ethylenediaminetetraacetic acid

ELISA: Enzyme linked immuno sorbent assay

EMEA: 2-[2-(2-methoxyethoxy) ethoxy] acetic acid-TEMPO

EMR: Electron magnetic resonance

EPR: Electron paramagnetic resonance

ESR: Electron spin resonance

ESI-MS: Electrospray ionization-Mass spectrometry

$F_0/F_T$ : ratio of fluorescence intensities with and without the quencher present

Fmoc: 9-Fluorenylmethoxycarbonyl

g: g-factor

GHz: gigahertz

GPI: Glycophosphatidylinositol

GUV: giant unilamellar vesicles

$H_0$ : representation of magnetic field

HBTU: O-(benzotriazol-1-yl)-1, 1, 3, 3-tetramethyluronium hexafluorophosphate

HAD: Heptadecanoic acid or Margaric acid

HDT: Heptadecanoic acid-TEMPO

HOBt: 1-hydroxybenzotriazole

HPLC: High performance liquid chromatography

hPrP: human Prion protein

iq-PCR: Immunoquantitative Polymerase Chain Reaction

k: Boltzmann constant

LUV: large unilamellar vesicle

$M_s$ : spin projection quantum number

mM: millimolar

mL: milliliter

Mtt: 4-Methyltrityl

$\eta$ : symbol for viscosity

NAT: Nonanoic acid-TEMPO

NaOH: Sodium hydroxide

NMR: Nuclear magnetic resonance

NO: Nitroxide

NPLC: Normal phase liquid chromatography

PBA: 1-pyrenebutyric acid

POPC: 1-palmitoyl-2-oleoyl-*sn*-glycero-3-phosphocholine

POPG: 1-palmitoyl-2-oleoyl-*sn*-glycero-3-phosphoglycerol

PROXYL: 2,2,5,5-tetramethyl-1-pyrrolidinyloxy

PrP: prion protein

PrP<sup>C</sup>: cellular form of Prion protein

PrP<sup>Sc</sup>: scrapie isoform of Prion protein

PT: Pyrene-TEMPO

recPrP: recombinant Prion protein

S: spin quantum number

SUV: small unilamellar vesicles

T: tesla

T<sub>m</sub>: phase-transition temperature

TEMPO: 2,2,6,6-tetramethylpiperidine-1-oxyl, 4-amino-2,2,6,6-tetramethylpiperidinyloxy

TFA: Trifluoroacetic acid

TSE: Transmissible Spongiform Encephalopathy

Zn: zinc

# Chapter 1: Introduction to Prion Protein

## 1.1: Overview

The discovery of infectious proteins, called Prions was unexpected. In 1982, Stanley B. Prusiner coined the term “Prion” to describe the transmissible proteinaceous infectious particles lacking nucleic acids for replication.<sup>1</sup> These particles were found to be different from other infectious agents like viruses, viroids, plasmids in their properties and mode of replication. It was discovered that the Prion protein (PrP) is an endogenous protein located predominately in the neuronal cells of the central nervous system (CNS). Mature human PrP is a membrane bound glycoprotein consisting of 208 amino acids. NMR studies on recombinant, full-length human, hamster, bovine and mouse PrP suggest that the C-terminal region encompassing the residues PrP (125-230) is primarily  $\alpha$ -helical in structure whereas the N-terminal region, corresponding to PrP (23-124), is unstructured<sup>2-5</sup> (Figure 1.1). The N-terminus encompasses the metal binding region which is a series of eight amino acids that repeats itself through the length of the peptide called an octarepeat or octapeptide. The normal cellular form of prion protein is denoted as PrP<sup>C</sup>. PrP is tethered to the surface of the cell membranes through a glycosylphosphatidylinositol (GPI) anchor.<sup>6</sup> PrP<sup>C</sup> is localized to clathrin-coated pits and lipid rafts on the membrane surface.<sup>7</sup> Lipid rafts are characterized by high concentrations of cholesterol and sphingolipids.<sup>8</sup> Clathrin-coated pits are thought to be

primarily responsible for the endocytic uptake of PrP whereas majority of the protein in both neuronal and non-neuronal cells is found in detergent-resistant lipid rafts. It is thought that PrP transits from the raft domain to the coated-pits, which then form vesicles to draw PrP and other GPI anchored proteins into the cell.<sup>9</sup>

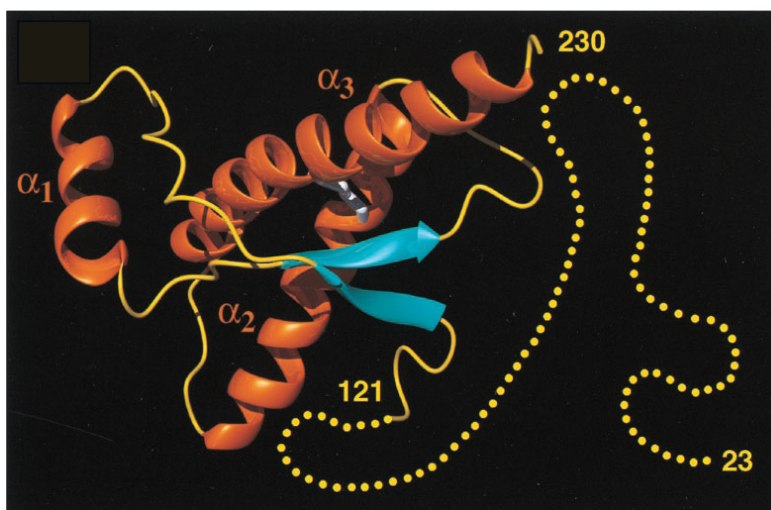


**Figure 1.1:** Ribbon diagram of the three-dimensional structure of the intact human prion protein, hPrP (23–230). The C-terminal region consists of three  $\alpha$ -helices and a short anti-parallel  $\beta$ -strand<sup>2</sup>. The N-terminus is unstructured and thus is not shown as a secondary structure cartoon.

The normal cellular PrP<sup>C</sup> is converted into a pathogenic form denoted PrP<sup>Sc</sup>, through a post-translational modification during which it acquires a high  $\beta$ -sheet content.<sup>9</sup> PrP<sup>Sc</sup> is the pathogenic isoform of PrP<sup>C</sup> which is insoluble and partially resistant to proteinase K digestion. The conversion of PrP<sup>C</sup> into PrP<sup>Sc</sup> leads to a class of neurodegenerative diseases known as prion diseases or transmissible spongiform encephalopathies

(TSEs). TSEs affect cattle (called mad cow's disease), sheep, goats (scrapie disease), deer, elk (Chronic wasting disease) and humans (Creutzfeldt-Jakob disease or CJD and Kuru). The accumulation of insoluble PrP<sup>Sc</sup> results in degeneration of the nerve cells, starting the onset of the disease.<sup>9</sup> Accumulation of pathogenic proteins is also the main cause for other neurodegenerative diseases like Alzheimer's, Parkinson's and Huntington's disease. Figure 1.2 shows the plausible model for the tertiary structure of human PrP<sup>Sc</sup> (huPrP<sup>Sc</sup>).

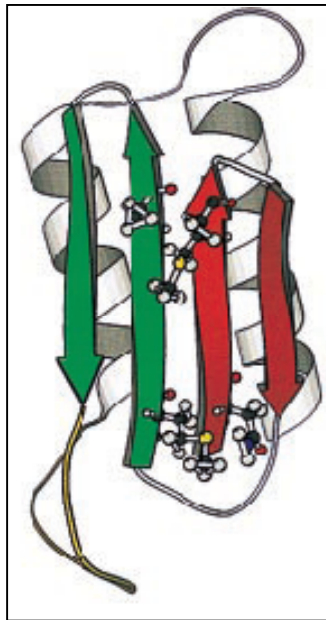


**Figure 1.2:** Plausible model for the tertiary structure of human huPrP<sup>Sc</sup>.<sup>9</sup> Note the increase in  $\beta$  sheet content shown in the secondary structure of huPrP<sup>Sc</sup>.

## 1.2: Physiological Functions of PrP<sup>C</sup>

Although a great deal of knowledge exists regarding the pathogenic role of PrP<sup>Sc</sup>, the physiological function of PrP<sup>C</sup> is still unknown. Experiments conducted on PrP knock-out mice showed no change in their normal behavior except for minor changes in circadian rhythms, some physiological parameters and low copper concentration in the brain.<sup>10-13</sup> The most important observation made from these experiments was that PrP<sup>C</sup> deficient mice were protected against scrapie disease and failed to propagate prions at least up to 13 months after inoculation. These studies led to the conclusion that endogenous PrP<sup>C</sup> was necessary for prion replication in mice. Several studies have been conducted suggesting various functions of PrP<sup>C</sup>. The ability to bind copper suggests that PrP<sup>C</sup> may be involved in copper metabolism.

The copper binding capability of PrP<sup>C</sup> through multiple octapeptide repeats present in the N-terminal region might have a direct impact on the regulation of presynaptic copper concentration, conformational stability of PrP<sup>C</sup>, and on cellular response to oxidative stress by regulating the redox balance.<sup>14,15</sup> In the context of the latter, PrP<sup>C</sup> is thought to act as a superoxide dismutase to protect the neurons from the reactive oxygen species such as superoxide, peroxide and redox active metal ions.<sup>16</sup> This theory was refuted by voltammetric data suggesting PrP without copper was not damaged by any reactive oxygen species.<sup>17</sup> Additionally to act as superoxide dismutase, PrP<sup>C</sup> must cycle through different oxidation states of copper, most likely Copper (I) and (III). Copper (I) cannot coordinate to the deprotonated amide bonds that are in the

octarepeat binding site.<sup>18</sup> Therefore, copper would not be able to cycle from copper (II) state to a different copper (I) state easily. Although superoxide dismutase activity of PrP might be possible, it is unlikely.

Cell culture experiments revealed the neuronal cell endocytosis cycle and constitutive internalization of the prion protein. It has been shown that PrP<sup>C</sup> is endocytosed from the plasma membrane via clathrin-coated pit and transferred to an endosomal compartment before being recycled back to the surface.<sup>19</sup> This process of internalization of PrP through endocytosis was believed to be mediated through its copper binding capability.<sup>20</sup> By cycling free copper (II) ions through the cell, PrP may protect the cell from the copper toxicity.<sup>21</sup>

### **1.3: PrP Self-Recognition**

Extensive research has been carried out to understand the normal function of PrP but it still remains elusive. Studies indicate that self-recognition might be an important factor in both the normal function and malfunction of PrP. PrP self-recognition is thought to be associated with metal binding. One of the major findings is the discovery that addition of copper or zinc to neuronal cells stimulates endocytosis of PrP. Copper binding by PrP has been studied extensively and a good deal of information is available about copper binding sites and coordination spheres. Three different studies address

the issue of PrP self-recognition. The physiological importance of self-recognition was brought to light by Moulliet-Richard et al., where they studied signal transduction pathways in murine 1C11 neuronal cells. They found that antibody mediated cross-linking of PrP on cultured cells stimulate signal transduction.<sup>22</sup> This research set the stage for the hypothesis that PrP dependant signaling might most likely involve a cofactor. This experiment shows that self-recognition of PrP can induce a biological reaction in neuronal cells. The likelihood of PrP cross-linking in nature is high, and might even play an important role in its biological function.

While working with solutions of full-length bovine PrP (BoPrP), Gonzalez-Iglesias et al. noticed that the solution turbidity increased upon addition of copper.<sup>23</sup> The appearance of turbidity was monitored by measuring the absorbance at 360 nm. Centrifugation of these turbid solutions yielded transparent supernatants with decreased protein concentration indicating the formation of insoluble aggregates. To test the specificity of copper over other metals, zinc and manganese were added to the solutions after copper was added. The addition of these metals had no effect on the measured absorbance. Subsequently, to verify the type of copper induced site binding, the protein-copper complex formation was monitored using Atomic force microscopy (AFM). The inspection of the supernatant obtained after 1 hr incubation and extensive washing of the centrifuged complexes revealed an amorphous mesh of protein of 3 nm that corresponded to that expected for a single layer of globular protein of about 23.5 kDa, the weight of the bovine PrP,  $\alpha$ BoPrP (24-242) used in the study (**Figure 1.3**). The constant thickness of the protein was interdispersed with holes and surface irregularities. A large polydispersity of proteins was seen in the direction parallel to the

mica surface. Based on turbidity and AFM measurements, they concluded that PrP molecules were oriented in a parallel fashion with  $\text{Cu}^{+2}$  cross-linking them.

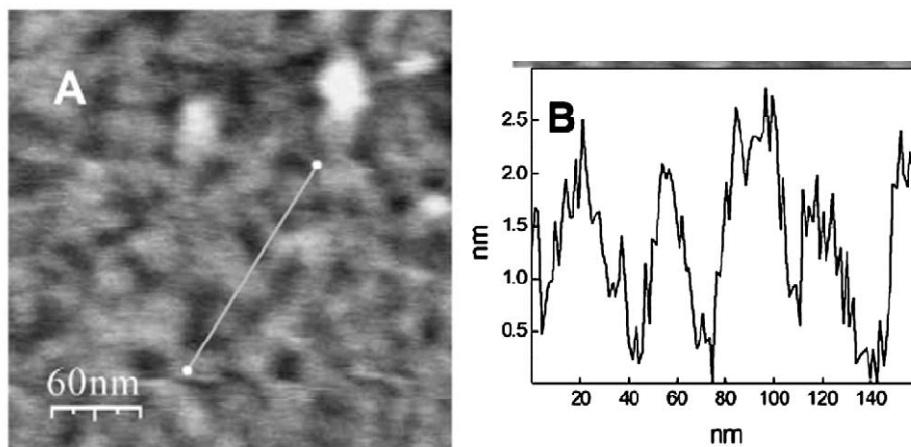


**Figure 1.3:** AFM analysis of the morphology of copper-bound  $\alpha\text{BoPrP}$  (24-242) insoluble complexes. (A) AFM image. (B) Distance profile of the selected region represented by the white bar on part (A). The horizontal axis corresponds to the distance related to the width of the selected segment while the vertical axis shows the thickness of the complex.<sup>23</sup>

In a subsequent study carried out by Morante et. al.,  $\text{Cu}^{+2}$  binding modes were explored using X-ray absorption spectroscopy and spectral modeling.<sup>24</sup> Two distinct copper conformations were deduced from the studies. The first conformation involved intra-repeat copper binding in peptides that contain only one or two octarepeat segments at sub-stoichiometric site occupancy. This structure agrees with the crystal

structure previously determined (Figure 1.4). Inter-repeat copper binding was also observed in complexes with four and six octarepeat copies and partial occupancy. This involved the coordination of copper to two histidine residues at equatorial positions (Figure 1.4).

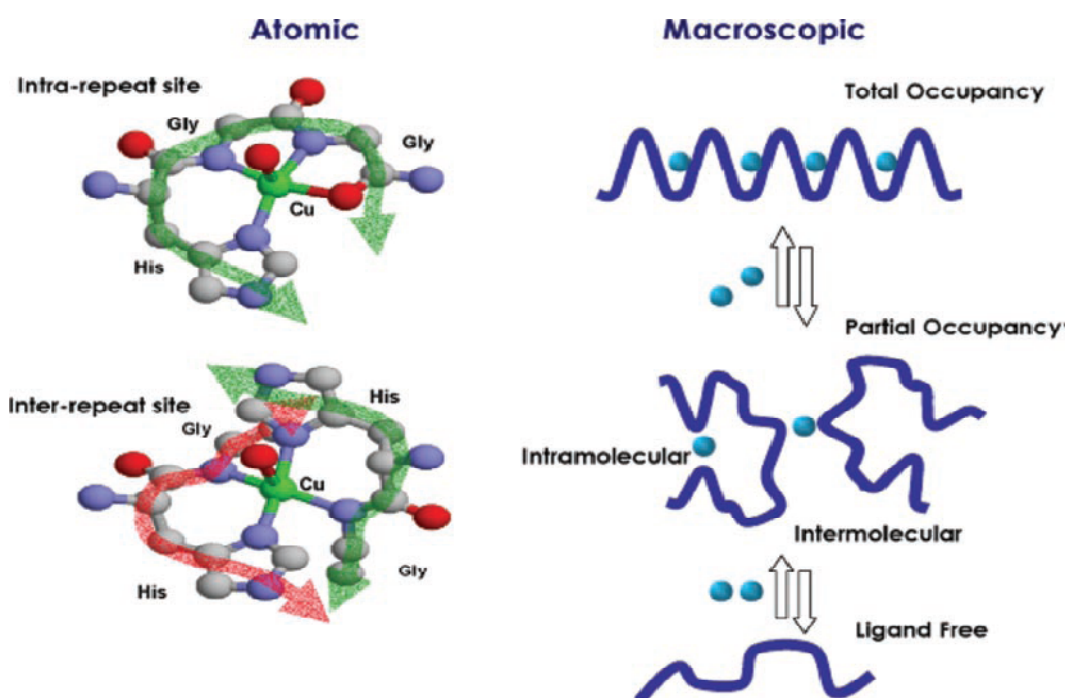


**Figure 1.4:** Intra-repeat and inter-repeat Cu(II) site geometries and its macroscopic relevance in the PrP Cu(II) binding process. The atomic model depicts the intra-repeat (upper part) and inter-repeat (bottom part) Cu(II) site geometries observed for Cu(II) bound to PrP octarepeat region. The thick green and pink lines represent the polypeptide chain backbones. On the right-hand side, the macroscopic process of Cu(II) binding to this region is summarized.<sup>24</sup>

The inter-repeat copper binding in PrP demonstrated that copper can induce homomeric or self-interactions. Another approach to studying interactions between PrP molecules employed by Leliveld et al., involved the use of fusion proteins. The N-terminus of sepharose-immobilized Glutathione S-transferase was linked to a variety of PrP-derived peptides spanning different lengths of the metal binding region.<sup>25</sup> When incubated with brain extracts from hamster, these fusion constructs could successfully capture PrP<sup>C</sup> in the presence of Cu<sup>+2</sup> and Zn<sup>+2</sup>. Although these studies do not provide molecular level detail on the nature of PrP-PrP interactions they clearly point to a role for the metal binding region in Cu<sup>+2</sup> and Zn<sup>+2</sup> dependant manner. Furthermore, Leliveld's experiment showed that metal-induced prion-prion interactions involve octarepeat domain alone; however, experiments were designed that monitored these interactions on a molecular level which will be discussed later.

#### **1.4: Importance of Membrane Location of PrP**

Membrane location of PrP has been shown to be an important factor that contributes to the conversion of normal cellular form PrP<sup>C</sup> to the pathogenic form PrP<sup>Sc</sup>. Several studies have been performed to analyze the interaction of the protein with the lipid membranes and consequences of these interactions. Time-resolved FTIR studies were conducted to study the changes in the secondary structure of the prion protein when binding to a raft like lipid-membrane through the GPI anchor using recPrP and native PrP<sup>C</sup>. The change in the structure of PrP<sup>C</sup> from random coil to  $\beta$ -sheets was

concentration dependant. NMR studies of the native PrP<sup>C</sup> anchored to the membranes showed that at low concentrations PrP<sup>C</sup> assumes a structure similar to recombinant PrP (recPrP) in solution and when the concentration reaches above the threshold at the membranes, the random coil is converted to intermolecular  $\beta$ -sheets.<sup>26</sup> The  $\beta$ -sheets are subsequently converted into dimers and oligomers on the membranes. The author speculates that the increase in concentration of PrP<sup>C</sup> in biological systems might be based on PrP accumulation either due to genetically caused overexpression or a different, as of yet unknown trigger. **Figure 1.5** shows the schematic representation of concentration dependant secondary structure changes of PrP<sup>C</sup> upon membrane anchoring.

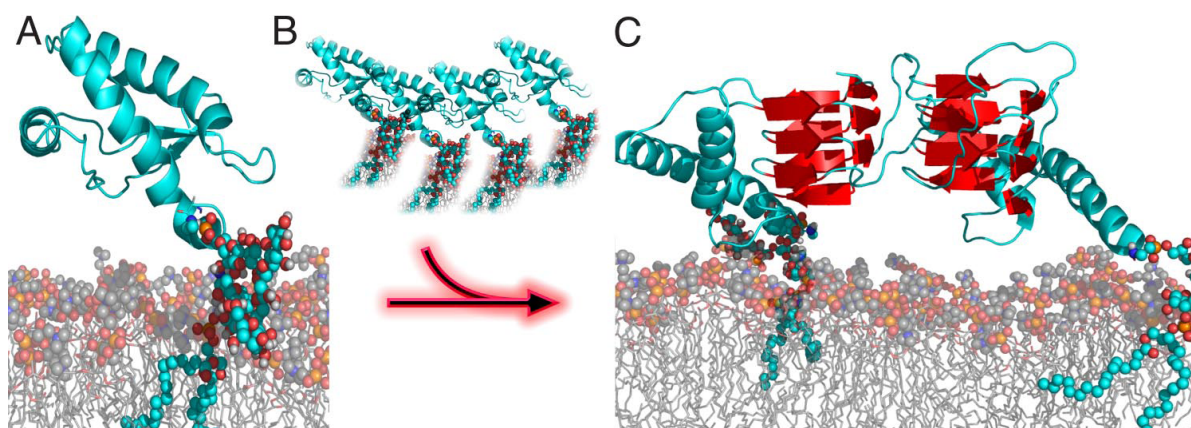


**Figure 1.5:** Concentration-dependent secondary structure changes upon membrane anchoring. (A) PrP<sup>C</sup> bound to the raft-like lipid bilayer exhibits the same secondary structure (at lower concentrations) as anchorless recPrP in solution in NMR studies. (B) An increased concentration of PrP<sup>C</sup> at the membrane leads to a structural transition

toward intermolecular beta sheet. (C) Schematic illustration of intermolecular  $\beta$ -sheet. This dimerization could well be the initial step on the pathway of the conversion into PrP<sup>Sc</sup>.<sup>26</sup>

In order to elucidate the molecular mechanism underlying the PrP-PrP interactions and their role in the transmission and pathogenesis of the TSEs, thermodynamic and structural studies were performed on soluble, recPrP from *E. coli* that is assumed to correspond to the structure of PrP<sup>C</sup> isoform of the prion protein. PrP<sup>C</sup> was covalently attached to cellular membranes *in vivo* via a C-terminal GPI anchor and measurements were made using far-UV circular dichroism. Results showed that the conversion of PrP<sup>C</sup> to PrP<sup>Sc</sup> might not be due to the direct influence of the raft lipids on the structure and stability of the membrane bound PrP<sup>C</sup> but caused by other factors like increased local PrP concentrations or high-effective concentration of membrane-associated conversion factors.<sup>27</sup> Also the study suggests that co-localization of PrP<sup>C</sup> and PrP<sup>Sc</sup> in contiguous membranes is a critical prerequisite for prion propagation *in vivo*. These results support the conclusions made from the time-resolved FTIR studies mentioned above.

Another study conducted on recPrP coupled covalently to a synthetic GPI anchor mimetic also provide experimental evidence to the data presented in the above studies.<sup>28</sup> This study shows that  $\beta$ -sheet-rich forms of PrP have higher affinities to the raft lipid components and aberrant prion molecules may start to accumulate within rafts, promoting protein-protein interactions, which ultimately result in aggregation and fibrillization of PrP. Also, the normal cellular form of PrP can bind to raft membranes but that does not induce aggregation of PrP. Finally, it was concluded that the lipid raft environment protects the  $\alpha$ -helical conformation of PrP, whereas the conversion is

initiated outside rafts.<sup>28</sup> Fluorescence, Circular dichroism (CD), Fourier transform infrared spectroscopy (FTIR), and Electron microscopy (EM) studies were conducted on the change in the structure of  $\beta$ -isoform of PrP with change in the membrane composition and pH.<sup>29</sup> Binding of  $\beta$ -PrP to negatively charged POPG vesicles resulted in a higher level of random coil and  $\beta$ -sheet structure, when compared with  $\beta$ -PrP in solution. This  $\beta$ -enriched form destabilizes the POPG membranes, leading to total release of the vesicle contents and subsequent formation of amorphous aggregates of PrP around the vesicles. Raft membranes composed of neutral DPPC, cholesterol and sphingomyelin induced a substantial unfolding of  $\beta$ -PrP upon binding. This membrane association of  $\beta$ -PrP with raft membranes did not destabilize the integrity of the raft lipids but led to the conversion of  $\beta$ -PrP into fibrils.<sup>29</sup>

Fluorescently labeled models of the membrane bound PrP were developed to investigate the prion-prion interactions and metal binding on a molecular level. Peptides encompassing the full metal binding region were anchored to small unilamellar vesicles (SUVs) and fluorescence measurements were taken as a function of added metal. Pyrene, a fluorophore was used as an anchor for the liposomes. **Figure 1.6** gives a general illustration of the idea of this research. This study provides a molecular description for PrP self-recognition as a function of  $\text{Cu}^{+2}$  and  $\text{Zn}^{+2}$  loading. As discussed in the previous studies mentioned above the structure of PrP is neither affected by the GPI anchor nor the cell membrane. The fluorescence assay was based on the proximity of the pyrene fluorophores located in the lipid membranes. When two pyrene molecules are close to each other in space, they give rise to an excimer signal in the emission spectrum distinct from that of the monomeric signal of pyrene.

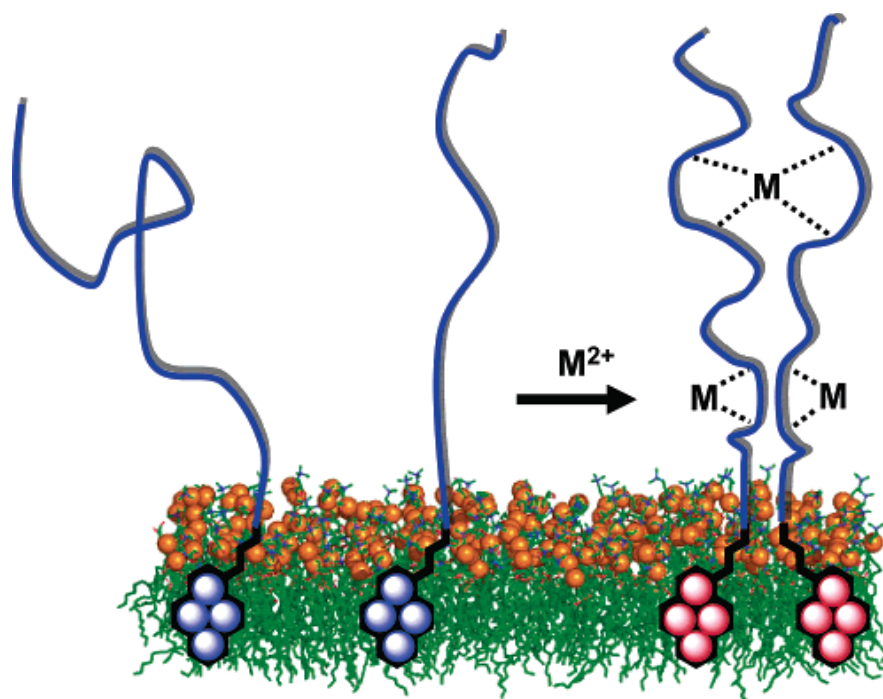


**Figure 1.6:** General illustration of pyrene-labeled peptides anchored to the outer surface of a SUV. When pyrene fluorophores (colored blue at the left) come into the proximity of one another, they form excimers (colored red at the right) which produce a distinct fluorescence signal at a longer wavelength.<sup>30</sup>

The excimer/monomer ratio (E/M) helped to illustrate the degree of interaction in a quantitative manner. **Figure 1.7** shows the results of the fluorescence experiments that were designed to monitor the PrP-PrP interactions as a function of added metal. A low intensity excimer peak was observed at 0 equivalents of added  $Cu^{+2}$  which led to the conclusion that the peptides interact with each other to a small degree even in the absence of any added metal. With an increase in the added equivalents of  $Cu^{+2}$  to peptide/liposome solution, there was an increase in the E/M ratio representing a 117% change. The results suggested that  $Cu^{+2}$  promoted interactions between PrP molecules.

Similar studies were conducted using  $Zn^{+2}$  which produced a pronounced increase in the E/M ratio, representing a 300% change.

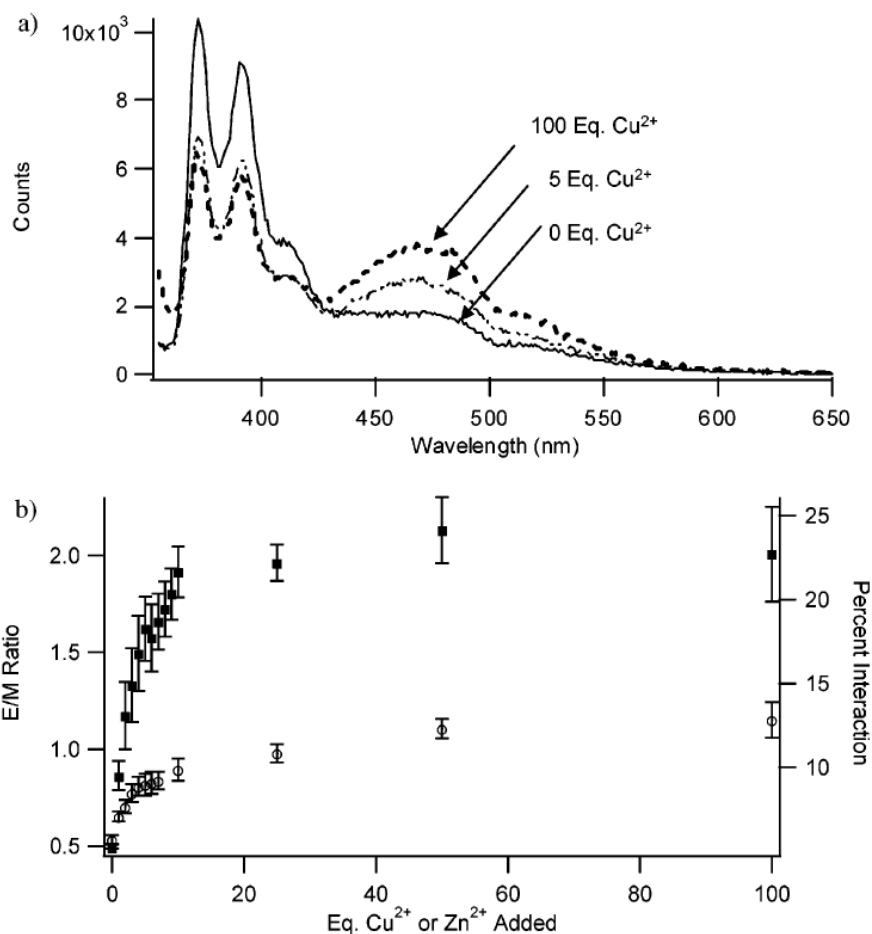


**Figure 1.7:** (a) Fluorescence spectra of the native PrP peptide ( $4.15 \mu M$ ) at three different  $Cu^{2+}$  loadings in a liposomal solution. (b) E/M ratio for the native PrP peptide as a function of titrated  $Cu^{2+}$  (O) and  $Zn^{2+}$  (■). The percent of interacting fluorophores presented at the right, y-axis, was calculated using eq 1. The metal ion concentration is reported in equivalents per peptide.<sup>30</sup>

Further research was conducted to determine the residues responsible for these interactions. Glutamine and tryptophan were found to be important in mediating the PrP self-interactions. Tryptophan was found to be responsible for the low-level interactions in the absence of any added metal. In conclusion, this research provides a plausible mechanism for PrP self-recognition and also suggests that dimmers or oligomers are sure to play an important role in  $\text{Cu}^{+2}$  or  $\text{Zn}^{+2}$  stimulated endocytosis.

### **1.5: Importance of Quantification of the Bound Peptide**

The importance of membrane location of PrP in context with the pathogenicity of the prion disease has been studied extensively. But, none of these studies were able to determine the amount of membrane bound PrP which does not allow for quantitative studies to be performed. Research has been conducted to quantify the amount of the pathogenic form and normal cellular form of prion protein in biological samples for diagnostic purposes using different techniques like enzyme linked immuno sorbent assay (ELISA) and recently immuno-quantitative polymerase chain reaction (iqPCR).<sup>31</sup> Quantification of membrane bound PrP provides a well-defined system to completely understand the behavior of prion-prion interactions. For instance, when discussing the fluorescence data in the previous section the percentage of molecules interacting was discussed. But if some PrP molecules are on the surface of the membrane and others are free in the solution the extent to which they interact may be different. Thus, the

percentage of interacting PrP molecules will also be a function of the percent bound and it would be nice to remove this variable. It also lays the foundation for quantitative studies in future which might further lead to a better understanding of the mechanism of self-recognition of PrP and its role in disease related and normal functions. Our study focuses on quantifying the membrane bound PrP using electron paramagnetic resonance (EPR) where the first step is to determine the amount of synthetic anchor molecules bound to model membranes. This study helps in developing a protocol for quantification of the bound peptide and the mechanism of metal-induced PrP-PrP interactions which can be applied to cellular models.

## Chapter 2: Electron Paramagnetic Resonance (EPR)

### 2.1: Introduction to EPR

Electron paramagnetic resonance (EPR) spectroscopy, also known as electron spin resonance (ESR) spectroscopy or electron magnetic resonance (EMR) spectroscopy is a spectroscopic technique that is used to detect unpaired electrons in a sample by their absorption of energy from microwave radiation (0.3-300GHz) when the sample is placed in a strong magnetic field. The concept of EPR is very similar to that of nuclear magnetic resonance (NMR). Both deal with the interaction of electromagnetic radiation with magnetic moments; in the case of EPR magnetic moments arise from electrons rather than nuclei. Free radicals and transition metal ions are the species which contain unpaired electrons and can be detected using EPR. The first observation of an electron paramagnetic resonance peak was made in 1945 by Zavoisky on transition metal ions.<sup>32</sup> The term electron paramagnetic resonance was introduced to account for contributions from electron orbital as well as spin angular momentum of the electron. An electron possesses a magnetic moment by virtue of its spin ( $S=1/2$ ) and acts as a magnet in the presence of a static, external magnetic field ( $H_0$ ). In the presence of an applied magnetic field, the magnetic moment has two allowed orientations or spin states, which have different energy levels. Transitions between the two spin states can be induced using electromagnetic radiation of the appropriate frequency applied perpendicular to

the external magnetic field  $H_0$ . **Figure 2.1** shows the behavior of a population of free electrons in the presence of an external magnetic field.

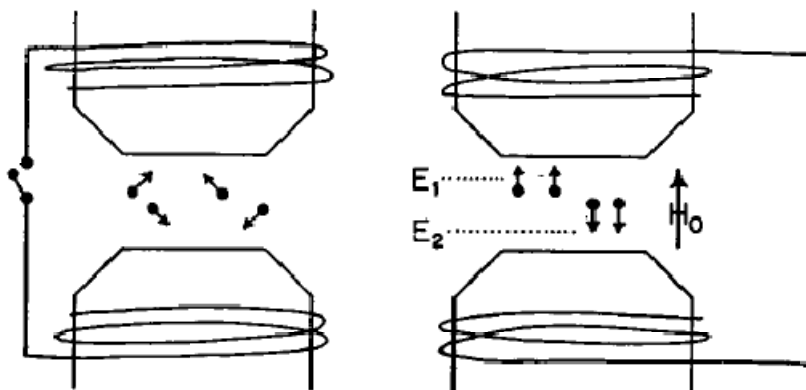


**Figure 2.1:** Pictorial representation of a population of free electrons in an external magnetic field ( $H_0$ )<sup>10</sup>.

Angular momentum about an axis may take only  $2S+1$  values, which is referred to as the multiplicity. So for an electron  $2(1/2)+1=2$ , thus there are two quantized states.

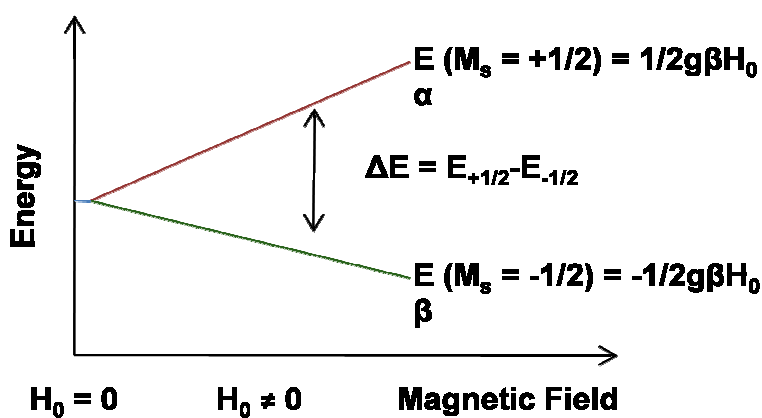


**Figure 2.2:** The  $M_s=+1/2$  and  $-1/2$  states have different energies in the presence of a magnetic field.

The energy difference ( $\Delta E$ ) between the two spin states will help us to determine the resonance condition.

$$\Delta E = h\nu = g\beta H_0$$

$h$  – Planck's constant

$\nu$  – Frequency

$g$  – g-factor

$H_0$  – Magnetic field strength

$\beta$  – Bohr magneton for the electron which is a collection of constants

Although EPR measures the absorption of energy, the spectrum is usually displayed as the first derivative of the absorption spectrum. The magnetic moment of an electron is substantially greater than the corresponding quantity of any nucleus, so a much higher frequency of electromagnetic radiation is required to bring about a spin resonance within an electron than a nucleus at identical magnetic fields. Hence, EPR is a more sensitive technique than NMR.

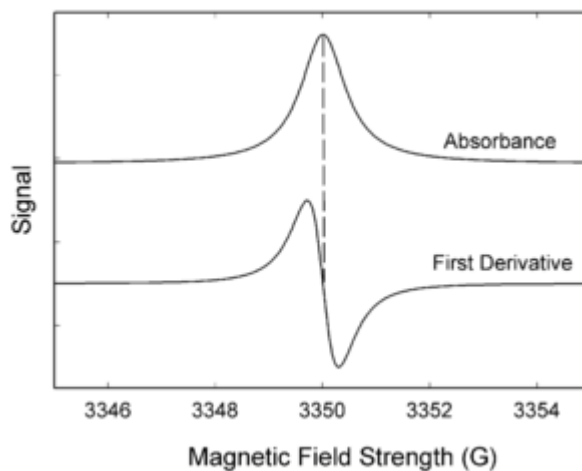


**Figure 2.3:** Absorbance spectrum is converted into the first derivative spectrum in EPR.

An EPR signal is characterized by four main parameters which are mentioned below:

g-value: The g-value gives us the position of a resonance. It is the measure of the local magnetic field experienced by the electron. The g-value of an EPR signal is analogous to the chemical shift value in NMR. The measurement of the g-value aids in the identification of an unknown signal. The g-value for a free electron as found in a large number of free radicals is 2.0023, while for transition metals it can be as high as 10.

Intensity of the EPR signal: The integrated area under the signal is proportional to the concentration of the unpaired electrons giving rise to the signal. A number of factors can alter the intensity of the signal like quenching due to high concentrations of the samples and saturation of the resonances. EPR signal intensities can be used for quantitative purposes.

Relaxation Times: The line width of an EPR signal depends on the relaxation of the spin states. **Figure 2.4** shows the relaxation of different spin states.

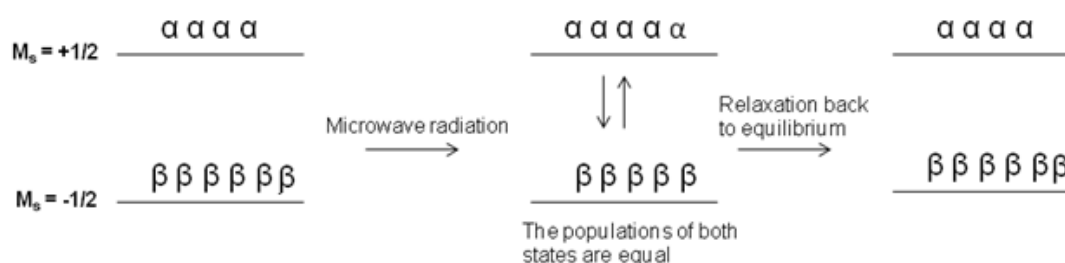


**Figure 2.4:** Affect of impingement of the microwave radiation on the distribution of the spin states and relaxation back to the equilibrium.

The distribution of the electrons between the  $M_s = +1/2$  and  $M_s = -1/2$  spin states can be perturbed by impinging microwaves on the sample. EPR signal intensity is proportional to the concentration of the unpaired electrons which depends on the population difference between the two spin states. In the presence of strong applied radiation the populations in the two states are equal. The system can return to the equilibrium via spin-lattice relaxation. The time constant for this process is called the spin-lattice relaxation time and denoted as  $T_1$ . It is the measure of the recovery rate of the spin population after a perturbation. If the value of  $T_1$  is too short, the system will relax extremely quickly and lead to line broadening. In some cases the resonance line can be too broad to detect at all. Electrons have a wide range of  $T_1$  values depending on their environment.

The Hyperfine Interaction: This interaction leads to the observation of multiplets or splitting in the EPR spectra. Often these are due to the presence of spin active nuclei that are near the unpaired electron. The nuclei produce a local magnetic field that changes the magnetic environment of the electron in a manner dependent on the number ( $n$ ) and nuclear spin ( $I$ ) of the nuclei. The magnitude of the splitting between the lines is called the hyperfine splitting constant denoted "A" or "a" depending on the units. The hyperfine interaction is of two types: 1) isotropic interaction that results from the delocalization of the unpaired electron onto the nucleus and 2) a dipolar interaction between spins of the electron and the nucleus that is anisotropic. If the molecular motion is rapid then the dipolar interaction will be averaged to zero. When this is the case the spectrum is referred to as being motionally narrowed.

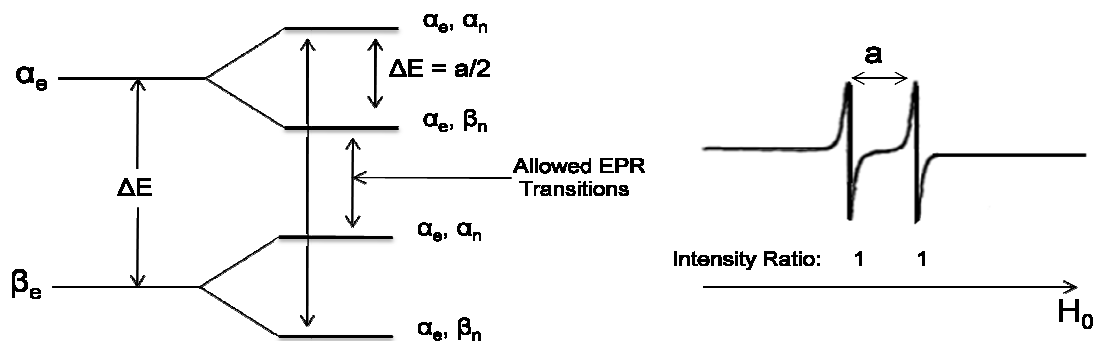
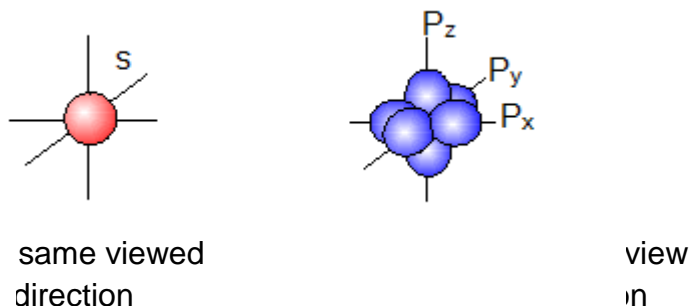


**Figure 2.5:** Energy diagram and the corresponding spectrum of a spin system with the value of  $I = \frac{1}{2}$  ( $2I+1 = 2$ ).

In general, there will be  $(2I+1)$  orientations of the nuclear spin in a magnetic field, all of which correspond to a different energy. The unpaired electron spin experiences these different orientations, so the EPR spectrum is split into  $(2I+1)$  lines. For  $n$  equivalent nuclei, the EPR spectrum consists of  $(2nI+1)$  lines.

Spectral Anisotropy: The orbitals containing electrons are not always spherical (isotropic). When this is the case their properties are different depending on their orientation and they are referred to as anisotropic.



In spin labels and transition metals, the electrons are primarily localized to p- or d-type orbitals. A number of EPR parameters are anisotropic, most notably the g-factor and the hyperfine coupling constant  $A$ . The g-value anisotropy is characterized by three principal g-values ( $g_{xx}$ ,  $g_{yy}$  and  $g_{zz}$ ) that correspond to the principal axes of the group containing the unpaired electron. The principal axes are determined by the symmetry.

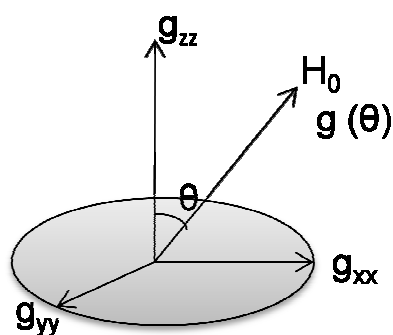


**Figure 2.6:** Variation of g-value with the magnetic field for an axially symmetric system.

For an isotropic system having equivalent principle axes i.e.,  $g_{xx} = g_{yy} = g_{zz}$ , the g-value is isotropic. In case of axial symmetry, as found in spin labels and transition metals,  $g_{xx} = g_{yy} \neq g_{zz}$ . In general,  $g_{zz}$  is defined as the g-value observed when the applied field is parallel to the symmetry axis while  $g_{xx}$  and  $g_{yy}$  are the g-values observed when the field is perpendicular to the axial symmetry. By convention,  $g_{zz}$  is usually taken to be the value at lowest field in a spectrum and  $g_{xx}$  is that at the highest field. In a single crystal the three principal g-values can be measured by rotating the crystal in the magnetic field so that they align with it. For any intermediate orientation the g-value depends on the angle ( $\theta$ ) between the magnetic field and the principal axes. Most samples we are interested in will not be single crystals; they will be liquids or randomly

oriented solids. Thus, the  $g$ -values will be spread out because the absorption of each molecule will depend on its own orientation ( $\theta$ ) with respect to the magnetic field. Anisotropy in  $A$  is just like that of the  $g$ -factor and is characterized by three principal  $A$ -values  $A_{zz}$ ,  $A_{xx}$  and  $A_{yy}$ . The anisotropy of  $A$  arises from the dipolar interaction of the magnetic field of the electron with the magnetic field of the nucleus. One very important example of hyperfine anisotropy is that involving stable nitroxide free radicals or spin labels which will be discussed later. The hyperfine interaction of the unpaired electron and the nitrogen nucleus ( $I = 1$ ) results in three lines. The unpaired electron is primarily localized to the  $2p$ -electron orbital on the nitrogen which is anisotropic; therefore the hyperfine interactions and  $g$ -values are also anisotropic.

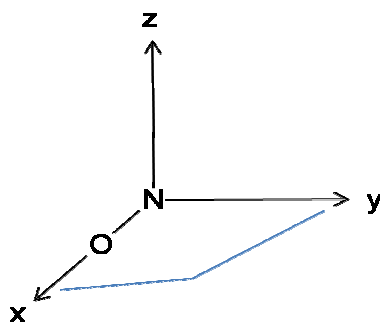


**Figure 2.7:** The molecular coordinate system of the nitroxide spin label used to define the direction of the applied magnetic field. The  $z$ -axis is parallel to the nitrogen  $2p$ -orbital associated with the unpaired electron.

Time Scale for EPR: If the molecular motions are rapid enough, anisotropic parameters will be averaged and the time scale required for averaging can be estimated by considering the frequency difference ( $\Delta\omega$  in rad/s) between the two parameter values under investigation. Molecular motion is characterized by the rotational correlation time, denoted  $\tau_r$ . This gives the average amount of time it takes for a molecule to rotate by 1 radian (about  $57.3^\circ$ ). We can characterize motion with a rate constant  $1/\tau_r$ . As a general guide, the time scale is “fast” if the  $1/\tau_r \gg \Delta\omega$  and “slow” if  $1/\tau_r \ll \Delta\omega$ .

## 2.2: Spin Labels

The term spin label was introduced by H. M. McConnell in the year 1965 to describe stable free radicals that can be used as reporter groups or probes. Spin labeling has developed into a major field of biochemistry and biophysics. Nitroxides are stable organic free radicals that, when attached to biomolecules or any other organic molecule can serve as EPR reporter groups. They are stable up to about  $80^\circ\text{C}$  and over a pH range of 3-10. Nitroxide spin labels are easily detectable even in micromolar concentrations. Spin labels detect molecular motion, intermolecular collisions, molecular ordering, local geometry, presence of other paramagnetic species and solvent polarity<sup>33</sup>. The nitroxide spin labels used for this research are 4-amino TEMPO and 3-carboxy PROXYL and the structures

are shown in **Figure 2.8**. Different functional groups present on the spin-labels allow us to attach them to different amino acids in a peptide sequence.

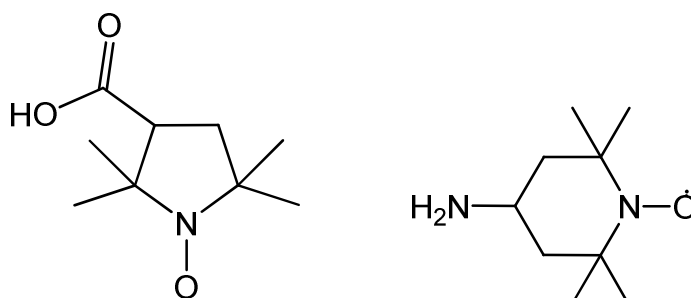


**Figure 2.8:** 3-carboxy PROXYL

4-aminoTEMPO

The NO group is called the nitroxide group and the unpaired electron is present in a molecular orbital formed from the 2p orbitals of nitrogen and oxygen. The ring with the NO group is called the nitroxide ring. The NO free radical is quite stable in both aqueous and organic solutions. The  $^{14}\text{N}$  nucleus has a magnetic moment with  $I = 1$  and is coupled to the moment of the unpaired electron, splitting the EPR spectrum into three resolvable hyperfine lines. When the nitroxide group is tumbling rapidly and isotropically, the motion is fast enough on the EPR time scale to average out the spectral anisotropies and the spectrum consists of three narrow lines of almost equal heights. This high degree of tumbling is observed for spin labels in non-viscous solutions. As the rate of tumbling decreases, the EPR spectrum alters. The effect of motion on the spectrum is characterized by rotational correlation time  $\tau_r$ . Majority of the spin label studies are based on the detection of rotational motion as a means of determining the local flexibility, local ordering, or overall tumbling dynamics in a

biomolecule. The correlation time is directly proportional to molecular volume ( $V$ ) and solution viscosity ( $\eta$ ) and is inversely proportional to temperature ( $T$ ), as described by the Stokes-Einstein relationship:

$$\tau_r = V\eta/kT$$

In the above equation,  $k$  is the Boltzmann's constant. Nitroxide EPR spectra are influenced by the rate of rotational motion relative to the range of electron spin frequencies within each hyperfine line. **Figure 2.9** shows a simulated nitroxide spin label spectra for different  $\tau_r$  values.

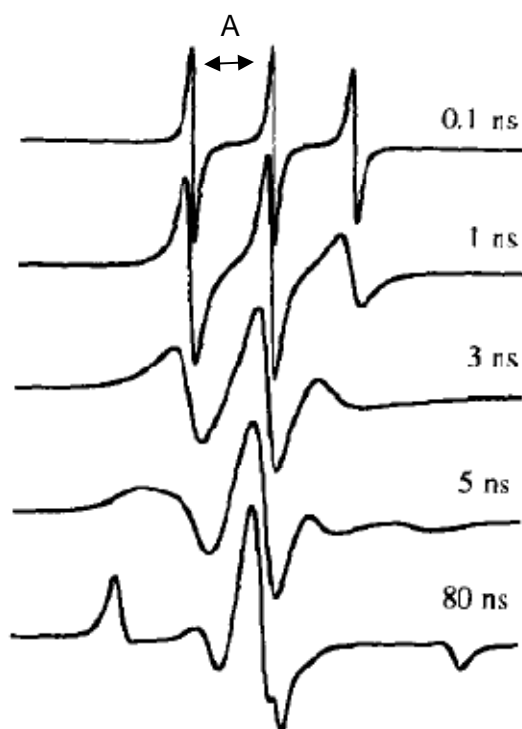


**Figure 2.9:** Simulated nitroxide spin label spectra for different  $\tau_r$  values.<sup>33</sup>

With increase in viscosity, molecular volume and decrease in temperature the hyperfine lines are broadened as depicted in the figure above.

### **2.3: EPR Instrumentation**

An EPR spectrometer mainly consists of the following components: a source of radiation and in majority of the cases the frequency of the radiation emitted from the source is around 9 GHz which falls in the X-band region of the microwaves. The microwave source of radiation is generally termed as a klystron. The microwave power can be incident on the sample either as a continuous wave (cw) or as a pulse. The microwaves are passed on to the sample located in the microwave cavity from the source via attenuator. The static magnetic field  $H$  is created using very strong magnets and must be very stable. The magnetic field is measured by magnetic flux density  $H$  and the recommended unit is tesla (T) ( $1\text{T}=10^4$  gauss). A resonator consisting of a resonant cavity is used to tune the frequency of the radiation emitted from the source. Microwaves reflected back from the cavity are detected by a diode, and the signal comes out as a decrease in current at the detector analogous to absorption of microwaves by the sample. EPR measurements can be carried out either by maintaining constant frequency and varying the magnetic field or vice versa; most commonly the frequency is kept constant. Samples for EPR can be gases, single crystals, solutions, powders, and frozen solutions. For solutions, solvents with high

dielectric constants are not advisable, as they will absorb microwaves. **Figure 2.10** shows the block diagram of a typical EPR spectrometer.

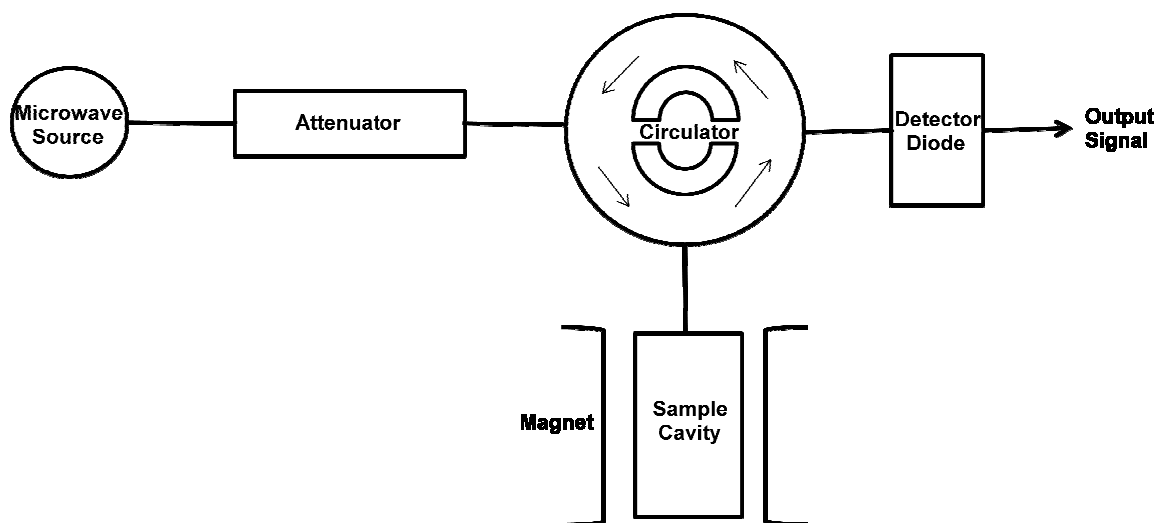


**Figure 2.10:** Block Diagram of a typical Electron Spin Resonance Spectrometer.

All the EPR experiments were carried out using an X-band (9.4 GHz) JEOL-JES-FA100 spectrometer with a  $TE_{102}$  cavity equipped with temperature control (University of North Carolina, Chapel Hill).

## Chapter 3: Materials and Methods

### 3.1: Experimental Design

The objectives of this research are:

- 1) To prepare a molecule capable of anchoring the majority of a PrP peptide sample to a liposome.
- 2) To develop a spin-label based assay in order to determine the percentage of molecules anchored to the liposome surface.

In order to anchor a peptide to a liposome a hydrophobic molecule was attached to the peptide. To determine the amount of peptide anchored to a liposome, a spin-labeled model molecule was used and it was detected using EPR. The EPR spectrum tells us about the motion of the molecule and by using a relaxation agent such as chromium oxalate the position of the spin-labeled molecule on the liposomes can be located. Liposomes mimic the cellular environment and aid in understanding the interactions between the cell membrane and peptide in vitro. The liposomes may consist of a single lipid bilayer (unilamellar) or multiple lipid bilayers (multilamellar). Based on their size, the unilamellar liposomes are divided into three classes: SUVs (small unilamellar vesicles), LUVs (large unilamellar vesicles) and GUVs (giant unilamellar vesicles). The SUVs encompass a wide size range between 25-100 nm. SUVs are a common choice for drug delivery.<sup>34</sup> Also, SUVs show reduced light scattering when compared to large unilamellar vesicles (LUVs).<sup>35</sup>

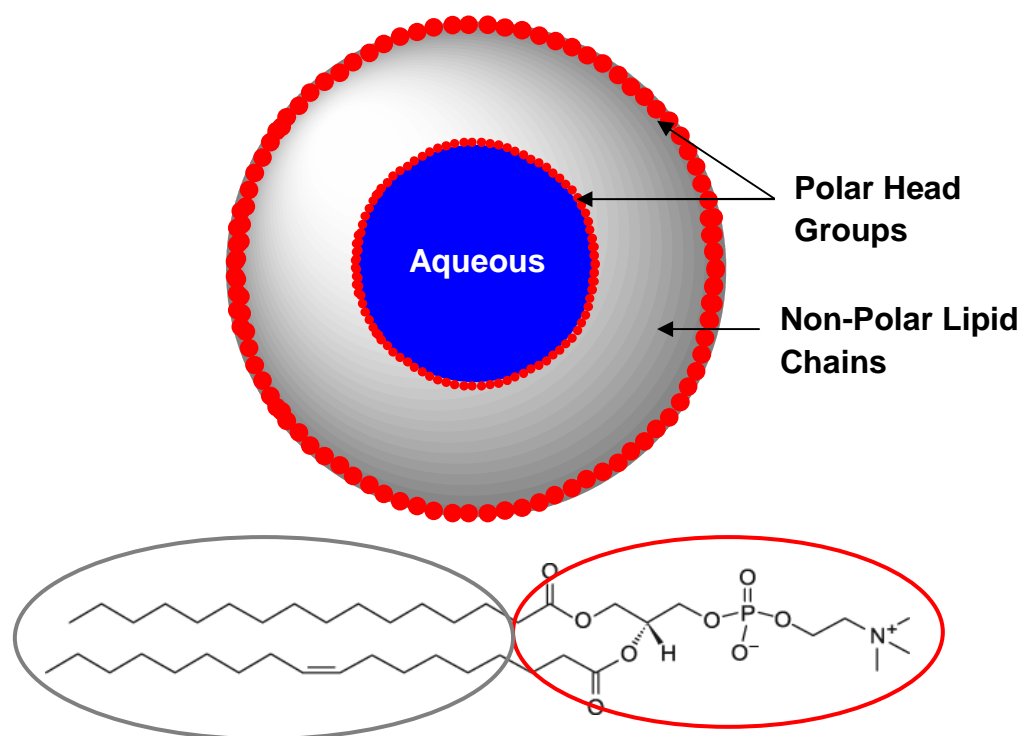


**Figure 3.1:** Structure of a unilamellar palmitoyl-oleyl-sn-glycero phosphatidylcholine (POPC) liposome consisting of polar and non-polar groups. The phosphatidylcholine head groups constitute the polar region and the lipid chains constitute the non-polar region of the liposome.

Lipophilic anchors containing the nitroxide spin-label were synthesized and added to the liposomes. These molecules might behave in different ways:

- 1) Some of the added lipophilic anchor might have the nitroxide portion sticking out into the surrounding aqueous solvent as shown in **Figure 3.2**.

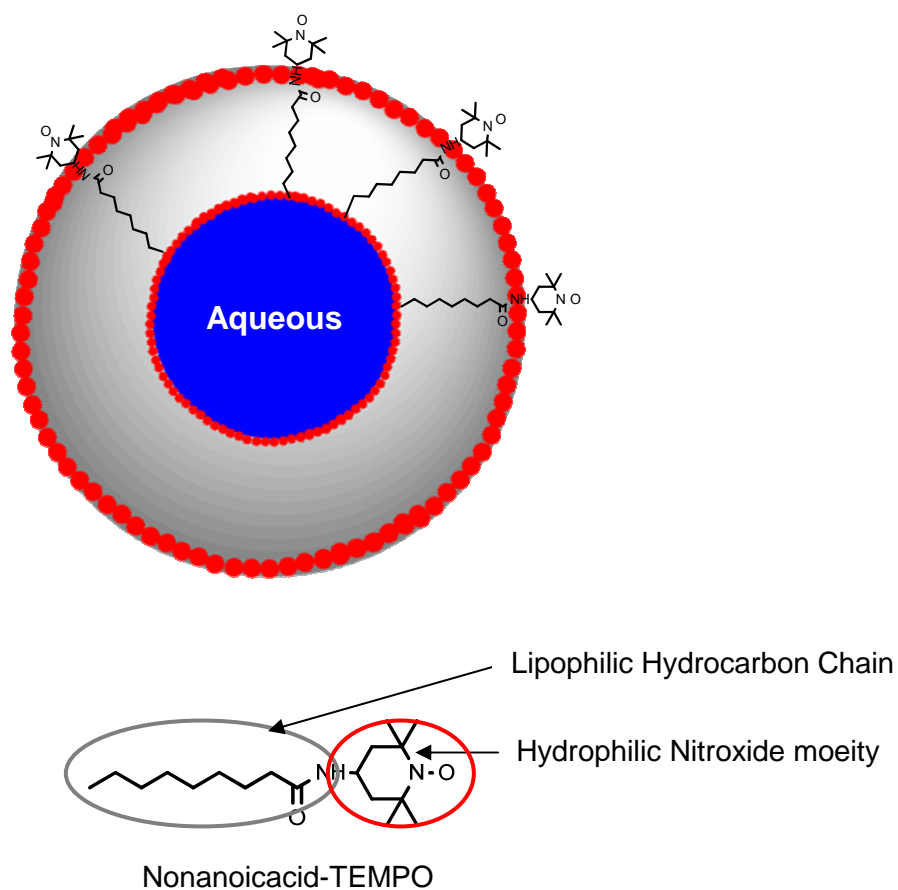


**Figure 3.2:** Illustration of one of the ways by which the spin-labeled lipophilic molecule is anchored to the liposome. The nine carbon lipophilic hydrocarbon chain of Nonanoic acid-TEMPO is inserted into the liposome membrane whereas the hydrophilic nitroxide moiety is sticking out of the membrane.

- 2) Some proportion of added lipophilic anchor sample might completely get inserted into the liposome membrane.
- 3) Or some of anchor might completely stay in the aqueous solution. **Figure 3.3** illustrates both cases 2 and 3.

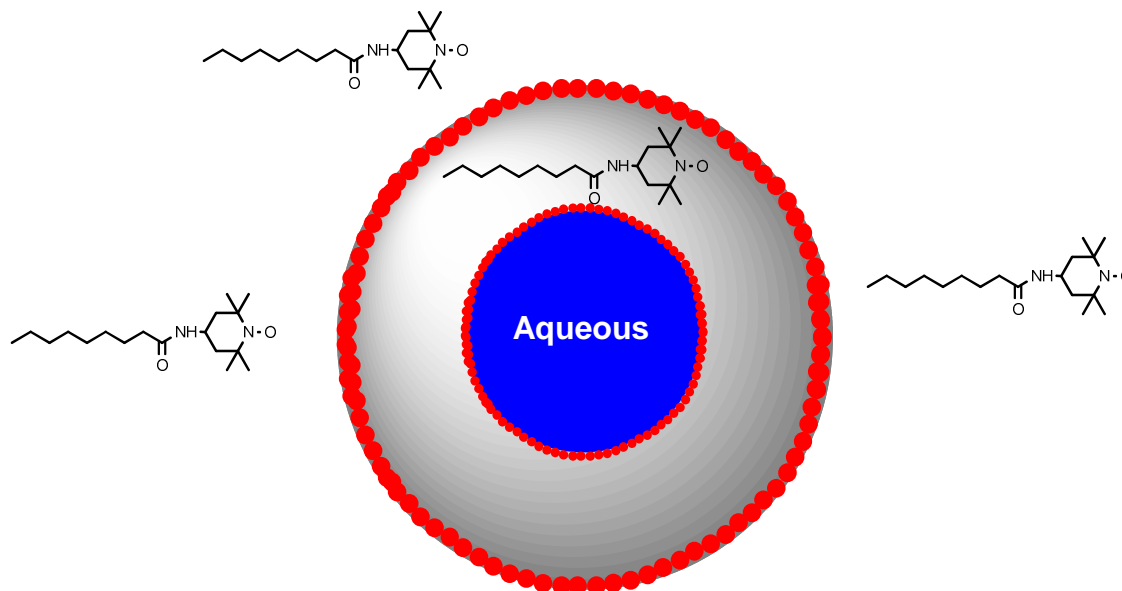


**Figure 3.3:** The lipophilic anchor completely inserts into the liposome or it might completely remain outside the liposome in the aqueous solvent. The lipophilic anchor shown in the figure is Nonanoic acid-TEMPO.

Given the structure of the spin-labeled anchor molecules, options 1 or 2 might dominate. This quenching of the EPR signal by a relaxation agent like chromium oxalate aids in differentiating these situations. The EPR spectrum of the nitroxide is very sensitive to the motion of the spin label and its proximity to other paramagnetic species including other spin-labeled molecules. Based on the concept of change in motion of the free radical due to its environment, we developed an assay to calculate the percentage of the anchored or bound spin label and unbound spin label. Signals of bound and unbound spin labels should be different and can potentially be separated mathematically, provided the signals are distinct, or by using relaxation agents. Although we did observe a difference in the EPR signals of bound versus unbound spin-labeled molecules we were unable to separate the signals mathematically so we relied

on the use of a relaxation agent. **Figure 3.4** shows the hypothetical EPR spectra of bound and unbound spin-labeled molecules.

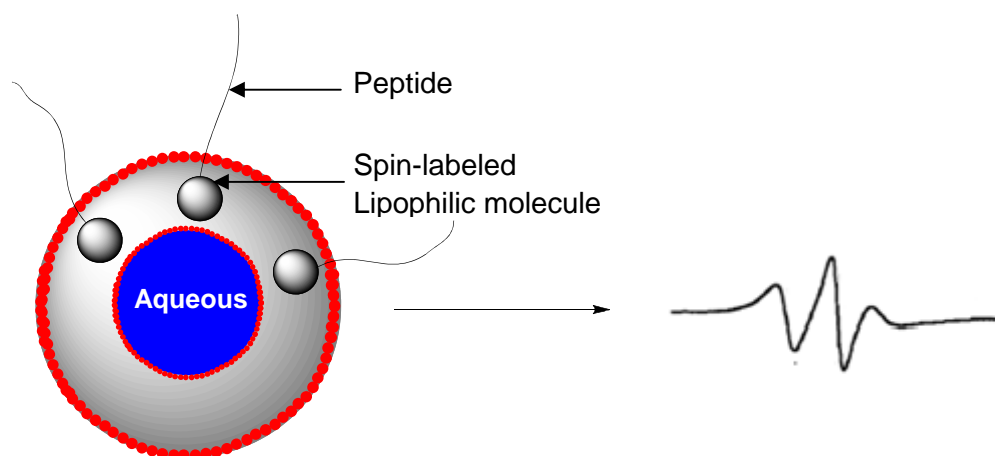


**Figure 3.4:** Hypothetical EPR spectrum of a bound spin-labeled molecule. The peptide is bound to the liposome through the lipophilic anchor and its motion is somewhat restricted so the spin-label will give a characteristic EPR signal for the bound peptide.

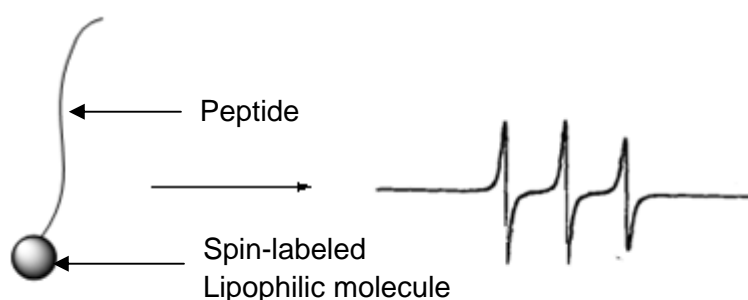


**Figure 3.5:** Hypothetical EPR spectrum of an unbound spin-labeled molecule. The peptide containing the spin-label and the lipophilic molecule is free in solution and gives a characteristic EPR signal which is significantly different from the bound peptide.

The relaxation agent interacts with the unbound spin-labeled molecule in a bimolecular collision and leads to broadening of the EPR signal; thus allowing the separation of the bound signal from the unbound signal of the lipophilic anchor provided the spin-label is shielded from the solvent and a water soluble relaxation agent is used. The integral of the EPR signal of the bound spin-label provides a measure of the amount of the lipophilic molecule anchored to the liposome. The lipophilic molecule was attached to the peptide model and quantitative experiments were carried out in the same manner as mentioned above.

### **3.2: Synthesis and Purification of the Spin-labeled Anchors**

The spin-labeled molecules were synthesized using an amide coupling reaction between a carboxylic acid and an amine. 1.6 mmol of carboxylic acid was dissolved in dichloromethane. To this solution 1.5 equivalents of 4-amino-TEMPO, 1.1 equivalents of diisopropylcarbodiimide (DIC) and 4 equivalents of diisopropylethylamine (DIPEA) were added and the reaction mixture was kept stirring overnight to ensure the completion of the reaction. The carboxylic acid was activated using DIC which is a coupling reagent. It improves the reaction by generating a reactive species with the free carboxylic acid. This reactive species reacts with the free amine to form an amide bond under room temperature conditions. A base like diisopropylethylamine is added to the reaction mixture to insure the amine group of 4-amino-TEMPO

does not get protonated and thus aids in the coupling reaction with the acid. **Figure 3.6** shows the reaction scheme for general method of synthesis of the anchor molecules.

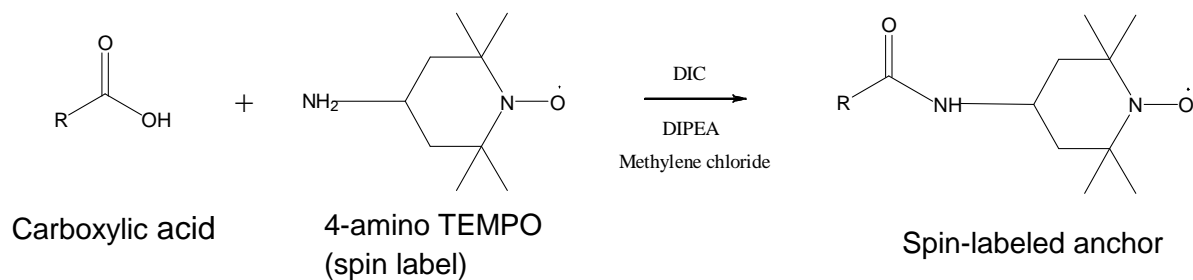


**Figure 3.6:** Reaction scheme for the general method of synthesis of the anchor molecules using amide coupling reaction.

Three different lipophilic molecules, and one hydrophilic molecule, each containing a spin-label were synthesized and tested for their ability to anchor to the POPC liposomes. The hydrophilic molecule serves as a control acting as a water-soluble non-anchoring species. **Figure 3.7** shows the structures of all the four molecules.

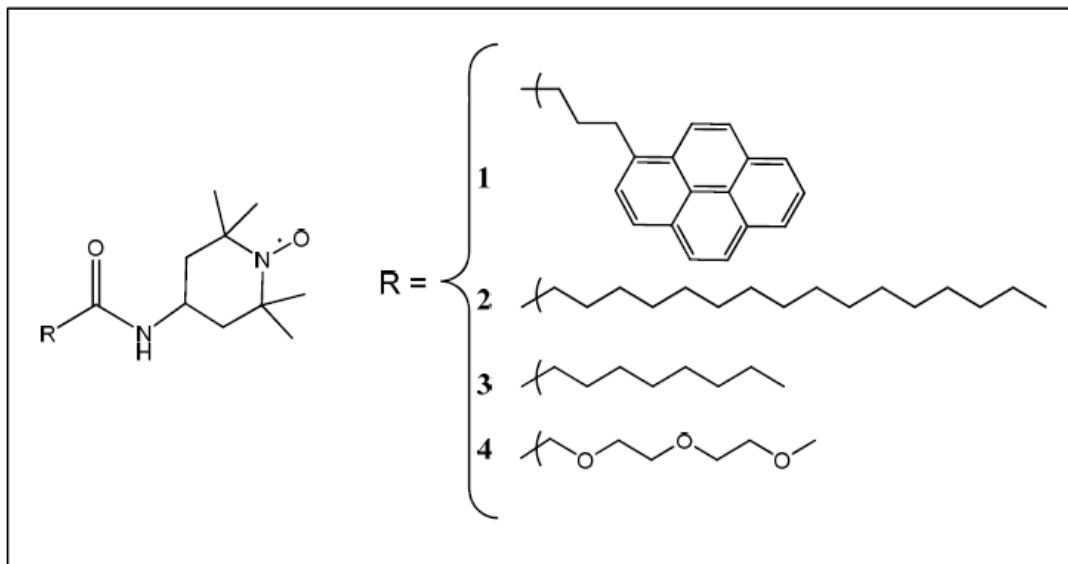
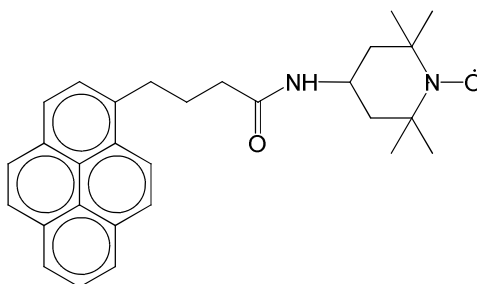


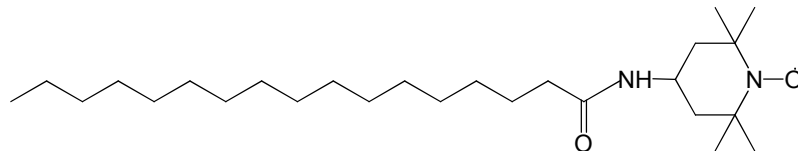
**Figure 3.7:** Lipophilic molecules (1-3) and a hydrophilic molecule (4) were coupled to the spin label 4-amino-TEMPO via an amide bond. Molecule 4 serves as control for 3, as they are essentially isosteric.

A brief description about each of these four molecules is given below:

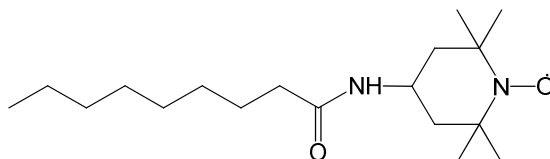
1. Pyrene-TEMPO (PT): Pyrene had been used with some success as an anchoring molecule to liposomes. It has an added advantage of acting as a fluorophore which gives us an opportunity to perform fluorescence experiments to further corroborate our results.



Molecular weight: 441.26 g/mol

2. Heptadecanoicacid-TEMPO (HDT):

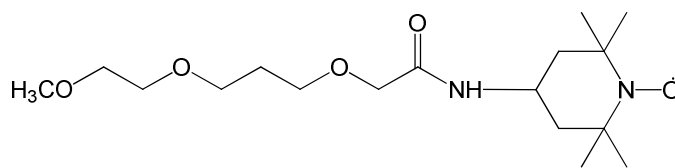
Molecular weight: 423.76 g/mol

3. Nonanoicacid-TEMPO (NAT):

Molecular weight: 311.46 g/mol

The presence of long hydrocarbon chains imparts a considerable amount of lipophilicity to the anchors HDT and NAT.

4. 2-[2-(2-methoxyethoxy) ethoxy] acetic acid-TEMPO (EMEAT): The polar oxygen containing chain and TEMPO render EMEAT very polar. Its size and shape are similar to NAT and thus will give an EPR spectrum for a completely unanchored molecule. Unlike NAT, EMEAT is soluble in water. It can be used to perform control experiments as it similar in size as NAT in terms of chain length which gives us a chance to compare the results of NAT and EMEAT.



Molecular weight: 331.45 g/mol
--------------------------------

The synthesized spin-labeled molecules were purified using different techniques:

Solvent Extraction: Also known as liquid-liquid extraction was used to separate the compounds based on their relative solubility in different immiscible solvents. The solvent system of choice for extracting the spin-labeled molecules was water/methylene chloride ( $\text{CH}_2\text{Cl}_2$ ). To rid the organic solution of the excess 4-amino-TEMPO a wash with dilute hydrochloric acid solution was also performed. 4-amino-TEMPO being polar was extracted into the water layer and the lipophilic anchor molecule was extracted into the methylene chloride layer. Any unreacted carboxylic acid (refer **Figure 3.6**) with a lipophilic side chain will also enter the methylene chloride layer. All the three lipophilic anchors (NAT, HDT, and PT) were extracted using the water/methylene chloride solvent system. The methylene chloride fraction was collected and the solvent was evaporated using a rotation evaporator leaving a solid residue behind. The compounds were further analyzed qualitatively and quantitatively using HPLC. Unlike the lipophilic anchors, EMEAT was comparatively less lipophilic in nature due to the presence of polar oxygen groups. Hence the solvents used for the extraction of EMEAT were ethyl acetate/water. Ethyl acetate being a comparatively more polar solvent than methylene chloride extracts the EMEAT molecule leaving the 4-amino-TEMPO in the water layer. The unreacted

carboxylic acid (2-[2-(2-methoxyethoxy) ethoxy] acetic acid) was extracted along with the target molecule. The percentage yields of the extracted compounds were determined at this stage. **Figure 3.8** shows the diagrammatic representation of the extraction technique.

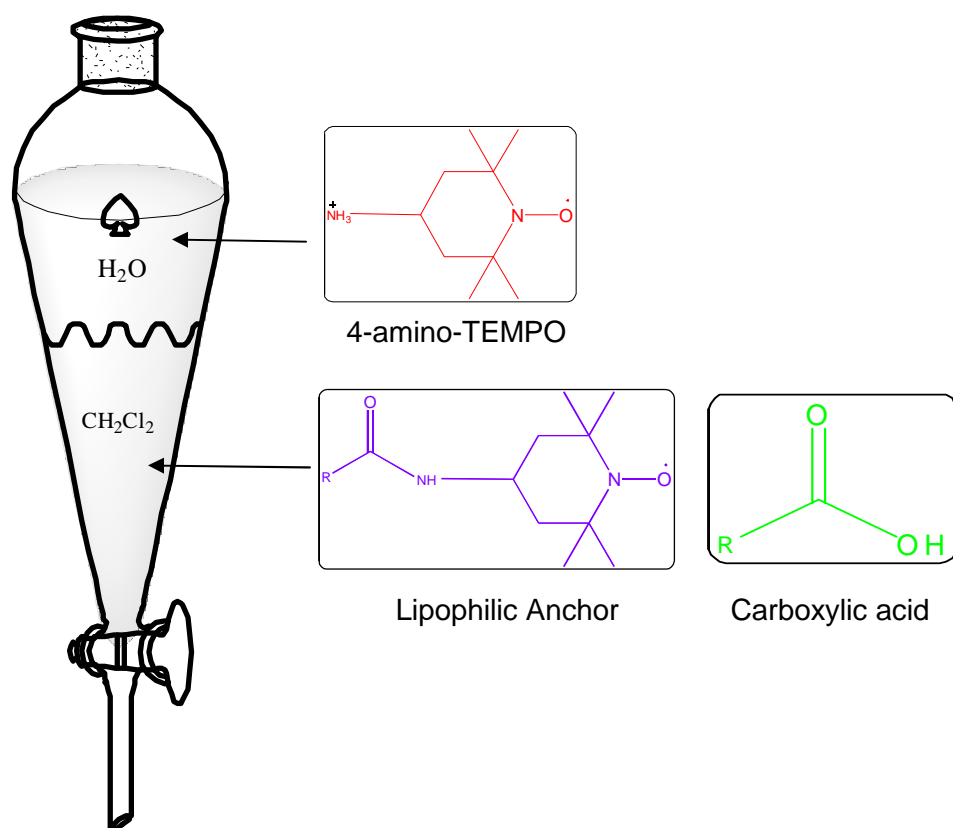


**Figure 3.8:** Pictorial representation of the extraction technique used to purify the lipophilic anchors and EMEAT.

The percentage yields of the synthesized anchor molecules are shown in **Table 3.1**. From the table it is evident that the percentage yields are low but considering the fact

that the amount of spin-label required for the EPR experiments was in the order of few milligrams, the values were not a matter of concern.

Compound	Percent yield (%)
Pyrene-TEMPO (PT)	45.3
Heptadecanoic acid- TEMPO (HDT)	51.2
Nonanoic acid-TEMPO (NAT)	14.8
2-[2-(2methoxyethoxy)ethoxy] acetic acid-TEMPO (EMEAT)	42.3

**Table 3.1:** Percentage yields of the synthesized anchor molecules.

Column Chromatography: It is a method used to purify individual chemical compounds from a mixture. EMEAT was further purified using a preparative silica gel column. The EMEAT was dissolved in 3-4 mL of ethyl acetate and eluted using a gradient flow of ethyl acetate and methanol. Initially 100% ethyl acetate was run through the column followed by an increase in the percentage of methanol. Methanol being a more polar solvent than ethyl acetate is expected to contain the eluted compound. The methanol fractions were collected and the solvent was evaporated using a rotation evaporator. The product was analyzed by normal phase HPLC using a silica gel column.

High Performance Liquid Chromatography (HPLC): To ensure the purity of the synthesized anchor molecules, the compounds were purified and analyzed by more than one technique. HPLC was used for the analysis of the purified compounds. A Vydac C-18 column was used for RPLC (reverse phase liquid chromatography) whereas a Microsorb-MV silica gel column was used for NPLC (normal phase liquid chromatography) runs. The HPLC data obtained was analyzed using Bio-rad software and HPLC grade solvents were obtained from Sigma-Aldrich. The lipophilic anchors were run on a reverse phase C-18 column by gradient elution using reverse phase solvents water and acetonitrile (ACN). A predetermined amount of the lipophilic anchor was dissolved in 1-2 mL of ACN making up the concentration of the anchor molecule to 2 mM. The sample was detected using a UV-Visible detector at 214 nm and 240 nm which are the absorption maxima for amide bond and TEMPO molecule respectively. For PT the absorption maxima of pyrene at 345 nm and amide bond at 214 nm were used. **Figure 3.9** shows the representative HPLC spectra of one of the anchor molecules, HDT.

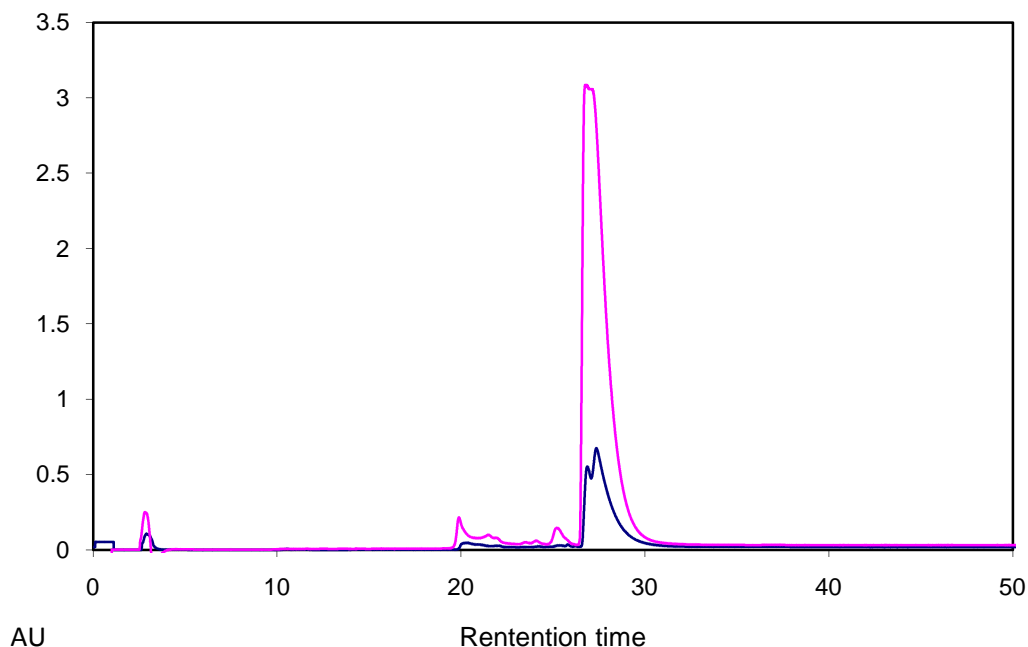


**Figure 3.9:** Representative HPLC Spectra for spin-labeled molecule HDT. The retention time of the molecule was 28 min.

A comparison of the retention times of both the lipophilic anchor and its corresponding carboxylic acid gives us an idea about the purity of the anchor molecule. It also rules out the possibility of the presence of any unreacted carboxylic acid in the final yield. PBA is a carboxylic acid containing a pyrene fluorophore. The absorption maxima of pyrene at 345 nm can be used to detect the signal in HPLC. The retention times of PBA and PT on a reverse phase C-18 column were found to be different from each other. The retention time of PBA was 4.5 min whereas the retention time of PT was found to be 6 min. From the data obtained it is evident that the synthesized anchor molecule, PT is pure and does not contain any unreacted carboxylic acid.

Normal phase silica gel column was used for the qualitative analysis of EMEAT. The sample was eluted by isocratic flow of solvents 70% Methanol and 30% ethyl acetate.

The solvents were decided based on the TLC (thin-layer chromatography) runs. The EMEAT sample was prepared by dissolving a predetermined amount of the compound in methanol such that the final concentration of the sample was 2 mM. The purified compounds were characterized by mass spectrometry and proton NMR.

### 3.3 Characterization of the Anchor Molecules:

The anchor molecules were characterized using mass spectrometry and Proton NMR. ESI-MS is a soft-ionization technique that typically does not fragment molecules during the ionization process. The ions are desolvated by the pressure and the heat of the nitrogen gas i.e. source temperature. The samples were injected into the ESI-MS with a KD scientific syringe pump at 250  $\mu\text{L/hr}$ , and the electric potential used to start ESI was 2600 V. The source temperature was 50<sup>0</sup>C and the nebulizer pressure was set at 25 psi. The source conditions were adjusted to give maximum signal to noise ratio. All the molecules were characterized in the positive ion mode due to the presence of the protonation site on the nitroxide free radical. The samples collected from HPLC runs were used to characterize by ESI-MS. The mass spectrum of one of the anchor molecules, HDT is shown in **Figure 3.10**.

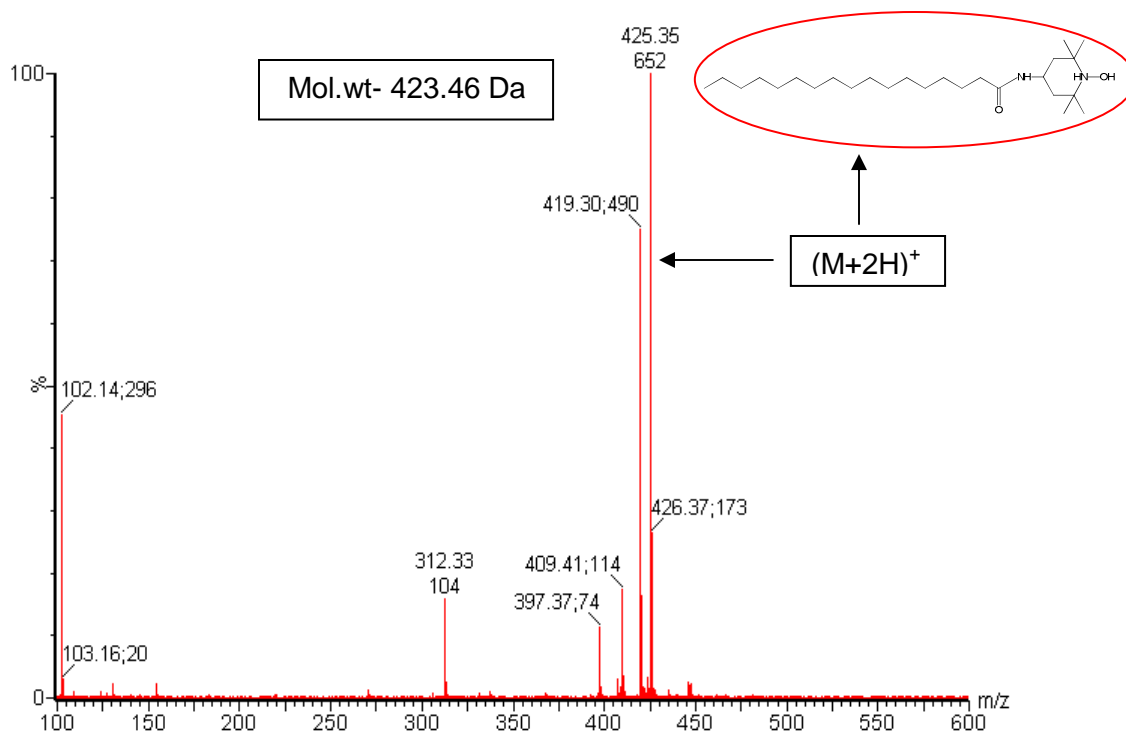


**Figure 3.10:** Representative ESI-MS spectrum of one of the lipophilic anchors, HDT. The molecular weight of the compound was 423.46 Da. A common observation of the mass spectra of the spin-labeled anchor molecules was the presence of  $(M+2H)^+$  peak. The possible structure of the ion which corresponds to that m/z value is shown in the figure (circled compound).

The mass spectra of the anchor molecules revealed interesting chemistry of the nitroxide spin-label i.e. the presence of  $(M+2H)^+$  peak in the mass spectra. The m/z value of 409 corresponds to the fragment produced as a result of loss of oxygen. But, from the ESI-MS data it was evident that the spin-labeled lipophilic anchors were synthesized and purified successfully although the data did show the presence of certain unknown peaks. Some of the peaks appear to be fragments and some might be the impurities in the solvent or samples used. After obtaining the data from mass

spectra which reassured the success of synthesis of the anchor molecules, they were used to test their ability to anchor to the liposomes using EPR. The plausible explanation for the  $(M+2H)^+$  peak is a disproportionation reaction between the nitroxide spin-labels which is shown in **Figure 3.11**.

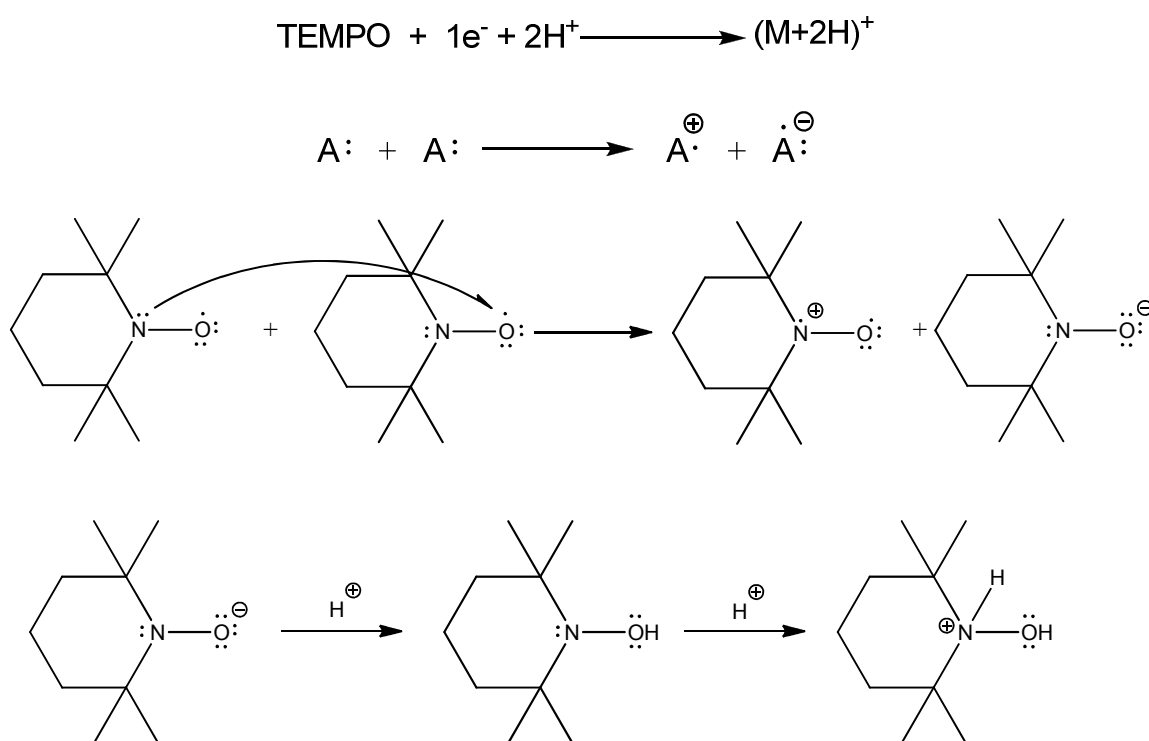


**Figure 3.11:** Schematic representation of the mechanism involved in disproportionation reaction between two spin-labeled nitroxide molecules. (A) represents the nitroxide radical.

To further ensure the identity of the lipophilic anchors proton NMR spectra were obtained for the molecules. Proton NMR gives us an idea about the environment of a

proton and types of protons present in a molecule. A Varian-300 MHz instrument was used to run the NMR samples and spin works software was used to analyze the data.

**Figure 3.12** shows the NMR spectrum of HDT.

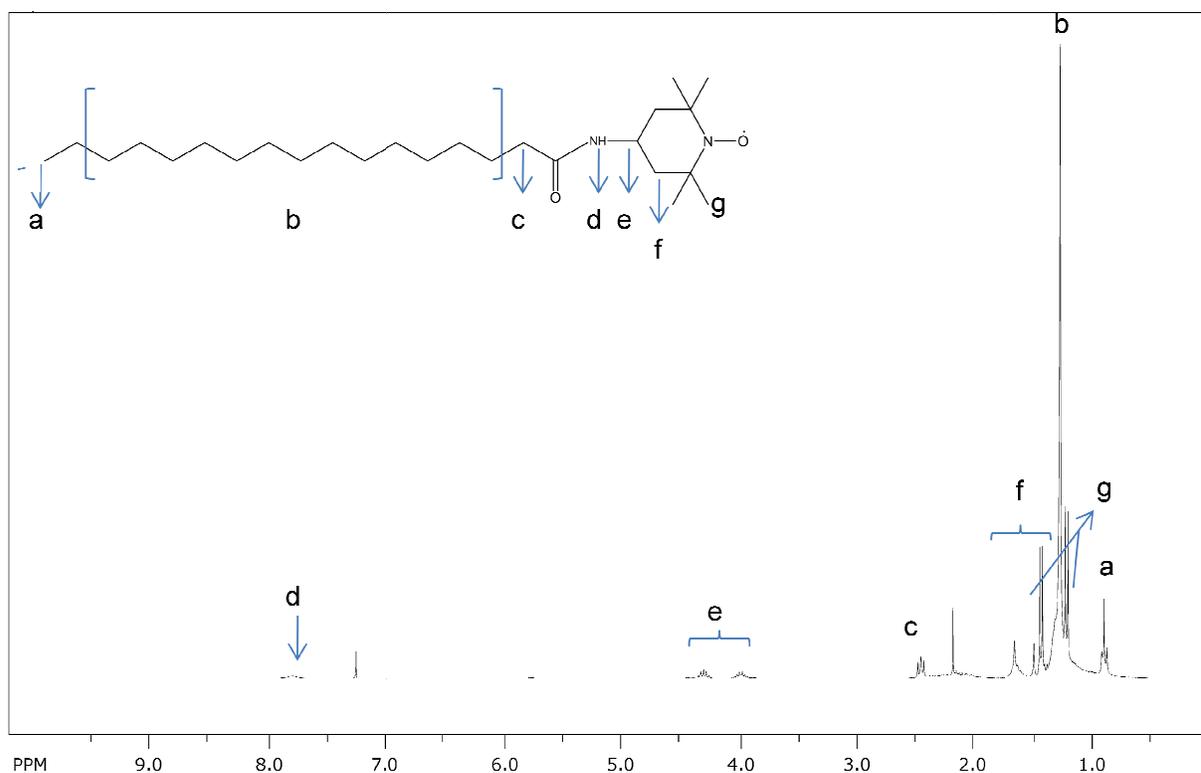


**Figure 3.12:** Representative Proton NMR spectrum of HDT. The assigned peaks represent the protons corresponding to the structure of the compound.

The peaks corresponding to proton g are indicated on either side of peak corresponding to proton b. Two peaks are assigned as e, where there is only a single e proton. This might be due to the different conformations attained by the molecule.

As mentioned earlier, nitroxide is a free radical and relaxes the protons which lead to broadening. This obscures the splitting and causes integrals to be unreliable. **Figure 3.13** shows the expanded portion of the NMR spectrum with peaks corresponding to proton e.

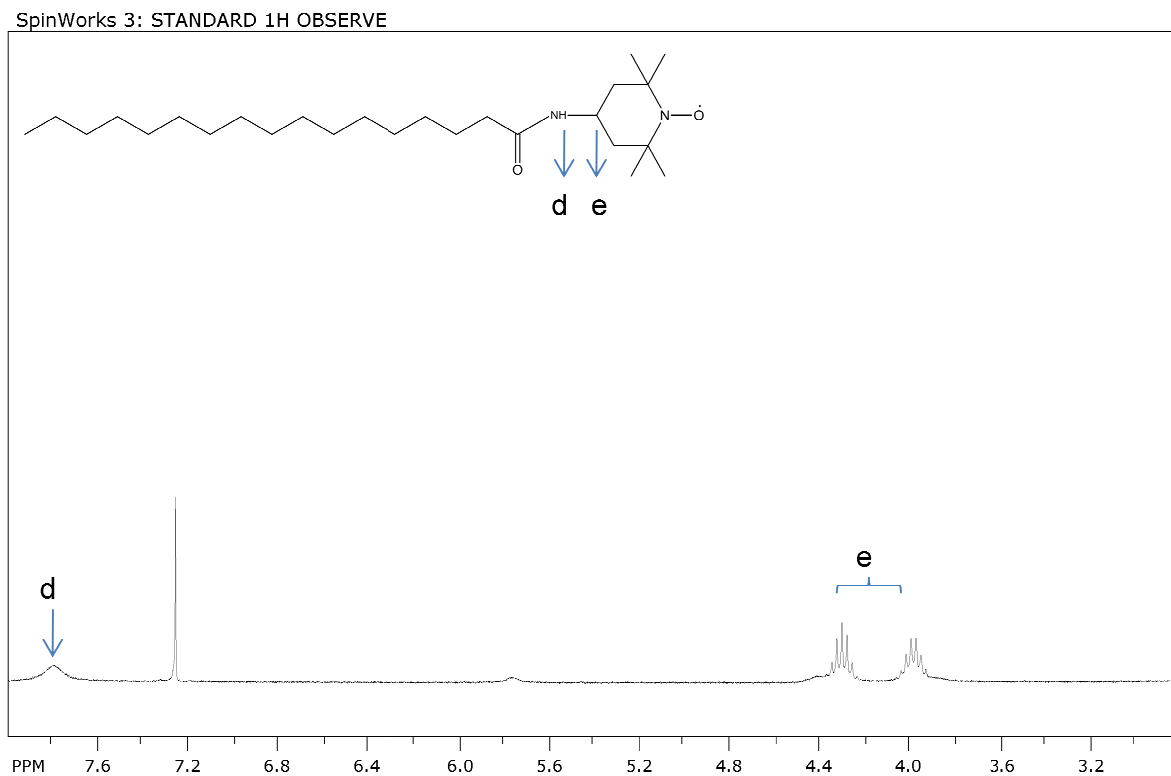


**Figure 3.13:** Expanded version of the Proton NMR spectrum of HDT in deuterated chloroform ( $\text{CDCl}_3$ ) for proton e.

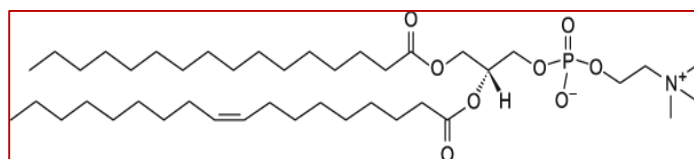
The proton NMR data and the ESI-MS data clearly showed the presence of the lipophilic anchor molecules and also revealed some interesting chemistry exhibited by the nitroxide spin-label. The synthesized anchors were further used for EPR

experiments to test their ability to anchor to the liposomes (data regarding the characterization of the other three molecules can be found in the appendix).

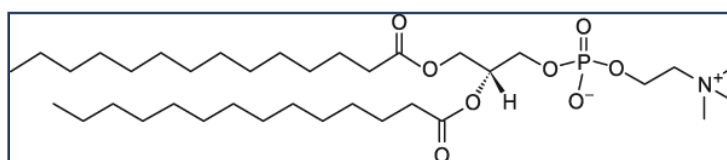
## Chapter 4: Liposomes

### 4.1: Preparation of Liposomes

Liposomes mimic the cellular environment and aid in understanding the interactions between the cell membrane and peptides *in vitro*. They serve as model membranes for the lipophilic anchors. Liposomes can be prepared using several techniques like sonication, extrusion etc. Single unilamellar vesicles (SUVs) were prepared by extrusion through polycarbonate membranes and filters. Extrusion can be used to prepare all lipid vesicles regardless of their composition although the properties of the lipid formulation might be affected by the composition. Neutral Glycerophospholipids, POPC (1-palmitoyl-2-oleoyl-*sn*-glycero-3-phosphocholine) and DMPC (1,2-dimyristoyl-*sn*-glycero-3-phosphocholine) used to prepare the SUVs were obtained from Avanti Polar Lipids Inc. The structures of these lipids are shown in **Figure 4.1**.



(a)



(b)

**Figure 4.1:** (a) Structure of POPC; (b) Structure of DMPC. Both contain a polar head group and a non-polar acyl lipid chain.

Extrusion is a technique in which a lipid suspension is forced through a polycarbonate filter with a defined pore size to yield particles having a diameter close to the pore size of the filter used. Extrusion must be done above the phase transition temperature ( $T_m$ ) of the lipid to avoid clogging of the pores by rigid membranes.<sup>36</sup> A predetermined amount of POPC was weighed, the amount depending on the specific experiment, and hydrated in Bistris buffer (pH-7.4) for 30 minutes giving a total lipid concentration of 35mM. SUVs for EPR and fluorescence studies were prepared by extrusion using a Mini-extruder (Avanti Polar Lipids Inc.). The solution was passed through a 100 nm polycarbonate membrane 21 times to ensure uniform size distribution of the vesicles. POPC liposomes were hydrated and extruded at room temperature which is above the phase transition temperature of the lipid ( $T_m = -2^{\circ}\text{C}$ ) whereas DMPC liposomes were prepared at  $30^{\circ}\text{C}$  as the phase transition temperature of DMPC is  $23^{\circ}\text{C}$ .<sup>37</sup> The preparation of liposomes using this procedure should result in a homogenous population of liposomes with >95% of the particles having a size range of 70-100 nm.<sup>38</sup> POPC liposomes were made fresh for each experiment and used within 48 hours whereas DMPC liposomes were used immediately after preparation. The stability of the liposomes was determined using a calcein leakage assay generally used for peptide studies. The structure of a liposome is shown in **Figure 4.2**.

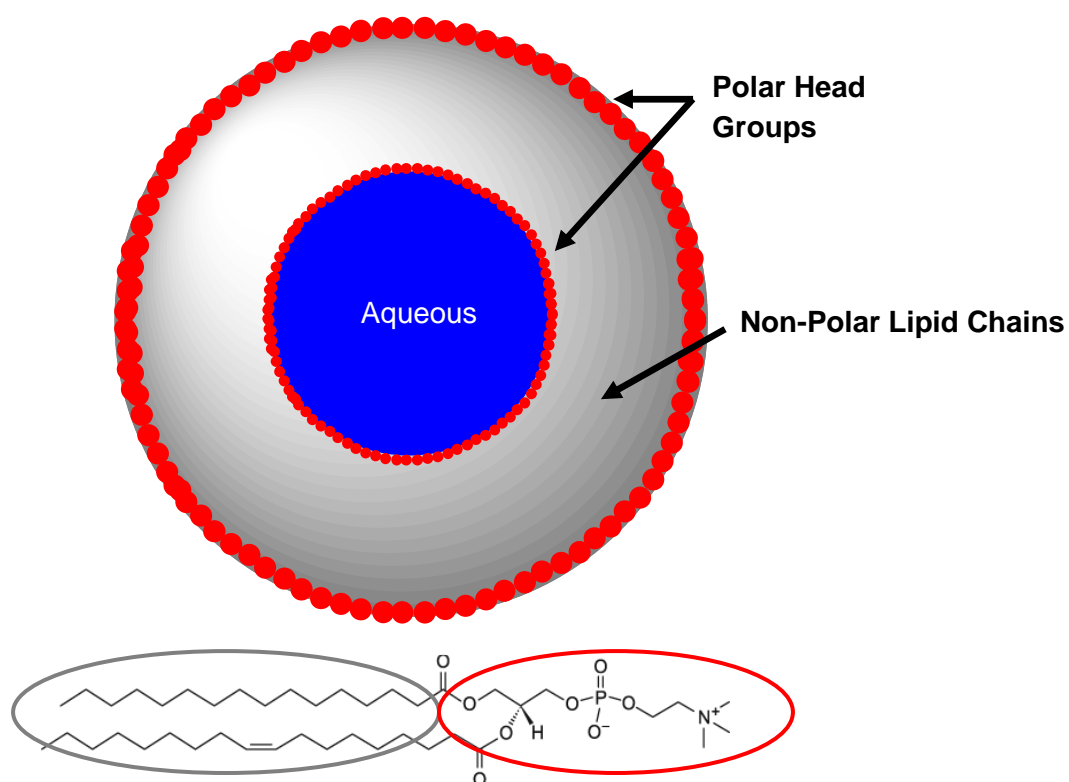


**Figure 4.2:** Structure of a Liposome showing the alignment of the non-polar lipid chains and polar head groups of the lipid in a unilamellar vesicle.

#### 4.2: Fluorescence Instrumentation

Fluorescence involves two processes, absorption and emission. Absorption of energy results in excitation to the singlet excited state upper vibrational level. The molecule in excited state can either lose excess energy as heat and return to the ground state, or undergo spontaneous emission in the form of fluorescence. The stability of the liposomes was determined by monitoring the emission spectra of calcein

which is a fluorophore. The emission spectra were measured using a PTI QM-4CW system with a 75 W xenon arc lamp as and with a spectral band pass of 2 nm.

### 4.3: Dye Release Assay

Molecules that display fluorescence properties are called fluorophores. These fluorophores possess conjugated double bonds containing delocalized electrons. Calcein is a stable, water-soluble fluorophore that can be encapsulated in liposomes. Upon encapsulation and at concentrations above 100 mM calcein fluorescence is self-quenched.<sup>39, 40</sup> Disruption of the vesicles or leakage from the vesicles results in dilution of the fluorophore. Dilution of the encapsulated, self-quenching calcein results in increase of fluorescence intensity. Calcein is also sensitive to pH changes. At pH values below 5 calcein fluorescence is not detectable.<sup>41</sup> The sensitivity of calcein fluorescence to different concentrations and pH values has been widely used in various experiments involving membrane permeability, peptide leakage assays<sup>42</sup>, to monitor vesicle fusion and lysis<sup>43</sup>, to test membrane-stabilizing effect of different synthetic compounds<sup>44</sup> etc. Calcein leakage assay was used to test the stability of the liposomal membranes which played the most important role as membrane models in our research. **Figure 4.3** shows the structure of calcein.

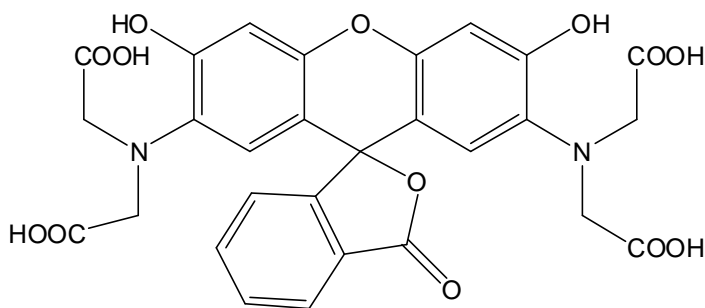


**Figure 4.3:** Structure of Calcein.

Chemical name: 2',7'- [bis(carboxymethyl)amino] fluorescein

Molecular weight: 622.54 g/mol

Addition of a detergent like Triton-X leads to the disruption of the liposomes and a 100% leakage of encapsulated calcein. The apparent percent leakage from the liposomes can be calculated using the following equation:

$$\% \text{ leakage} = [1 - (F_0/F_T)] * 100 \%$$

$F_0$  and  $F_T$  are the initial fluorescence before introduction of the anchor and after the addition of 10% Triton-X, respectively. The fluorescence experiments were carried out to qualitatively analyze the stability of the liposomes and check for their shelf-life so that they could be successfully used for the EPR experiments. **Figure 4.4** shows a pictorial representation of the overall idea of the calcein leakage assay.

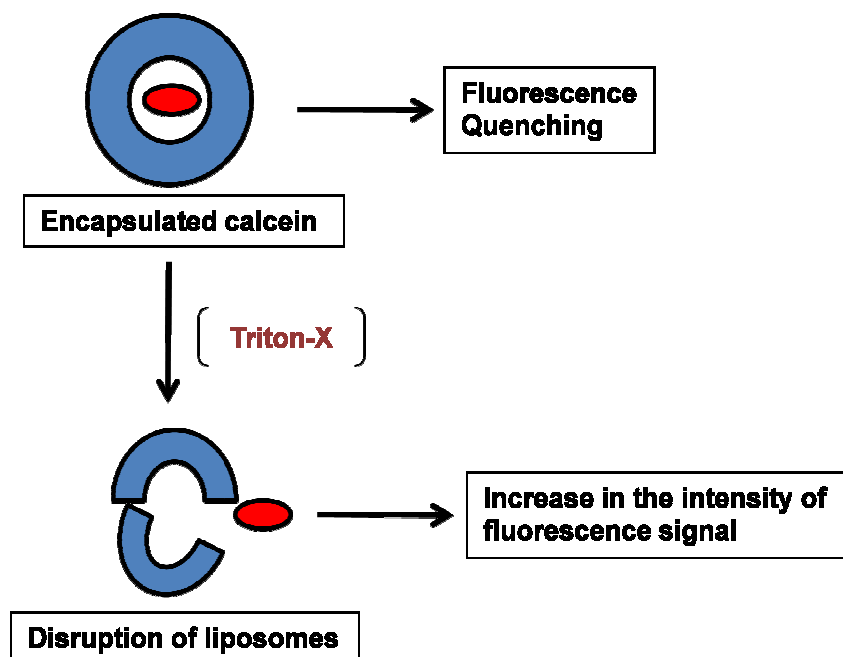


**Figure 4.4:** Pictorial representation of calcein leakage assay. The blue circle depicts the liposome and the red circle depicts the calcein fluorophore.

A defined amount of dried DMPC or POPC were weighed to give a starting concentration of approximately 35 mM and suspended in a calcein-containing buffer. The initial concentration of calcein was 70 mM and the composition of the buffer was 10 mM Bis-Tris, 150 mM NaCl, 1 mM EDTA. The pH of the buffer was adjusted to 7.4 using 1 mM NaOH to ensure the detectability of calcein fluorescence upon dilution. The pH of the buffer was determined using a model Accunet Basic AB 15 pH meter (Fischer Scientific) using a three point calibration. The resulting solution was vortexed for a minute (3 times). Calcein-containing lipid suspension was extruded 21 times through the 0.1 $\mu$ m polycarbonate filters and allowed to sit for minimum of an hour in the refrigerator before using. The unencapsulated calcein was removed by gel filtration or size exclusion chromatography on a Sephadex G-50 column (GE healthcare). The eluent

buffer used for the gel filtration was 10 mM Bis-Tris, 150 mM NaCl , 1 mM EDTA, pH-7.4. The fraction containing the encapsulated calcein was collected and the concentration was determined using a UV-Vis spectrophotometer from the absorption at 495 nm, considering  $\epsilon = 80,000 \text{ M}^{-1} \text{ cm}^{-1}$ .<sup>45</sup> This solution was further diluted so the concentration of the liposomes upon complete lysis would not saturate the fluorescence detector. This concentration was approximately 45  $\mu\text{M}$ . Fluorescence experiments were conducted at an excitation wavelength of 494 nm and an emission wavelength of 512 nm. **Figure 4.5** shows the fluorescence spectra of calcein in DMPC liposomes before and after the addition of Triton X. The fluorescence intensity of calcein was observed to be greater even before the addition of Triton X, that is the intensity decreased after its addition to the encapsulated liposomes. The buffer solution was used as a blank for the experiments. The experiments were performed in triplicate to ensure the reliability of the data. The increased intensity of the calcein in DMPC liposomes clearly pointed out the stability issues with the liposomes. The reason might be attributed to the transition temperature of the DMPC liposomes ( $23^{\circ}\text{C}$ ); due to considerably high transition temperature, the storage of the liposomes was inconvenient. They had to be stored at temperatures above  $25^{\circ}\text{C}$  i.e. slightly above the room temperature and failure to maintain the required conditions of storage could result in disruption of the liposomes which explains the high intensity seen in **Figure 4.5**.

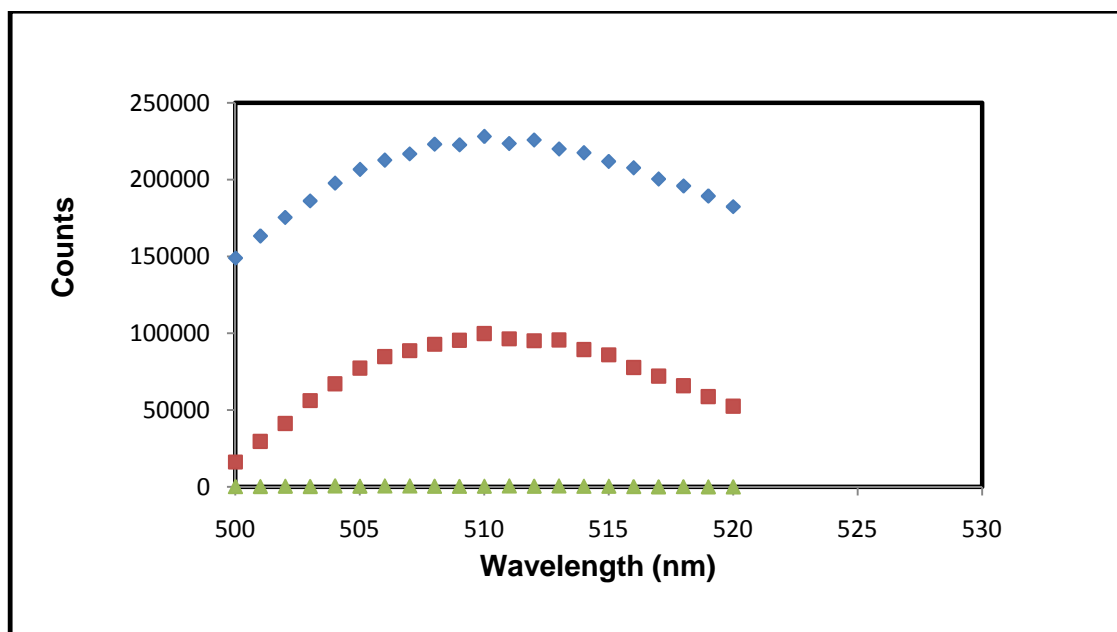


**Figure 4.5:** Fluorescence spectra of calcein encapsulated in DMPC liposomes in the presence (red squares) and absence of (blue diamonds) of Triton X. The fluorescence spectrum of the blank buffer solution (green triangles) is also shown in the figure. The fluorescence intensity is plotted against the emission wavelength of calcein.

The fluorescence spectra of DMPC encapsulated calcein evidently shows that the extruded liposomes were unstable and couldn't be used for further experiments. Hence, DMPC lipid was replaced by POPC which is a neutral phospholipid with a transition temperature of  $-2^{\circ}\text{C}$ . The POPC liposomes were expected to be much more stable due to a very low transition temperature which not only increases the stability but also the shelf-life of the liposomes. **Figure 4.6** shows the fluorescence spectra of the encapsulated calcein in POPC liposomes before and after addition of Triton X.

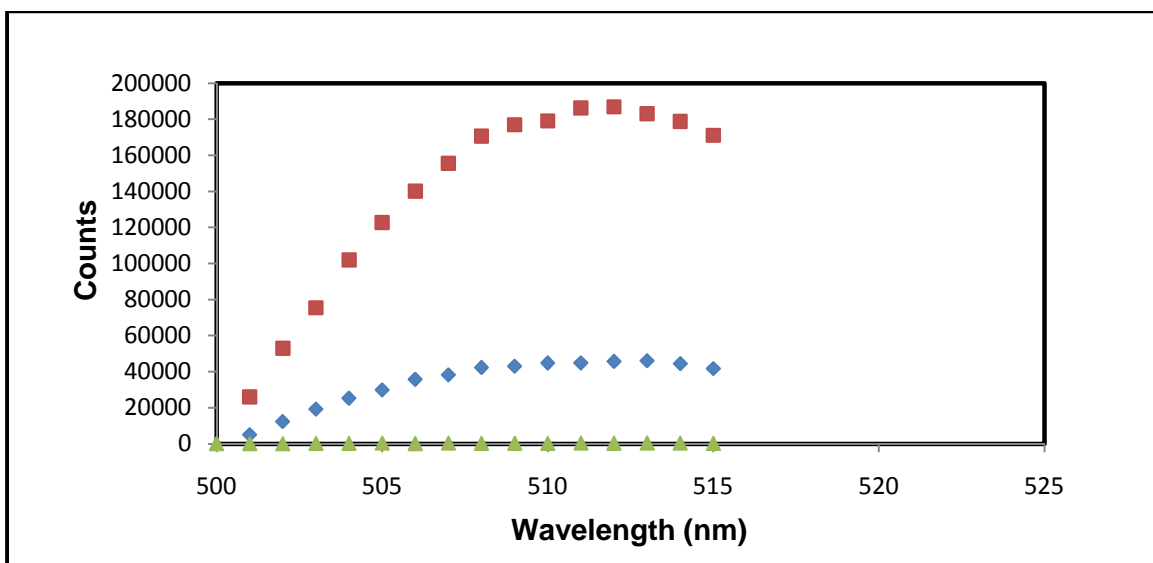


**Figure 4.6:** Fluorescence spectra of encapsulated calcein in POPC liposomes in the presence (red squares) and absence (blue diamonds) of Triton X. The blank spectrum of the buffer solution (green triangles) is also shown in the figure. The fluorescence intensity of the encapsulated dye is increased by several folds upon addition of Triton X.

The fluorescence intensity of encapsulated calcein in POPC liposomes was as expected. Due to quenching of the fluorescence of calcein within the liposomes the intensity is less. Upon addition of Triton X, the liposomes were disrupted and the calcein was diluted which resulted in about five fold increase in the fluorescence intensity. All the experiments were run in triplicate. The data clearly show that the extruded POPC liposomes were stable. EPR experiments involve the addition of lipophilic anchors to the liposomes so the next step was to make sure that addition of these molecules did not lead to disruption of the liposomes. Previously synthesized and purified anchors were added to the liposomes by adding an aliquot of the anchor solution and subsequent

stirring of the liposome (POPC) solution such that the anchor to lipid molar ratio would be 1:100.<sup>46</sup> Fluorescence measurements were obtained immediately. **Figure 4.7** shows the fluorescence spectra of POPC liposomes upon addition of different anchor molecules in the presence and absence of Triton-X used as a reference for 100% disruption.

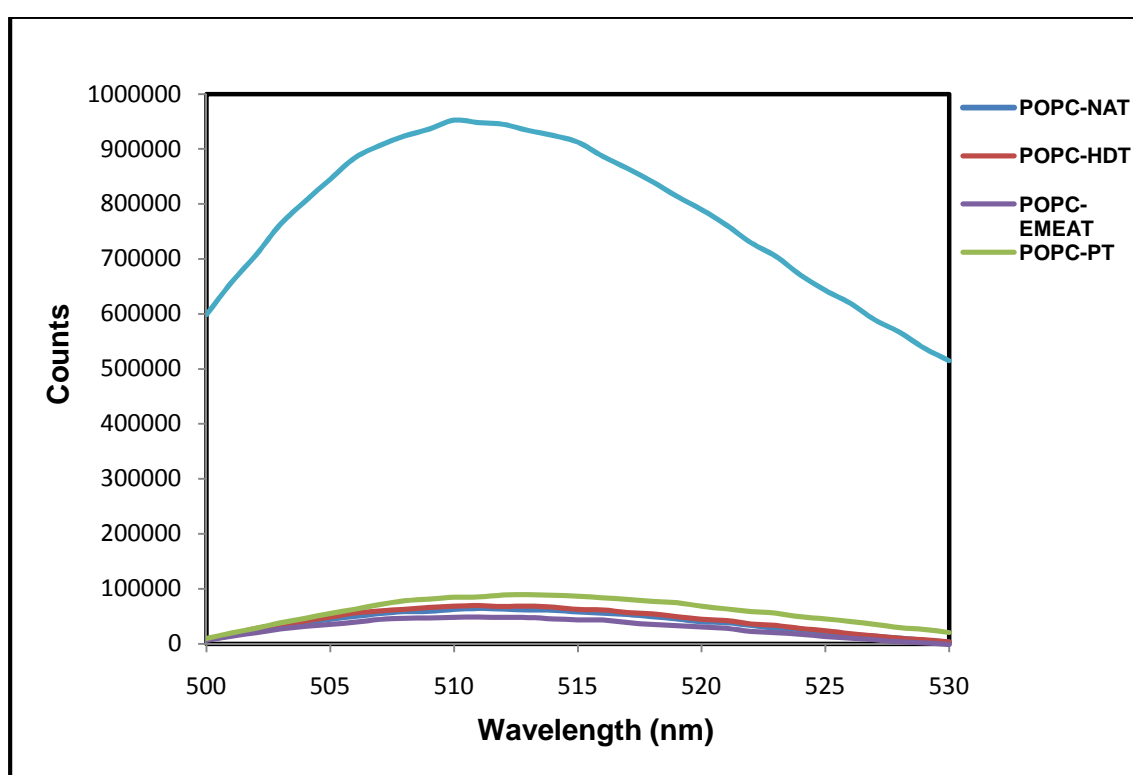


**Figure 4.7:** Fluorescence spectra of encapsulated calcein in POPC liposomes upon addition of anchor molecules. The blue line depicts the spectrum of the encapsulated liposomes after the addition of Triton X. The anchor to liposome ratio was maintained at 1:100.

The spectra shown in **Figure 4.7** prove that the POPC liposomes remain intact even upon addition of the anchor molecules. There is almost 10 fold increase in intensity after the addition of Triton X which results in 100% disruption of the liposomes.

### **Dye Release Assay Conclusions:**

The calcein release assay used to assess the stability of the liposomes proved to be very useful in choosing the right lipid to prepare the liposomes. The data obtained from the addition of the anchor molecules to the encapsulated calcein demonstrate that the POPC liposomes remained intact even upon addition of the lipophilic molecules. These data help in proving the reliability of the qualitative and quantitative results obtained from the EPR experiments.

## **Chapter 5:**

### **Quantification of the Lipophilic Anchors by EPR**

#### **5.1: Control Experiments**

EPR was used to quantitate the amount of lipophilic anchors attached to the liposomes, which act as model membranes, using the spin-label approach. Spin-labels are nitroxide free radicals bearing substituents which endow them with specific properties, most importantly the ability to be detected by EPR. Three of the spin-labels synthesized and purified in the lab possessed lipophilic properties (NAT, HDT, and PT) and one of them was hydrophilic (EMEAT) in nature. Apart from providing evidence of a change in a sample, spin-labels often yield significant information about the molecular basis of the change. Spin-labels can be detected at moderately low levels (micromolar and submicromolar) and have been used to qualitatively characterize the membranes and their components and also to quantitatively measure membrane structure and dynamics.<sup>47</sup> The first sets of EPR experiments were performed to assess the interaction of the anchor molecules with the liposomes. POPC liposomes were prepared by extrusion through the polycarbonate membranes and the final concentration was determined to be 2 mM based on the weight of the dry lipid. Stock solutions of the spin-labeled molecules were prepared and their concentration was determined by EPR. A calibration curve was plotted using known concentrations of a standard spin-label 4-amino TEMPO (4-AT) and the solvent used was kept the same. All the concentrations

were determined based on the values obtained from the calibration curve. The EPR spectrum is a first derivative spectrum of the absorption curve so by integrating the first derivative curve followed by subsequent integration of area under the curve of the absorption spectrum the concentration of the spin-label in the sample can be determined. The behavior of the spin-label changes with a change in the solvent and this is clearly shown in the **Figure 5.1**.

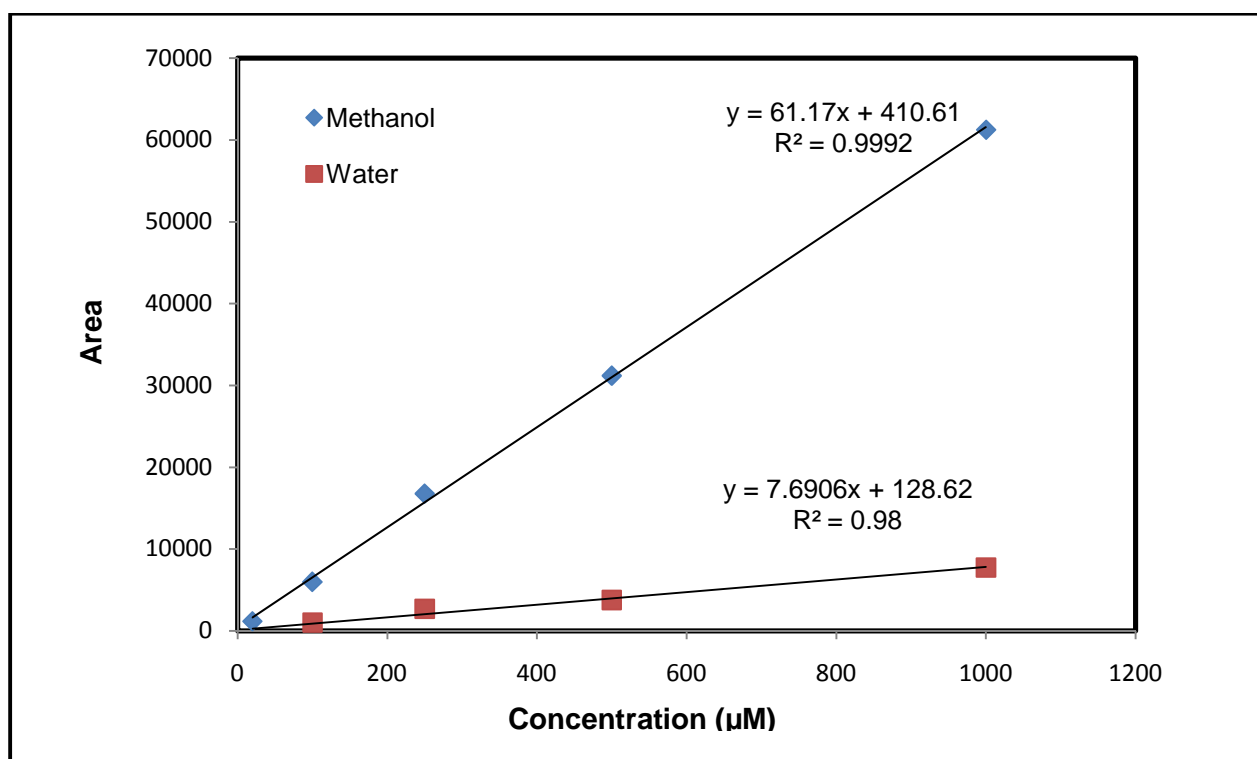
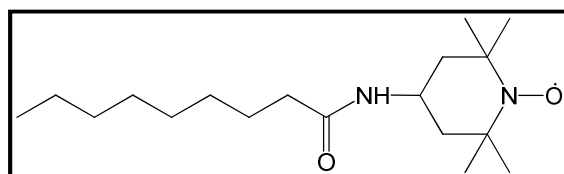
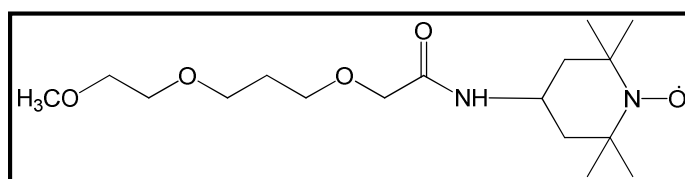


**Figure 5.1:** Calibration curves of 4-AT in water and methanol. The known concentrations of the spin-label molecule are plotted against the area under the curve of the corresponding concentration.

The behavior of the spin-label molecule is different in methanol when compared to water as shown in the figure. This might be attributed to the differences in the dielectric constants of the two solvents which plays a major role in affecting the motion of the spin-label and thus the spectrum. Moreover, a lot more oxygen dissolves in methanol than water and this causes the broadening in the lines we observe. The dielectric constant of water is 80 and methanol is 30. The concentration of the stock solutions were determined by using the calibration curve and subsequently samples were prepared such that the liposome to anchor molecule ratio was close to 100:1. All the anchor solutions were prepared in methanol (Fischer-scientific) and added to the liposomes. **Figure 5.2** shows the EPR spectra of EMEAT vs NAT in Methanol. The structures of EMEAT and NAT are shown below.



Nonanoic acid-TEMPO (NAT)



2-[2-(2-methoxyethoxy) ethoxy] acetic acid-TEMPO (EMEAT)

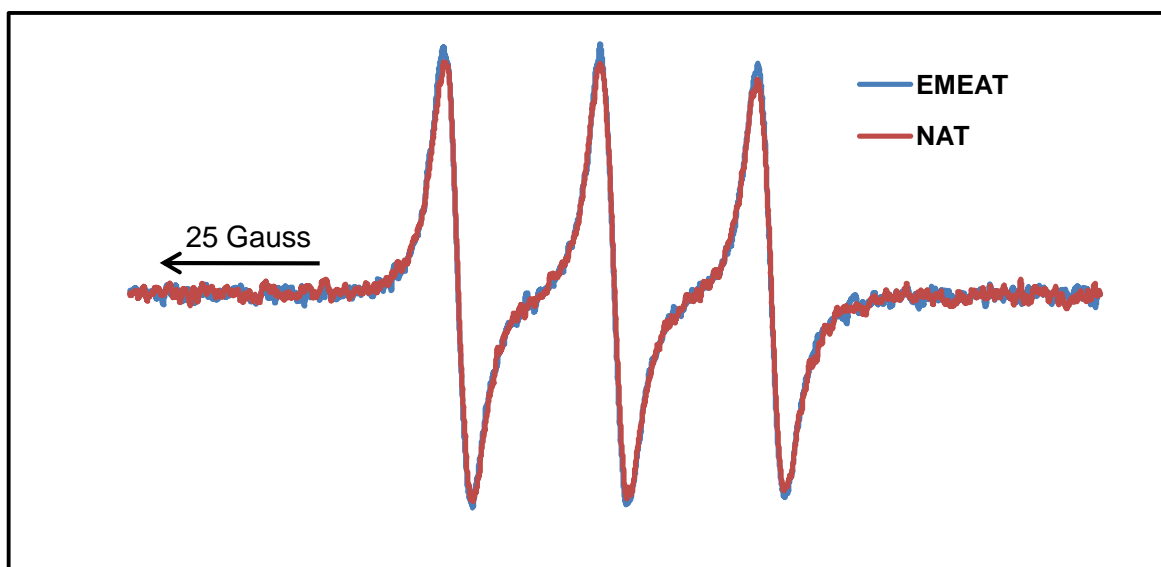


**Figure 5.2:** EPR spectra of EMEAT vs NAT in methanol. Magnetic field (B) is plotted on the x-axis and arbitrary intensity on y-axis. The EPR spectra of both the compounds have been measured for the same concentrations.

EMEAT is a hydrophilic molecule and is similar in size and shape to NAT which makes it a control for NAT. Both EMEAT and NAT have nitroxide spin-label which gives three hyperfine lines in its EPR spectrum. Any change in the line shape suggests the difference in environment or hindrance to the motion of the spin-label. As expected, NAT behaved similar to EMEAT in the solvent methanol. This demonstrates that the EPR spectra of both the molecules are comparable. EMEAT was added to the liposomes after extrusion and was vortexed approximately for one minute. **Figure 5.3** shows the EPR spectra of EMEAT in the presence and absence of liposomes.

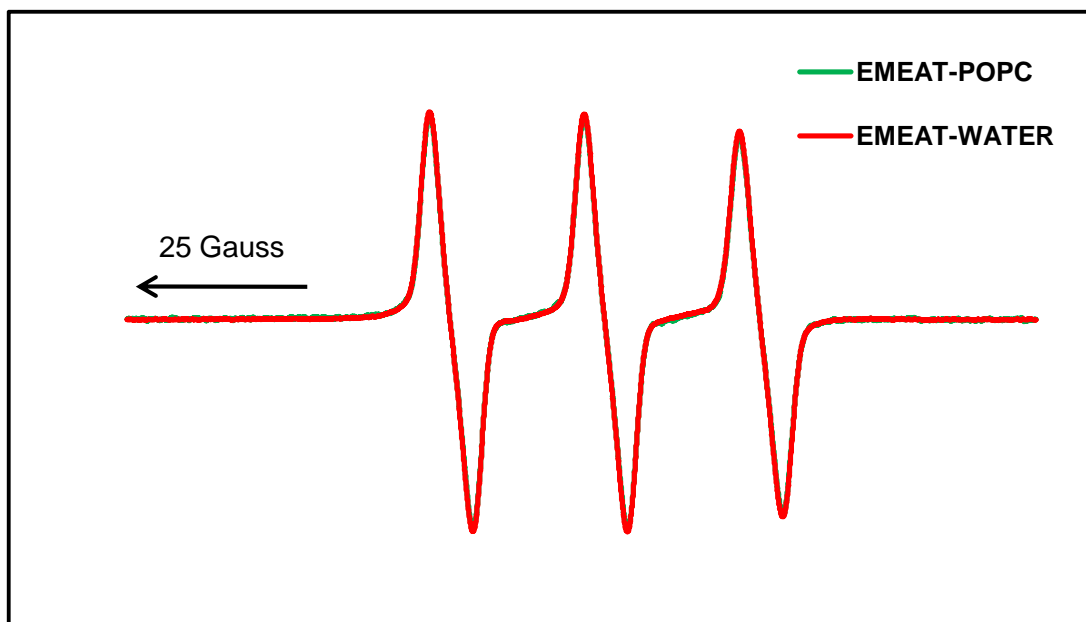


**Figure 5.3:** EPR spectra of EMEAT in the presence and absence of liposomes. EMEAT showed same behavior both in the solvent water as well as in the presence of POPC liposomes. The concentration of EMEAT was the same both in the liposomes and the solvent.

Since EMEAT is hydrophilic in nature, it cannot anchor to the lipophilic acyl chains of the liposome. The line shape and intensity remained the same and this clearly suggests that the behavior of the molecule remains the same both in the solvent as well as the liposomes. Also, this data helped in establishing EMEAT as a control molecule for the experiments. Subsequently, the lipophilic molecules were added to the POPC liposomes and the EPR spectra were obtained. **Figure 5.4** shows the EPR spectra of NAT in the presence and absence of liposomes.

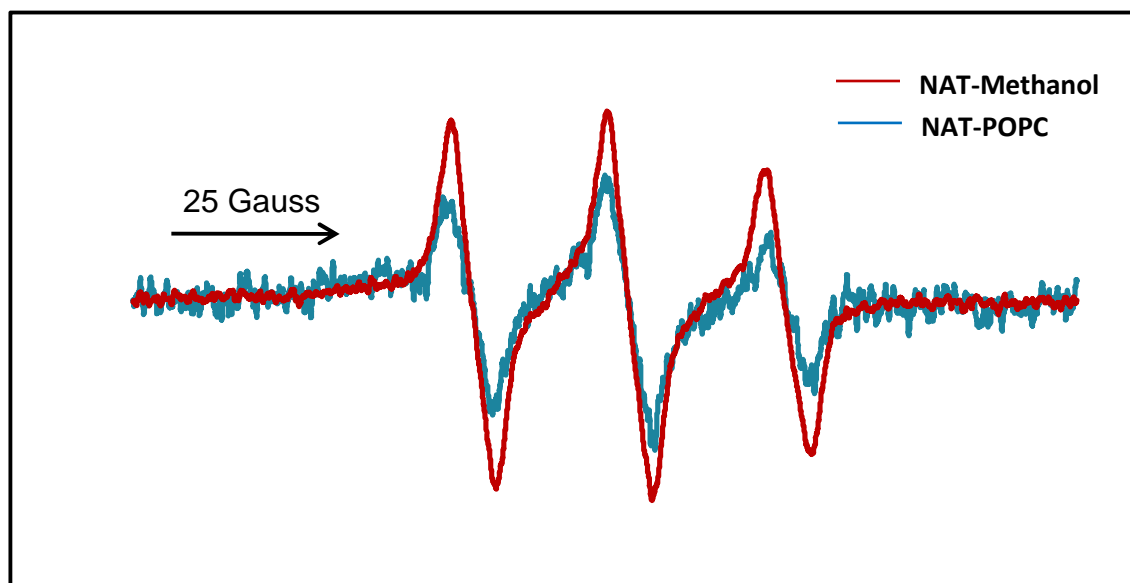
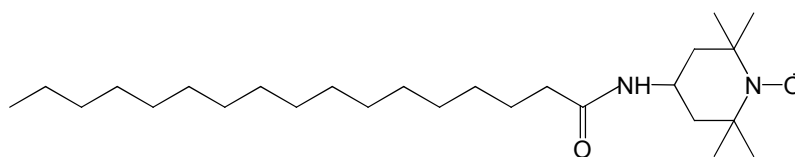


**Figure 5.4:** EPR spectra of NAT in the presence and absence of liposomes. Both the spectra are area normalized. There is a subtle change in the line shape of the hyperfine lines for NAT in liposomes and the signal to noise ratio is a bit low (noisy signal: NAT-POPC).

The behavior of the lipophilic anchor NAT was different in the solvent and the liposomes. This difference not only suggests a change in the environment of the spin-label but also a certain level of hindrance to the motion of the spin-label which is depicted in the line shape of the spectrum for NAT-POPC. In conclusion, the preliminary EPR data suggests that the lipophilic molecules do interact with the POPC liposomes whereas EMEAT does not. Thus EMEAT proved to be a molecule of choice to act as a control for NAT.

## 5.2: Lipophilic Anchors

To determine the efficiency of the lipophilic anchors, they were added to the liposomes and EPR spectra were obtained for all the molecules. The anchors were added to the liposomes in two different ways; (1) In the first method the lipophilic anchors were added to the liposomes after extrusion (2) In the second method the anchors were added to the lipid solution and extruded subsequently. In both the cases the ratio of anchor to lipid was approximately maintained at 1:100. **Figure 5.5** shows the spectra of HDT in the presence and absence of liposomes. In this case the anchor was added to the liposomes after extrusion. The structure of HDT is shown below.



Heptadecanoic acid-TEMPO (HDT)

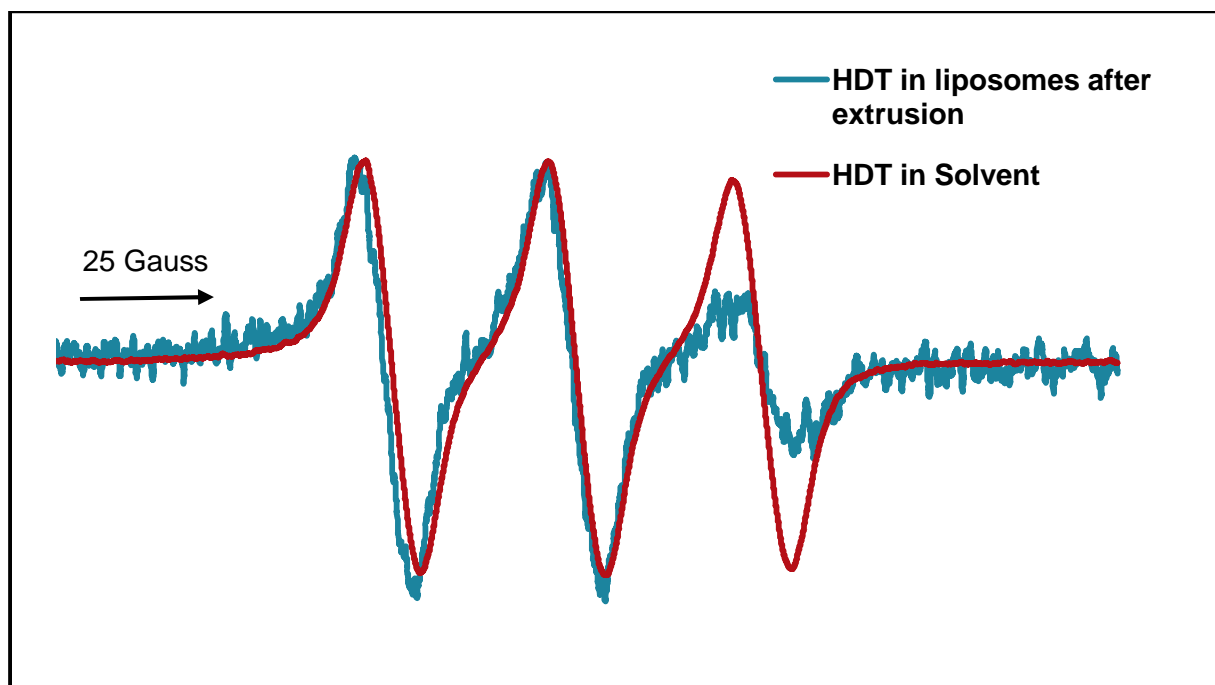


**Figure 5.5:** EPR spectra of HDT in the presence and absence of liposomes. In this case HDT was added to the liposomes after extrusion. Also, among the synthesized anchors, HDT has the longest hydrocarbon chain which imparts high lipophilicity to the anchor. In the figure the magnetic field is plotted against the arbitrary intensity.

There was a change in the hyperfine line shape of the EPR spectrum of HDT in liposomes which indicated a change in the environment of the spin-label. The change in environment resulted in hindrance to the motion of the spin-label anchored to the liposome depicted in the spectrum. The EPR spectrum of HDT added during extrusion also showed similar results as expected. **Figure 5.6** shows the EPR spectra of HDT added during extrusion.

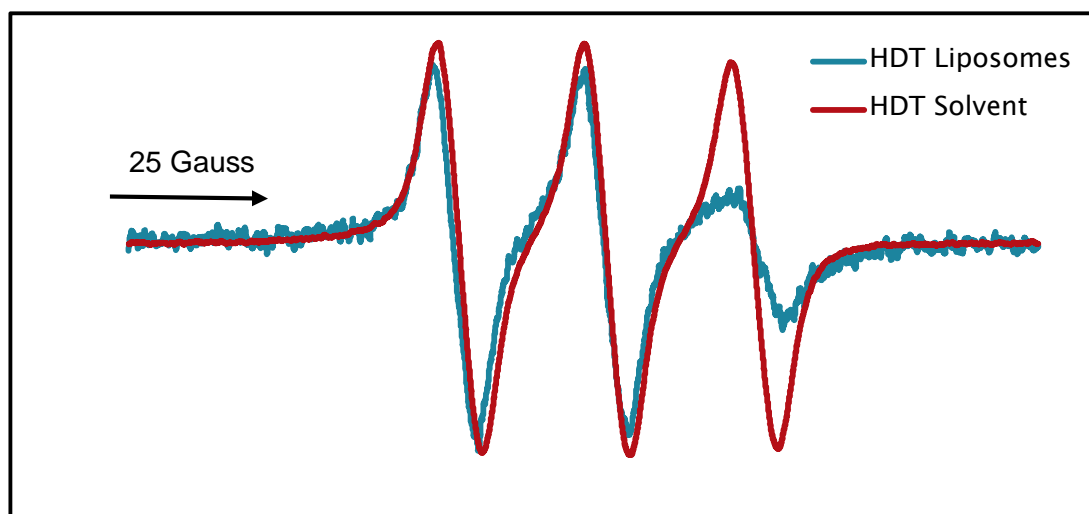


**Figure 5.6:** Comparison of the EPR spectra of HDT added to the liposomes during extrusion to HDT in solvent methanol.

In conclusion, the lipophilic anchors were anchored to the liposome which was evident in the spectra obtained and the method of addition of the anchor did not bring about a change in its ability to anchor to the liposomes. The EPR spectra of HDT showed pronounced difference in line shape when compared to the other lipophilic molecules (c.f. Appendix) and this might be due the high lipophilicity of the hydrocarbon chain which helps in better penetration into the lipophilic portion of the liposome.

### 5.3: Quantification of the Membrane Bound Anchor Using a Relaxation Agent

The synthesized lipophilic anchors proved to anchor to the liposomes and the next step was to determine the amount of bound anchor to the liposome. Attempts to use mathematical simulations to determine the percent bound anchor were not successful as the signal from the bound spin-label could not be separated from the unbound spin-label. Hence, the method of quantitation used to calculate the percent bound was based on relaxation agents. When an anchor is added to the liposomes, some of it or most of it might bind to the liposomes depending on how efficient the anchor is and the rest of the anchor molecules remain in solution (unbound). Relaxation agents like chromium oxalate react with the spin-labeled anchor molecules present in the solution through a bimolecular collision. This bimolecular collision results in relaxation of the spin-label which can be seen as line broadening in the EPR spectra. Based on the concept of line broadening the signal of the bound spin-labeled anchor can be separated from the unbound spin-label.

Relaxation agents also help in determining the position of the spin-label on the liposome. If the spin-label is free in the solution, it involves in a bimolecular collision reaction with chromium oxalate resulting in relaxation of the spin shown as line broadening in the EPR spectrum. If the spin label is anchored to the liposome with the entire molecule inserted into the hydrophobic part of the liposome, it will no longer be available for the collision with the relaxation agent. Thus, we can actually determine the position of attachment of the anchor molecule. As mentioned in chapter 3 there are

other ways of attachment of the anchor molecule as mentioned in case 2 and 3 (c.f. 3.1). Chromium oxalate has been widely used as a relaxation agent to determine the mobility of modified, spin-labeled proteins on the membranes<sup>48</sup> and position of the spin-labeled molecules on a model membrane<sup>49</sup>. **Figure 5.7** illustrates the scheme for separating the signals of bound and unbound spin-labeled molecules using chromium oxalate as the relaxation agent.

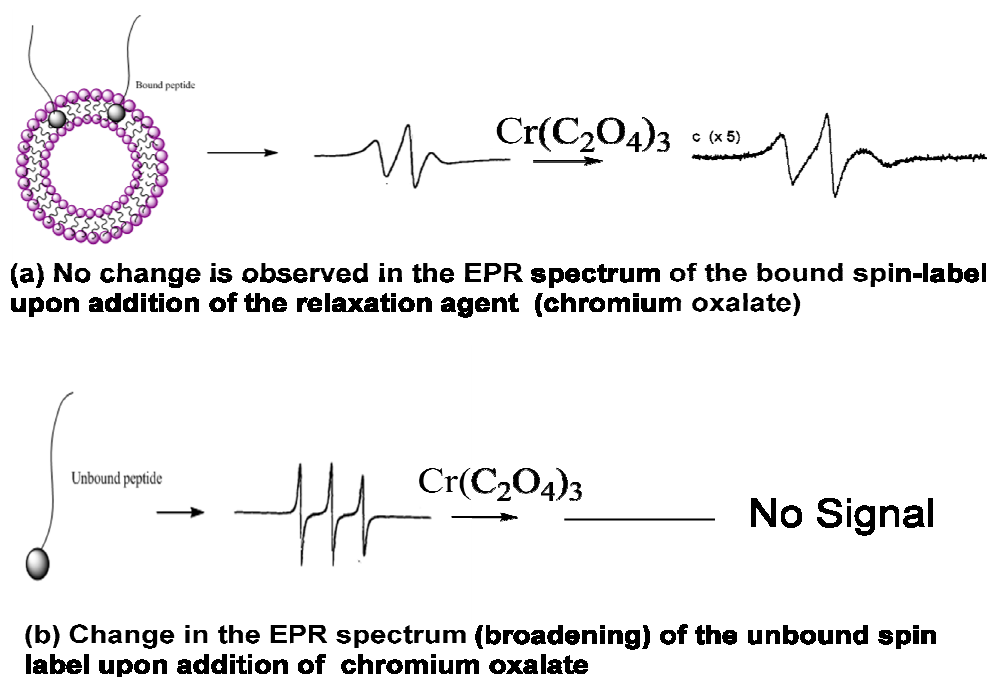


**Figure 5.7:** Scheme for separating the signals of bound from unbound spin-label using Chromium oxalate  $[\text{Cr}(\text{C}_2\text{O}_4)_3]$ . Chromium oxalate is a polar relaxation agent soluble in water.

After separating the signal of the bound spin-labeled anchor with the help of a relaxation agent, the amount of the spin-label giving rise to the signal was calculated. Kaleidagraph 4.0 software was used to make all the calculations. **Figure 5.8** shows the

diagrammatic representation of the method used for calculating the amount of bound spin-labeled anchor.

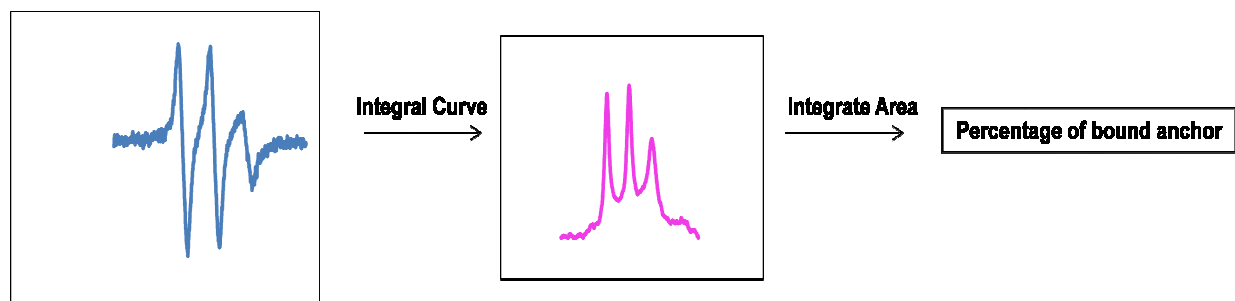


**Figure 5.8:** Diagrammatic representation of the method used for calculating the percentage of bound spin-labeled anchor using the kaleidagraph software.

The solution of the liposomes with the anchor potentially consists of both bound and unbound spin-label. The integrated area for the EPR spectrum of this sample will be considered to contain 100% of the anchor and the percentage of bound anchor will be calculated by comparing the integrated area of the corresponding sample treated with chromium oxalate. The potassium salt of chromium oxalate (sigma-aldrich) was used for these quantitative experiments.

In order to minimize errors in preparation of the samples and to obtain uniform and reproducible results, the samples of the lipophilic anchor added to the liposomes with and without chromium oxalate were prepared from a common stock solution. This was to ensure that we had the same concentration of the anchor in both the solutions so that the results would be comparable. **Figure 5.9** gives a pictorial representation of preparation of the samples from a common stock solution of the anchor and liposomes.

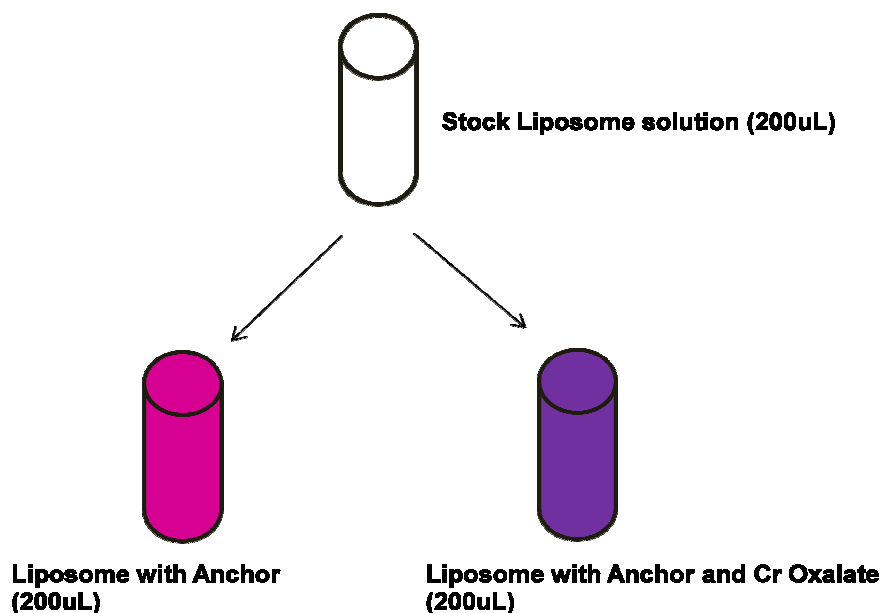


**Figure 5.9:** Pictorial representation of the experimental design used to obtain uniform and reproducible results with minimum errors possible.

EMEAT, being the control molecule is expected to remain in the solvent without anchoring to the liposomes. Hence, the EPR signal of the corresponding sample was expected to undergo total broadening due to bimolecular collision between chromium and the spin-label of EMEAT. The EPR signal for EMEAT in liposomes with chromium represents the unbound spin-label. **Figure 5.10** shows the EPR spectra for EMEAT in liposomes with and without chromium.

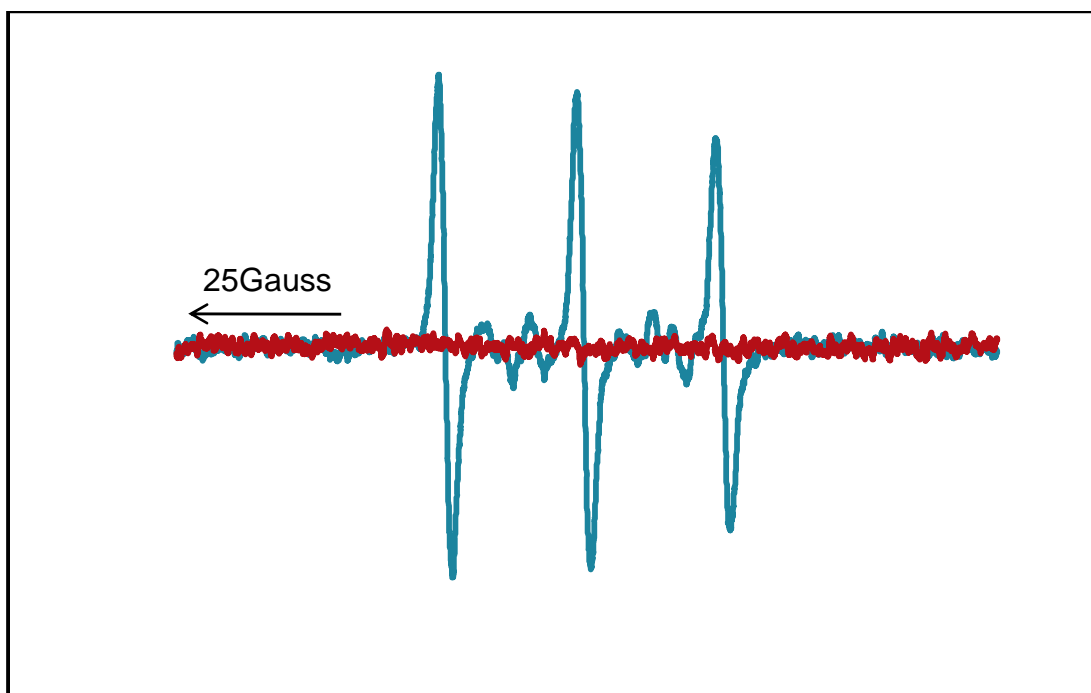


**Figure 5.10:** EPR spectra of EMEAT in liposomes with (blue) and without (red) chromium. EMEAT was added to the liposome solution after extrusion. The concentration of chromium oxalate in solution was 20 mM.

The signal for EMEAT after the addition of chromium was completely broadened indicated by the flat line (red) in the spectra shown above. This data was a clear proof of the ability of chromium to collide with the unbound spin-label and thus separating the signals of the unbound spin-labeled anchor from the bound spin-labeled anchor. Similar experiments were repeated with the spin-labeled lipophilic anchors. The runs were made in triplicate to ensure the reproducibility and reliability of the data. **Figure 5.11** shows the spectra of HDT in liposomes with and without chromium oxalate.

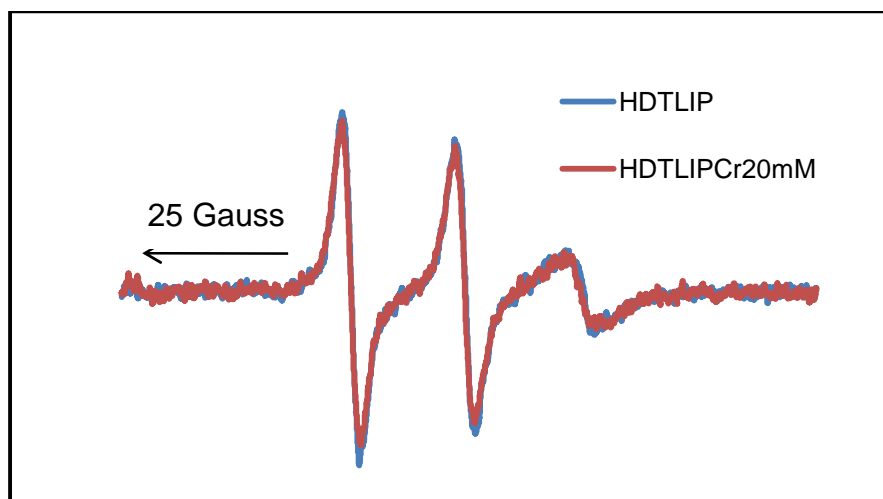


**Figure 5.11:** Representative EPR spectra of HDT in liposomes with (red) and without (blue) chromium. The anchor was added to the liposome after extrusion.

**Figure 5.12** shows the absorption spectra corresponding to the first derivative spectra of HDT shown in figure 5.11.

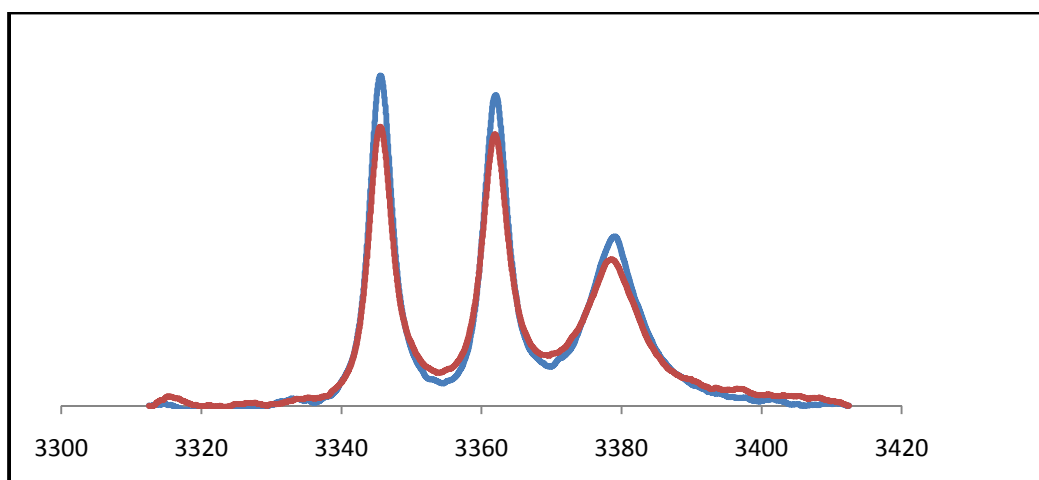


**Figure 5.12:** Representative absorption spectra of HDT in liposomes with (red) and without (blue) chromium. X-axis represents the magnetic field in gauss (units).

The absorption spectra of HDT are shown to give a clear picture of the difference in signals of the bound and unbound HDT. The concentration of HDT was maintained the same between the two samples so that results would be comparable. The EPR spectrum of HDT in the presence of chromium showed subtle changes when compared to the spectrum of HDT without chromium. It was evident from the spectra that most of the HDT added was anchored to the liposome making it an efficient anchor. The integrated area was calculated for both the signals and the percentage HDT bound to the liposomes was determined to be around 80%. This shows that almost all of the HDT was bound to the liposomes. The same experiment was repeated using PT and the percentage of bound PT was found to be 76%. **Figure 5.13** shows the EPR spectra of PT in liposomes with and without chromium oxalate.

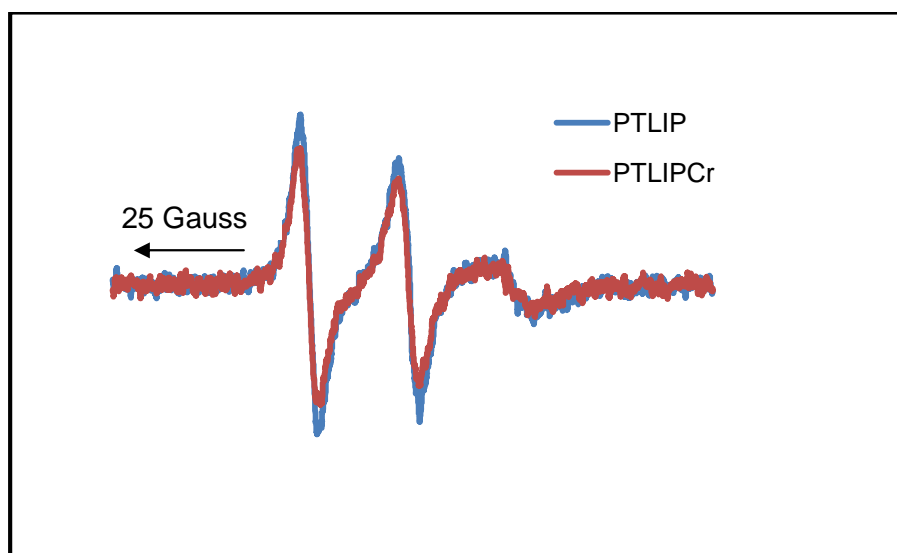


**Figure 5.13:** EPR spectra of PT in liposomes with (red) and without (blue) chromium oxalate.

In order to make sure that the obtained results were reliable, chromium was added to the lipophilic anchors and the resulting EPR spectra is shown in **Figure 5.14**.

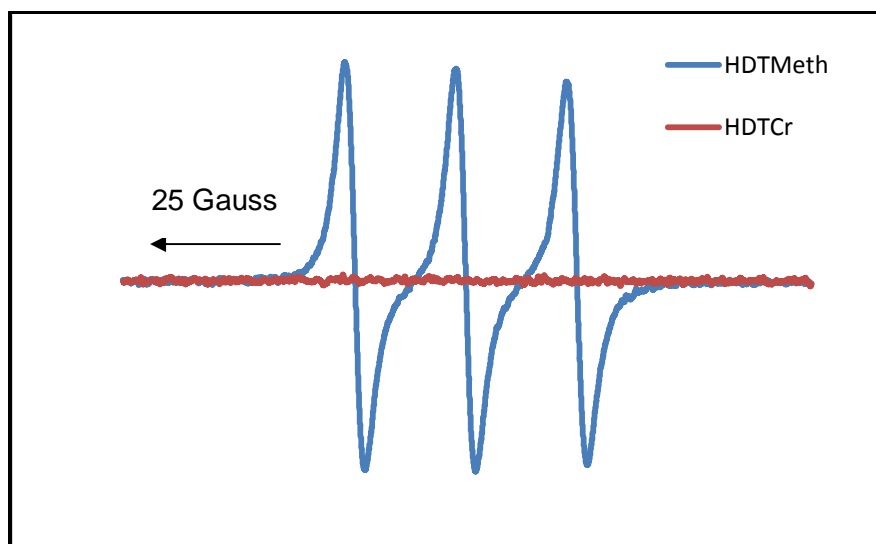


**Figure 5.14:** Representative EPR spectra of HDT in solvent methanol with (red) and without (blue) chromium. The signal from HDT with chromium can be seen as a flat line which is a result of broadening. It is very clear that the unbound HDT collides with the chromium resulting in total relaxation of the spin-label.

The integrals for the spectra obtained by adding chromium oxalate were different for some of the experimental runs. **Table 5.1** shows the data for percent bound anchor for each anchor and **Table 5.2** shows the values for each of the triplicate runs of HDT.

Lipophilic Anchor	Percent Bound (%)
HDT added to the liposomes after extrusion	159
HDT added to the liposomes before extrusion	80
NAT added to the liposomes after extrusion	148
PT added to the liposomes after extrusion	76

**Table 5.1:** Values for percent bound anchors to the liposomes

HDT Run number	Percent bound (%)
Run 1	86
Run 2	108.5
Run 3	141.4

**Table 5.2:** Representative values for triplicate run of percent bound anchor of HDT

The integrals obtained after adding chromium were expected to be less than the integrals for the spectrum without chromium; the reason being the absence of broadening of the signal from the unbound anchor. The spectrum for the anchor without chromium accounts for the total amount of the anchor present in the solution whereas the spectrum with chromium accounts only for the bound anchor. However, in some

cases the amount of anchor bound was found to exceed 100% after addition of chromium oxalate. The high values for the integrals of chromium might be due to slight broadening of the signal which results in apparent increase in the integrated area. This might be due to change in polarity of the solvents because chromium oxalate is dissolved in water whereas the anchor is present in methanol. The change in polarity might cause more of the lipophilic anchor to partition into the liposome. Or, the chromium oxalate may collide inefficiently with some of the spin-label protruding from the surface of the liposome leading to incomplete broadening of the signal. In conclusion, the use of relaxation agent proved to be useful in determining the amount of the bound spin-label with a few inevitable aberrations.

#### **5.4: Solid Phase Peptide Synthesis**

The final step of the research was to synthesize a model peptide with the most efficient lipophilic anchor also containing a nitroxide spin-label attached to one of the amino acids in the sequence and to quantify the amount of peptide anchored to the liposomes. The model peptides were synthesized using solid phase peptide synthesis on a PS3 Protein Technologies, Inc. peptide synthesizer using an Fmoc (9-Fluorenylmethoxycarbonyl) protecting group strategy. The lipophilic anchor was attached via a peptide bond to the side chain of a lysine residue as was 3-carboxy-PROXYL (sigma-aldrich) a free radical. 3-carboxy-PROXYL (CP) is a nitroxide spin-

label which contains carboxylic acid group in the side chain (c.f. 2.2). The carboxylic acid group helps in forming the peptide bond with the amino acid.

SPPS utilizes resins which are the insoluble polymeric supports to create an open gel system where peptides can be synthesized. Peptides are built from the C-terminus to the N-terminus. The first step is the removal of the protecting group on the swelled resin to create a free amine. This free amine becomes the active site of the resin where the first amino acid will attach. Then, a side chain protected N<sup>α</sup> amino acid is attached to the solid support resin via an amide bond linkage (**Figure 5.16**). This reaction is improved by the coupling reagents which generate a reactive species from the free carboxyl group of the amino acid. This reactive species then reacts rapidly with the free amine to create a peptide bond under room temperature conditions. Common coupling agents used in SPPS include dicyclohexylcarbodiimide (DIC), 1H-benzotriazol-1-yloxy-tri(dimethylamino)phosphonium hexafluorophosphate (BOP), and the uronium salt O-(benzotriazol-1-yl)-1,1,3,3-tetramethyluronium hexafluorophosphate (HBTU). Using these coupling reagents can sometimes result in side reactions that lead to racemization or epimerization of the amino acid. 1-hydroxybenzotriazole (HOBt) is a common additive used to prevent racemization.

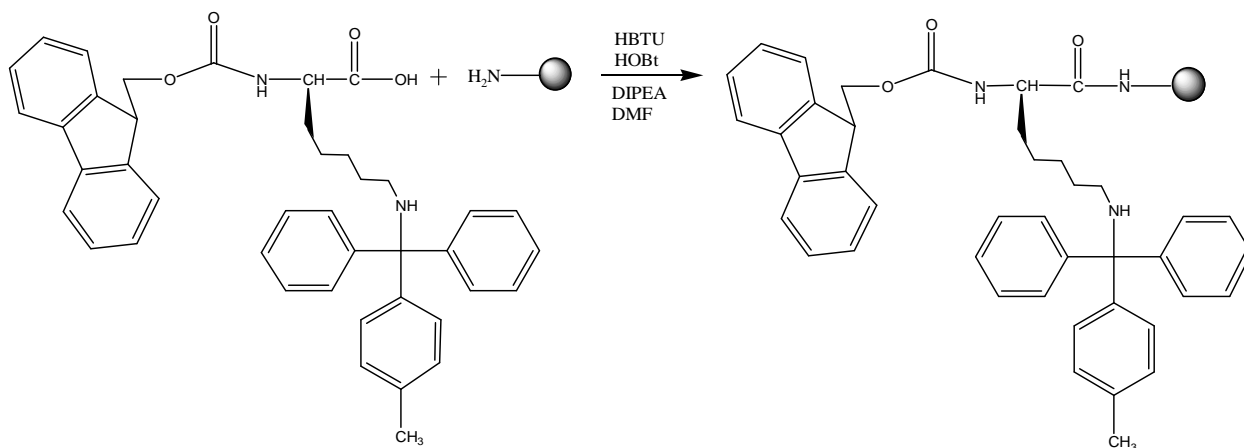


**Figure 5.16:** Attachment of First Amino Acid (Fmoc-Lys(Mtt)-OH) to a resin in SPPS

Once the first amino acid is attached, the Fmoc protecting group is removed on the attached amino acid with a secondary amine (**Figure 5.17**), allowing for a new Fmoc protected amino acid to be coupled to the peptide chain in the same way. This process of removing the protecting group and attaching a new amino acid is repeated until the desired peptide chain is produced. Heptadecanoic acid (HDA) was the anchor of choice due to its proven efficiency to anchor to the liposomes in EPR experiments.

1-pyrenebutyric acid was already proved to attach well to the peptide in previous experiments conducted in our lab. To attach the anchor and the spin-label to the C-terminus of a peptide, a 4-Methyltrityl (Mtt) side chain protected amino acid was used.

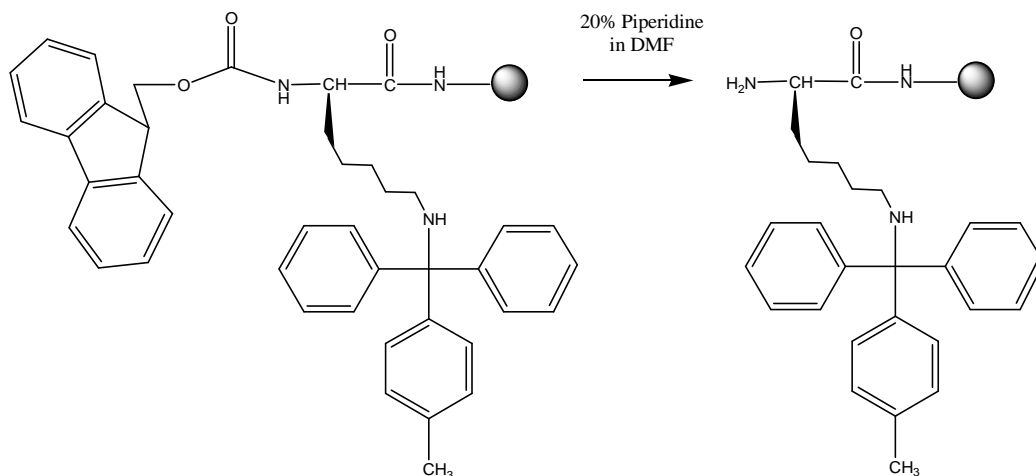


**Figure 5.17:** Removal of Fmoc protecting group from the peptide chain.

Mtt group is an acid-labile group which can be removed easily with mild acids like 1% trifluoroacetic acid (TFA), which is desirable because all other protecting groups, including the resin, are stable under mild acidic conditions. To attach the molecules (anchor and spin-label), the Mtt protected lysine is attached using SPPS. Then, the Mtt group is selectively removed with 1% TFA, leaving the amine group on the lysine side chain unprotected (**Figure 5.18**).

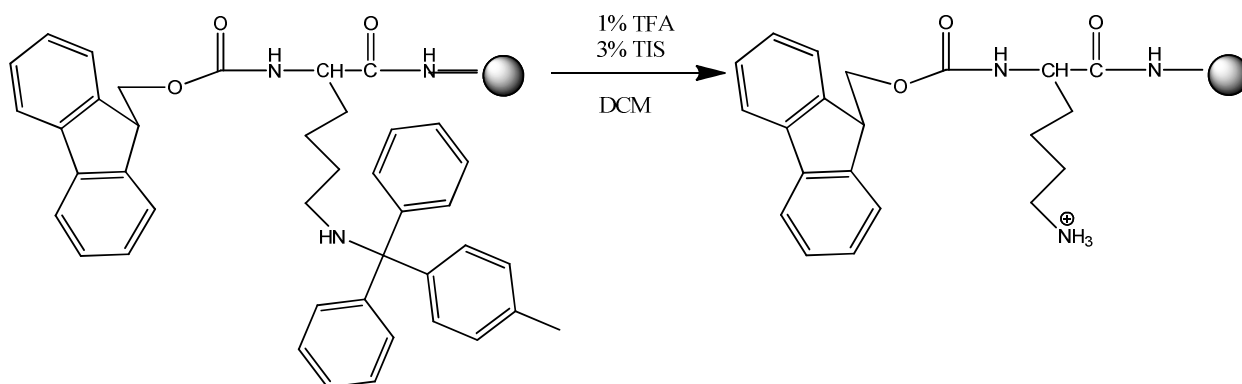


**Figure 5.18:** Removal of methytrityl protecting group from lysine.

To create a spin-labeled peptide with an anchor attached to it, the molecules can be linked to the lysine side chains under standard SPPS conditions (**Figure 5.19**). In the figure, the attachment of pyrene is shown as an example.

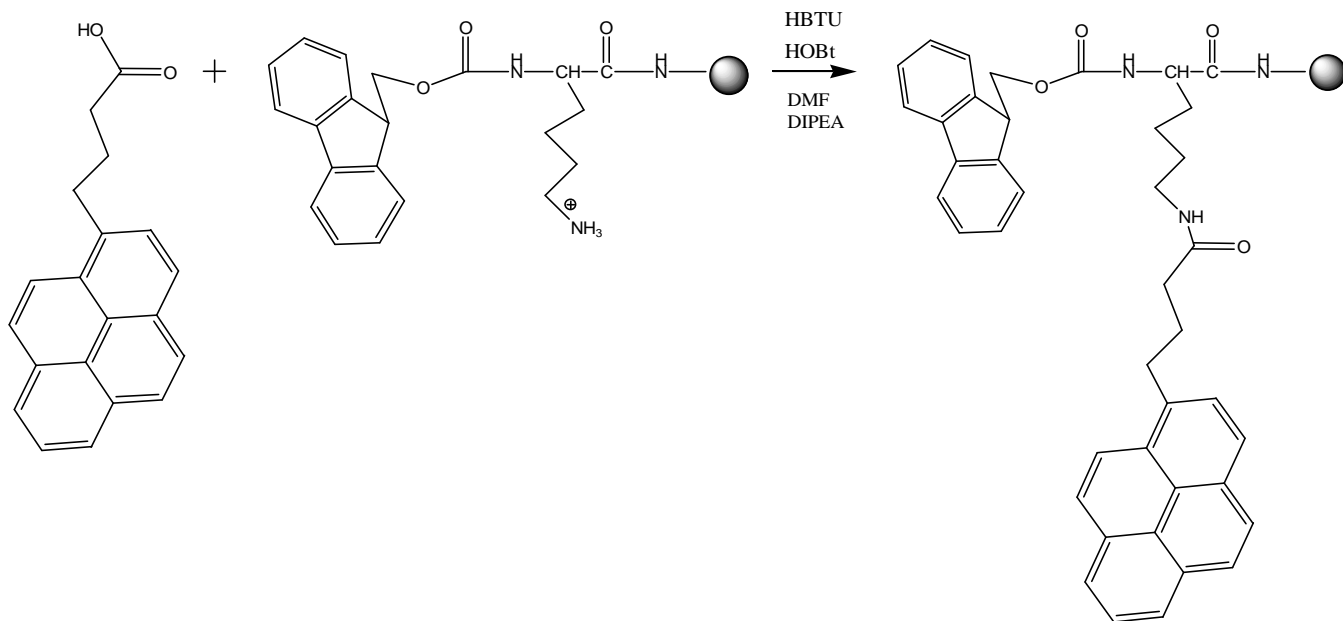


**Figure 5.19:** Reaction showing the attachment of the anchor 1-pyrenebutyric acid to the lysine amino acid.

Once the desired peptide chain is built, the peptide is cleaved from the resin using 95% TFA with added scavengers such as water and triisopropylsilane to reduce the side reactions. The peptide models are then purified using reverse-phase HPLC and characterized using mass spectrometry (ESI-MS).

### 5.5: Synthesis of the Peptide Model

A small nine amino acid length peptide was planned to be synthesized to which the spin-label and the anchor would be attached (**Figure 5.20**).

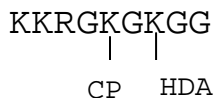


**Figure 5.20:** Model peptide with HDA and CP attached to the side chain of the lysine amino acid. Glycine spacers were used to reduce the steric hindrance from the resin and the rest of the amino acids.

In the process of attaching the HDA molecule to the peptide chain, methyltrityl protecting group was removed and the HDA was coupled immediately. Following this, acetic anhydride was added to acetylate any free lysine side chains. Then, the Fmoc protecting group on the lysine that had the newly attached anchor molecule was removed, and the synthesis of the peptide was continued. Fmoc protected amino acids, HBTU and HOBt were obtained from Novabiochem and all other chemicals were obtained from Sigma-Aldrich.

All peptides were synthesized at the 0.1 millimole scale, with a fourfold excess of amino acid, HBTU, CP and HDA. 100  $\mu\text{L}$  of diisopropylethylamine was used during each step. All reactions took place in a glass vessel with a glass frit at the bottom. Rink amide MBHA resin was used as the solid support, and swelled for at least 30 minutes in N, N-dimethylformamide (DMF) before use. The resin was deprotected using 20%

piperidine in DMF for 45 minutes before adding the first amino acid. Coupling times ranged from 30-60 minutes in DMF, and reagents (amino acid, HOBt, HBTU, diisopropylethylamine) were allowed to react for approximately one minute before addition to the solid support peptide system. Ninhydrin tests were utilized to test the completion of attachment of HDA, CP, and to monitor the deprotection of Mtt group.

To attach HDA and CP, HBTU, HOBt, and diisopropylethylamine were allowed to react for approximately five minutes before addition to the peptide chain. Reaction time ranged from 5-7 hours, as monitored by ninhydrin tests. Acetylation of the free amino terminus was performed using approximately 1 mL of acetic anhydride in the presence of 100  $\mu$ L diisopropylethylamine. Peptide cleavage was performed using 95% TFA, 2.5% water, and 2.5% triisopropyl silane and allowed to react for 100-120 minutes. The TFA mixture was drained from the reaction vessel and the resin was rinsed with clean TFA, and the peptide was precipitated using ethyl ether. The solution was centrifuged to isolate the solid peptide and water was added to dissolve the peptide after the TFA and ethyl ether were decanted.

The peptide solution was then lyophilized and purified using a Bio-Rad Biologic Duo-flow HPLC. A Vydac reverse phase C-18 column was used with a gradient of 100% water to 100% acetonitrile over 40 minutes for all peptides. The peptide fractions collected from HPLC were analyzed using ESI-MS to determine the purity and success of peptide synthesis. In order to monitor the attachment of the anchor HDA and the spin-label CP to the lysine residues, small amounts of resin was collected. These samples were cleaved and analyzed using HPLC and ESI-MS. Analysis revealed some unexpected results. It was difficult to continue the synthesis after the attachment of HDA

to lysine which may be due to steric hindrance caused by the long hydrocarbon chain. Therefore 1-pyrenebutyric acid was chosen and attached to the lysine residue. Another problem was the attachment of the amino acid after 3-carboxy PROXYL group. In order to overcome this problem, the coupling time was increased. According to the EPR data and the ESI-MS data we know that both the molecules were attached to the lysine residues but peptide as a whole was not detectable. The fragment  $\text{K}^{\text{GKGG}}$  with CP and PBA attached to the lysine residues was observed in the mass spectrum of the peptide. **Figure 5.21** shows the mass spectrum of the whole length peptide containing PBA and CP attached to the lysine residues.

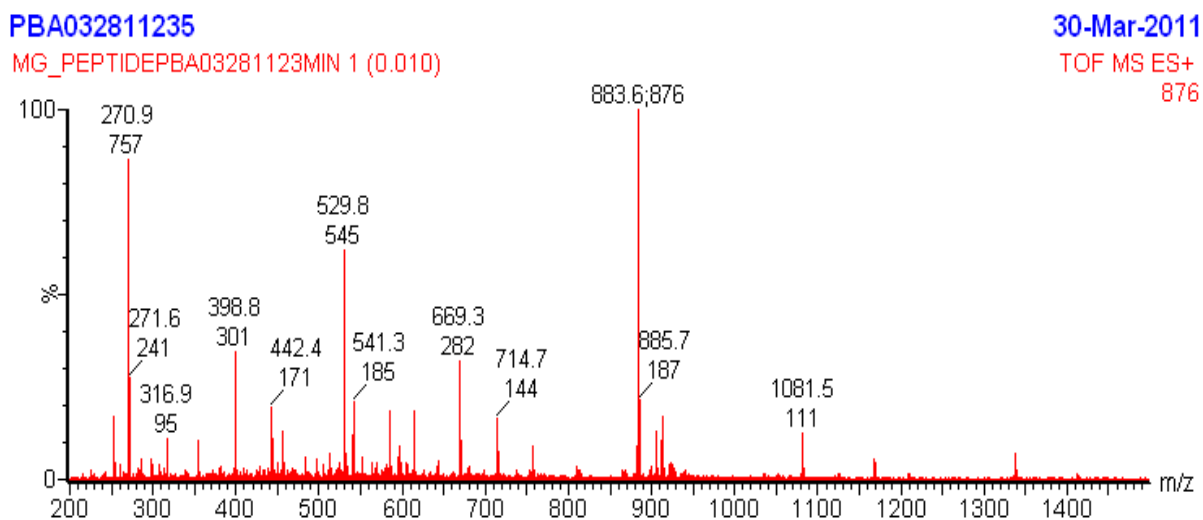


**Figure 5.21:** An ESI-MS spectrum in positive ion mode of RPLC purified peptide containing PBA and CP attached to the lysine residues of the C-terminus. The  $m/z$  values 883, 669, and 529.8 correspond to different fragments of the peptide containing either one or both of the molecules attached to the lysine residues.

The fragments corresponding to some of the peaks observed in the spectrum are shown in **Table 5.3**.

m/z value	Peptide Fragment
883.6876	(CP)KG(PBA)KGG
669.3282	G(CP)KGKGG
529.8545	(PBA)KGG

**Table 5.3:** The peptide fragments corresponding to the m/z values are shown above.

The fact that the peptide gave an EPR signal itself proves the presence of the CP free radical but the EPR line shape for the peptide in liposomes was not as expected. The integrals for the chromium experiment were also not reliable. If the lipophilic molecule was anchored to the liposome, the motion of the spin-label might be hindered which is shown in the line shape. The EPR spectrum of the peptide with the liposomes did not show any hindrance to the motion of the spin-label. Moreover, the mass of the entire peptide with the attached molecules was not seen in the mass spectrum. In conclusion, though the synthesis of the peptide did not end up as expected there was evidence for the attachment of the anchor molecule and the spin-label. The EPR spectrum of the peptide model in liposomes with and without chromium is shown in **Figure 5.22**.

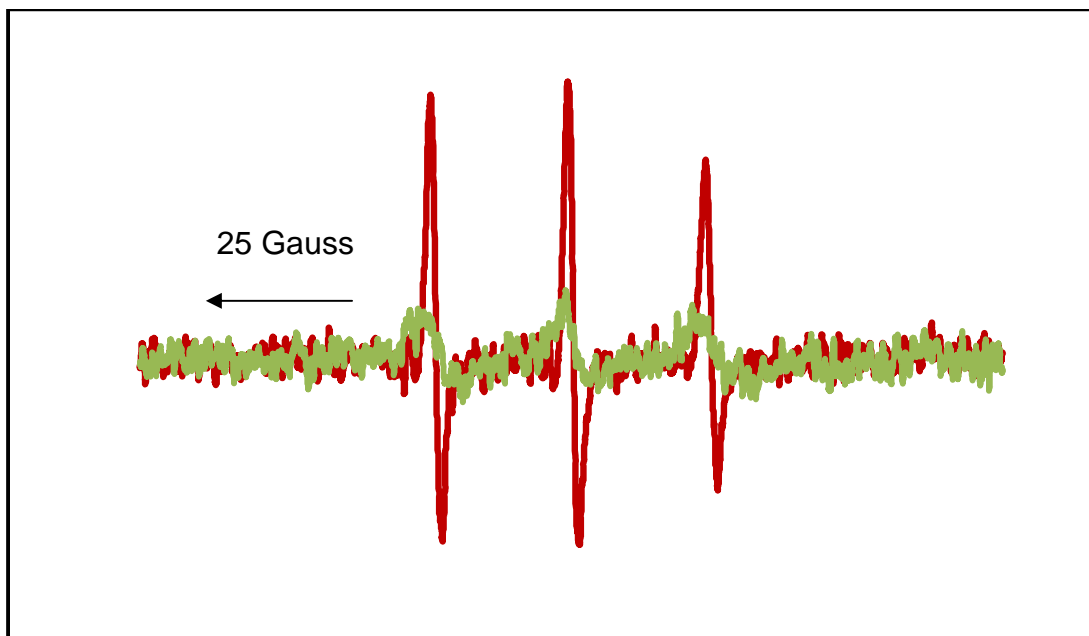


**Figure 5.22:** EPR spectra of the peptide model in liposomes with (green) and without (red) chromium.

From the EPR spectra, it is evident that the signal of the spin-label has been quenched. However, just because it quenches doesn't mean it isn't anchored – the spin label might be with the peptide outside of the liposome. Determining the position of the spin-label on the liposome would be the key to unravel this puzzle.

## Chapter 6: Final Conclusions and Future Studies

This study gives a novel perspective on prion research. Several studies were conducted to understand the prion-prion interactions but none of them could quantify the amount of these interactions. Experiments conducted in the past have proven that the attachment of PrP to a synthesized liposomal surface does not result in significant structural changes as observed by far-UV circular dichroism. These studies also proved that the structure of mammalian PrP<sup>C</sup> in a liposome is identical to the recombinant PrP in solution.<sup>26</sup> Also, when PrP incorporated into model liposomes was attached to a synthetic GPI anchor mimetic, it maintained the same conformation as the native GPI bound PrP.<sup>27</sup> The results from this study pave the way for future experiments where prion-derived peptides are anchored to the surface of the liposomes. Given the discussion above, the results from these studies should provide an insight into the behavior of the prion protein in its native environment.

The first challenge in the research was to synthesize spin-labeled lipophilic molecules in the lab which could anchor majority of the PrP sample to the liposome. The anchors were selected based on their lipophilicity rendered due to the long hydrocarbon chains or a series of aromatic rings in the molecule. Spin-labeled lipophilic anchor molecules were successfully synthesized using a simple amide coupling reaction. Characterization of these molecules led us to some interesting observations about the behavior of the spin-label. For instance, the ESI-MS spectra of the spin-labeled lipophilic anchors showed  $(M+2H)^+$  peak instead of the regular  $(M+H)^+$  peak.

The proton NMR spectra of the molecules showed that the spin-labeled molecules might exist in different conformations due to the presence of the nitroxide moiety.

The most important goal of the research was to develop a spin-label based assay for the quantification of the bound anchor. Spin-labels are widely used in peptide chemistry to monitor the behavior of both pathogenic and non-pathogenic proteins. The synthesized anchor molecules proved to be efficient in anchoring to the liposomes. EPR results clearly proved that majority of the TEMPO molecule was embedded into the liposomes. The spin-labeled molecule, EMEAT, selected to act as the control molecule for all the EPR experiments was not anchored to the liposomes. This was evident in the chromium oxalate assay where the signal from the molecule in liposomes in the presence of chromium got completely flattened. The spin-labeled assay was based on the capability of a relaxation agent to separate the bound signal from the unbound signal of the lipophilic anchor.

The quantitation experiments using the chromium oxalate were successful to some extent. The major problem was the increase in integral values of the anchor after addition of the relaxation agent which was uncanny. The plausible explanation for the integrals might be difference in the behavior of the spin-labeled anchor in solutions of different ionic strength. Chromium, being a polar molecule increases the ionic strength of the solution which in turn might help in penetration of the unbound anchor into the liposome. Also, the spin label might experience relaxation due to dipolar interactions with the  $\text{Cr}(\text{C}_2\text{O}_4)_3$ . The strategy used for the synthesis of the peptide model by attaching the lipophilic anchor and the spin-label separately posed a lot of difficulties. The steric hindrance of the lipophilic chain of HDA did not allow the

progress of the synthesis any further. ESI-MS results of the peptides with HDA or PBA as the anchor and CP as the nitroxide spin-label showed different fragments of the peptide but not the entire peptide. But, both ESI-MS and EPR results showed that the anchor molecules and the spin-label were attached to the peptide. A change in strategy might help in successful synthesis of the PrP peptide encompassing the metal-binding region. In conclusion, a spin-label based assay has been developed to calculate the percentage of bound anchor to the liposomes.

Studies planned for the future would be to design a peptide containing both the anchor and the spin-label attached to it and use this assay to determine the percentage bound peptide to the liposomes. Additionally, PrP-PrP interactions can be monitored and quantified as a function of added metal at a molecular level using EPR.

## REFERENCES

- (1) Prusiner, S. Novel proteinaceous infectious particles cause scrapie. *Science* **1982**, *216*, 136-144.
- (2) Zahn, R.; Liu, A.; Luhrs, T.; Riek, R.; von Schroetter, C.; Lopez Garcia, F.; Billeter, M.; Calzolari, L.; Wider, G.; Wuthrich, K. NMR solution structure of the human prion protein. *Proc. Natl. Acad. Sci. U. S. A.* **2000**, *97*, 145-150.
- (3) Donne, D. G.; Viles, J. H.; Groth, D.; Mehlhorn, I.; James, T. L.; Cohen, F. E.; Prusiner, S. B.; Wright, P. E.; Dyson, H. J. Structure of the recombinant full-length hamster prion protein PrP(29-231): the N terminus is highly flexible. *Proc. Natl. Acad. Sci. U. S. A.* **1997**, *94*, 13452-13457.
- (4) Riek, R.; Hornemann, S.; Wider, G.; Glockshuber, R.; Wuthrich, K. NMR characterization of the full-length recombinant murine prion protein, mPrP(23-231). *FEBS Lett.* **1997**, *413*, 282-288.
- (5) Kristensson, K.; Feuerstein, B.; Taraboulos, A.; Hyun, W. C.; Prusiner, S. B.; DeArmond, S. J. Scrapie prions alter receptor-mediated calcium responses in cultured cells. *Neurology* **1993**, *43*, 2335-2341.
- (6) Harris, D. A. Trafficking, turnover and membrane topology of PrP. *Br. Med. Bull.* **2003**, *66*, 71-85.
- (7) Gorodinsky, A.; Harris, D. A. Glycolipid-anchored proteins in neuroblastoma cells form detergent-resistant complexes without caveolin. *J. Cell Biol.* **1995**, *129*, 619-627.
- (8) Prusiner, S. B. Prions. *Proceedings of the National Academy of Sciences of the United States of America* **1998**, *95*, 13363-13383.
- (9) Engstrom, A.; Lindstrom, B. General Introduction. *Biophys. J.* **1962**, *2*, i6.
- (10) Tobler, I.; Gaus, S. E.; Deboer, T.; Achermann, P.; Fischer, M.; Rulicke, T.; Moser, M.; Oesch, B.; McBride, P. A.; Manson, J. C. Altered circadian activity rhythms and sleep in mice devoid of prion protein. *Nature* **1996**, *380*, 639-642.
- (11) Colling, S. B.; Collinge, J.; Jefferys, J. G. R. Hippocampal slices from prion protein null mice: disrupted Ca<sup>2+</sup>-activated K<sup>+</sup> currents. *Neurosci. Lett.* **1996**, *209*, 49-52.
- (12) Brown, D. R.; Qin, K.; Herms, J. W.; Madlung, A.; Manson, J.; Strome, R.; Fraser, P. E.; Kruck, T.; von Bohlen, A.; Schulz-Schaeffer, W.; Giese, A.; Westaway, D.; Kretzschmar, H. The cellular prion protein binds copper in vivo. *Nature* **1997**, *390*, 684-687.
- (13) Rizzardini, M.; Chiesa, R.; Angeretti, N.; Lucca, E.; Salmona, M.; Forloni, G.; Cantoni, L. Prion protein fragment 106-126 differentially induces heme oxygenase-1 mRNA in cultured neurons and astroglial cells. *J. Neurochem.* **1997**, *68*, 715-720.
- (14) Milhavet, O.; Lehmann, S. Oxidative stress and the prion protein in transmissible spongiform encephalopathies. *Brain Res. Brain Res. Rev.* **2002**, *38*, 328-339.
- (15) Brown, D. R.; Schmidt, B.; Kretzschmar, H. A. Effects of copper on survival of prion protein knockout neurons and glia. *J. Neurochem.* **1998**, *70*, 1686-1693.

- (16) Bonomo, R. P.; Imperlizzeri, G.; Pappalardo, G.; Rizzarelli, E.; Tabbi, G. Copper(II) binding modes in the prion octapeptide PHGGGWGQ: a spectroscopic and voltammetric study. *Chemistry* **2000**, *6*, 4195-4202.
- (17) Kroneck, P. M.; Vortisch, V.; Hemmerich, P. Model studies on the coordination of copper in biological systems. The deprotonated peptide nitrogen as a potential binding site for copper(II). *Eur. J. Biochem.* **1980**, *109*, 603-612.
- (18) Shyng, S. L.; Huber, M. T.; Harris, D. A. A prion protein cycles between the cell surface and an endocytic compartment in cultured neuroblastoma cells. *J. Biol. Chem.* **1993**, *268*, 15922-15928.
- (19) Pauly, P. C.; Harris, D. A. Copper stimulates endocytosis of the prion protein. *J. Biol. Chem.* **1998**, *273*, 33107-33110.
- (20) Rachidi, W.; Vilette, D.; Guiraud, P.; Arlotto, M.; Riondel, J.; Laude, H.; Lehmann, S.; Favier, A. Expression of prion protein increases cellular copper binding and antioxidant enzyme activities but not copper delivery. *J. Biol. Chem.* **2003**, *278*, 9064-9072.
- (21) Elfrink, K.; Ollesch, J.; Stohr, J.; Willbold, D.; Riesner, D.; Gerwert, K. Structural changes of membrane-anchored native PrP(C). *Proc. Natl. Acad. Sci. U. S. A.* **2008**, *105*, 10815-10819.
- (22) González-Iglesias, R.; Elvira, G.; Rodríguez-Navarro, J. A.; Vélez, M.; Calero, M.; Pajares, M. A.; Gasset, M. Cu<sup>2+</sup> binding triggers  $\alpha$ BoPrP assembly into insoluble laminar polymers. *FEBS Lett.* **2004**, *556*, 161-166.
- (23) Morante, S.; Gonzalez-Iglesias, R.; Potrich, C.; Meneghini, C.; Meyer-Klaucke, W.; Menestrina, G.; Gasset, M. Inter- and intra-octarepeat Cu(II) site geometries in the prion protein: implications in Cu(II) binding cooperativity and Cu(II)-mediated assemblies. *J. Biol. Chem.* **2004**, *279*, 11753-11759.
- (24) Leliveld, S. R.; Dame, R. T.; Wuite, G. J.; Stitz, L.; Korth, C. The expanded octarepeat domain selectively binds prions and disrupts homomeric prion protein interactions. *J. Biol. Chem.* **2006**, *281*, 3268-3275.
- (25) Fujimoto, K.; Roots, B. I.; Burton, R. M.; Agrawal, H. C. Morphological and biochemical characterization of light and heavy myelin isolated from developing rat brain. *Biochim. Biophys. Acta* **1976**, *426*, 659-668.
- (26) Eberl, H.; Tittmann, P.; Glockshuber, R. Characterization of recombinant, membrane-attached full-length prion protein. *J. Biol. Chem.* **2004**, *279*, 25058-25065.
- (27) Hicks, M. R.; Gill, A. C.; Bath, I. K.; Rullay, A. K.; Sylvester, I. D.; Crout, D. H.; Pinheiro, T. J. Synthesis and structural characterization of a mimetic membrane-anchored prion protein. *FEBS J.* **2006**, *273*, 1285-1299.
- (28) Kazlauskaitė, J.; Sanghera, N.; Sylvester, I.; Venien-Bryan, C.; Pinheiro, T. J. Structural changes of the prion protein in lipid membranes leading to aggregation and fibrillization. *Biochemistry* **2003**, *42*, 3295-3304.

- (29) Gofflot, S.; El, M. B.; Zorzi, D.; Melen, L.; Roels, S.; Quatpers, D.; Grassi, J.; Vanopdenbosch, E.; Heinen, E.; Zorzi, W. Immuno-quantitative polymerase chain reaction for detection and quantitation of prion protein. *J. Immunoassay Immunochem* **2004**, *25*, 241-258.
- (30) Gaffney, B. J.; McNamee, C. M. Spin-label measurements in membranes. With appendix: a use of computers in EPR spectroscopy. *Methods Enzymol.* **1974**, *32*, 161-198.
- (31) Voss, J.; Hubbell, W. L.; Hernandez-Borrell, J.; Kaback, H. R. Site-directed spin-labeling of transmembrane domain VII and the 4B1 antibody epitope in the lactose permease of *Escherichia coli*. *Biochemistry* **1997**, *36*, 15055-15061.
- (32) Mouillet-Richard, S.; Ermonval, M.; Chebassier, C.; Laplanche, J. L.; Lehmann, S.; Launay, J. M.; Kellermann, O. Signal transduction through prion protein. *Science* **2000**, *289*, 1925-1928.
- (33) Millhauser, G. L.; Fiori, W. R.; Miick, S. M. In [24] *Electron spin labels*; Kenneth Sauer, Ed.; Methods in Enzymology; Academic Press: 1995; Vol. Volume 246, pp 589-610.
- (34) González-Iglesias, R.; Elvira, G.; Rodríguez-Navarro, J. A.; Vélez, M.; Calero, M.; Pajares, M. A.; Gasset, M. Cu<sup>2+</sup> binding triggers  $\alpha$ BoPrP assembly into insoluble laminar polymers. *FEBS Lett.* **2004**, *556*, 161-166.
- (35) Morante, S.; Gonzalez-Iglesias, R.; Potrich, C.; Meneghini, C.; Meyer-Klaucke, W.; Menestrina, G.; Gasset, M. Inter- and intra-octarepeat Cu(II) site geometries in the prion protein: implications in Cu(II) binding cooperativity and Cu(II)-mediated assemblies. *J. Biol. Chem.* **2004**, *279*, 11753-11759.
- (36) Kennedy, A.; Hmel, P. J.; Seelbaugh, J.; Quiles, J. G.; Hicks, R.; Reid, T. J. Characterization of the main phase transition in 1,2-dipalmitoyl-phosphatidylcholine luvs by <sup>1</sup>H NMR. *J. Liposome Res.* **2002**, *12*, 221-237.
- (37) Podgornik, R. Liposomes in Gene Delivery by Danilo D. Lasic. *Biophys. J.* **1998**, *74*, 2138-2139.
- (38) Davidsen J FAU - Mouritsen, Ole G.; Mouritsen OG FAU - Jorgensen, Kent; Jorgensen K Synergistic permeability enhancing effect of lysophospholipids and fatty acids on lipid membranes. *Biochimica et Biophysica Acta* **2002**, *1564*, 256-262.
- (39) Perin, M. S.; MacDonald, R. C. Fusion of synaptic vesicle membranes with planar bilayer membranes. *Biophys. J.* **1989**, *55*, 973-986.
- (40) Kaneshiro, E. S.; Wyder, M. A.; Wu, Y.; Cushion, M. T. Reliability of calcein acetoxymethyl ester and ethidium homodimer or propidium iodide for viability assessment of microbes. *J. Microbiol. Methods* **1993**, *17*, 1-16.
- (41) (24) Russell, A. L.; Kennedy, A. M.; Spuches, A. M.; Venugopal, D.; Bhonsle, J. B.; Hicks, R. P. Spectroscopic and thermodynamic evidence for antimicrobial peptide membrane selectivity. *Chem. Phys. Lipids* **2010**, *163*, 488-497.
- (42) Kendall DA FAU - MacDonald, R C.; MacDonald RC A fluorescence assay to monitor vesicle fusion and lysis. *Biophys J.* **1989**, *55*, 973-986.

- (43) Hara, M.; Yamano, Y.; Sakai, Y.; Kodama, E.; Hoshino, T.; Ito, M.; Miyake, J. Stabilization of liposomal membranes by carotenoids: Zeaxanthin, zeaxanthin glucoside and thermozeaxanthin. *Materials Science and Engineering: C* **2008**, *28*, 274-279.
- (44) Litvinchuk, S.; Lu, Z.; Rigler, P.; Hirt, T. D.; Meier, W. Calcein release from polymeric vesicles in blood plasma and PVA hydrogel. *Pharm. Res.* **2009**, *26*, 1711-1717.
- (45) Kenward, A. G.; Bartolotti, L. J.; Burns, C. S. Copper and zinc promote interactions between membrane-anchored peptides of the metal binding domain of the prion protein. *Biochemistry* **2007**, *46*, 4261-4271.
- (46) Ladokhin, A. S.; Jayasinghe, S.; White, S. H. How to measure and analyze tryptophan fluorescence in membranes properly, and why bother? *Anal. Biochem.* **2000**, *285*, 235-245.
- (47) Tobler, I.; Deboer, T.; Fischer, M. Sleep and sleep regulation in normal and prion protein-deficient mice. *J. Neurosci.* **1997**, *17*, 1869-1879.
- (48) Liu, J.; Rutz, J. M.; Klebba, P. E.; Feix, J. B. A site-directed spin-labeling study of ligand-induced conformational change in the ferric enterobactin receptor, FepA. *Biochemistry* **1994**, *33*, 13274-13283.
- (49) Lloyd-Williams, P. Albericio, F., Giralt, E. *Chemical Approaches to the Synthesis of Peptides and Proteins*; CRC Press, LLC: Florida, **1997**.

## APPENDIX: SPECTROSCOPIC DATA

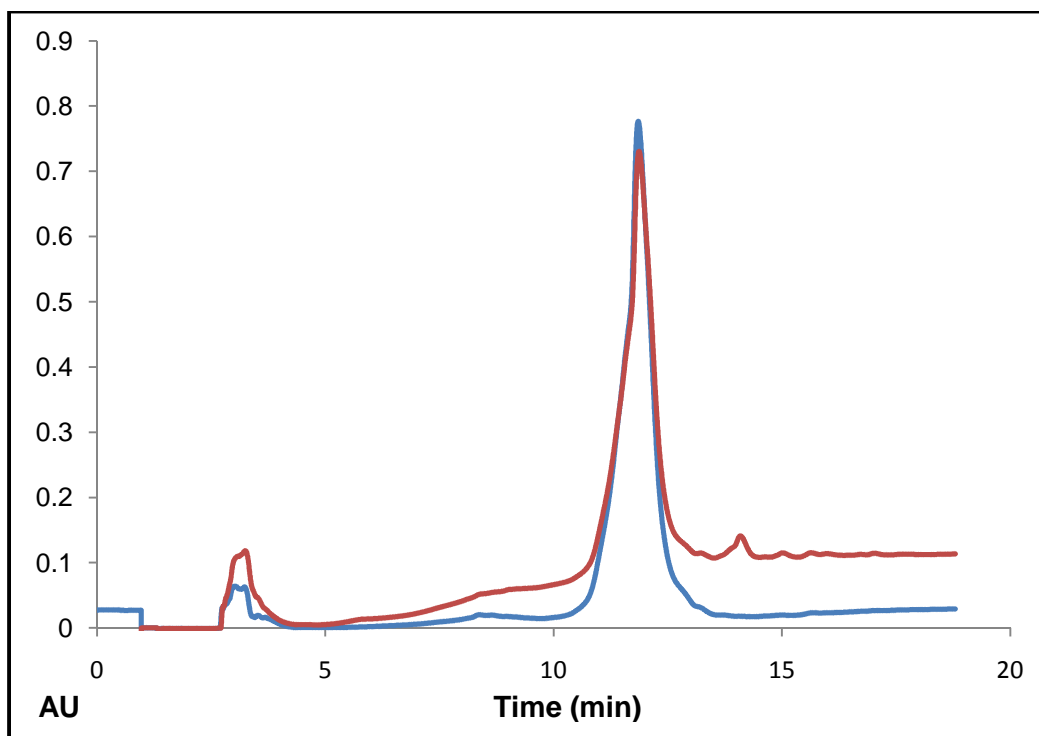
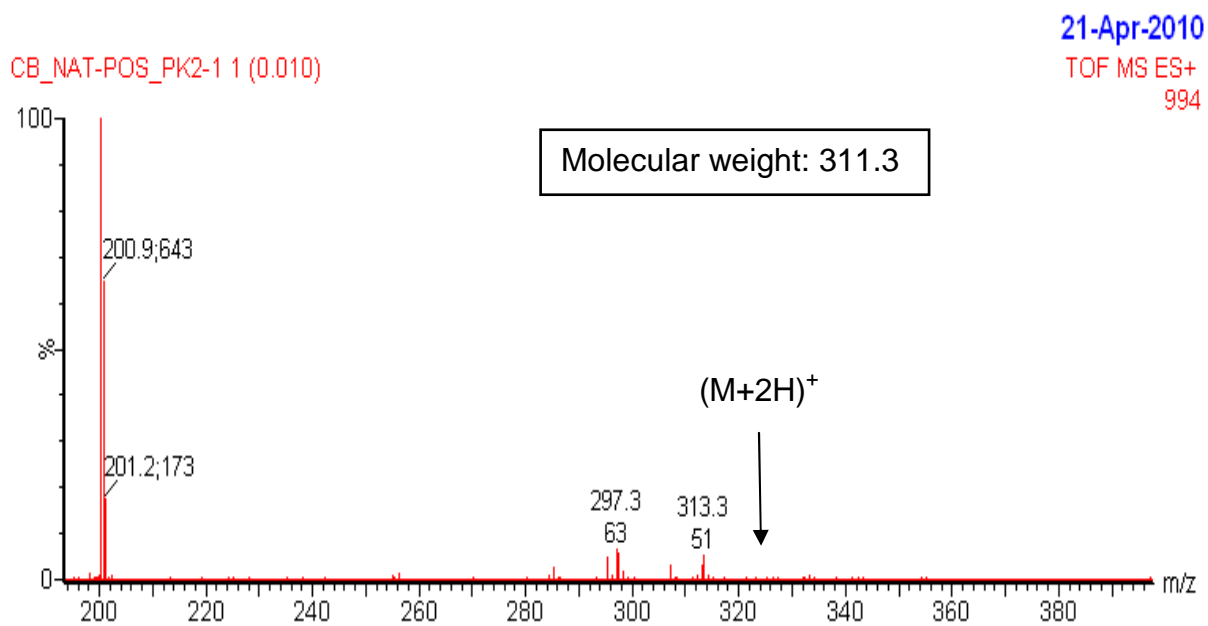
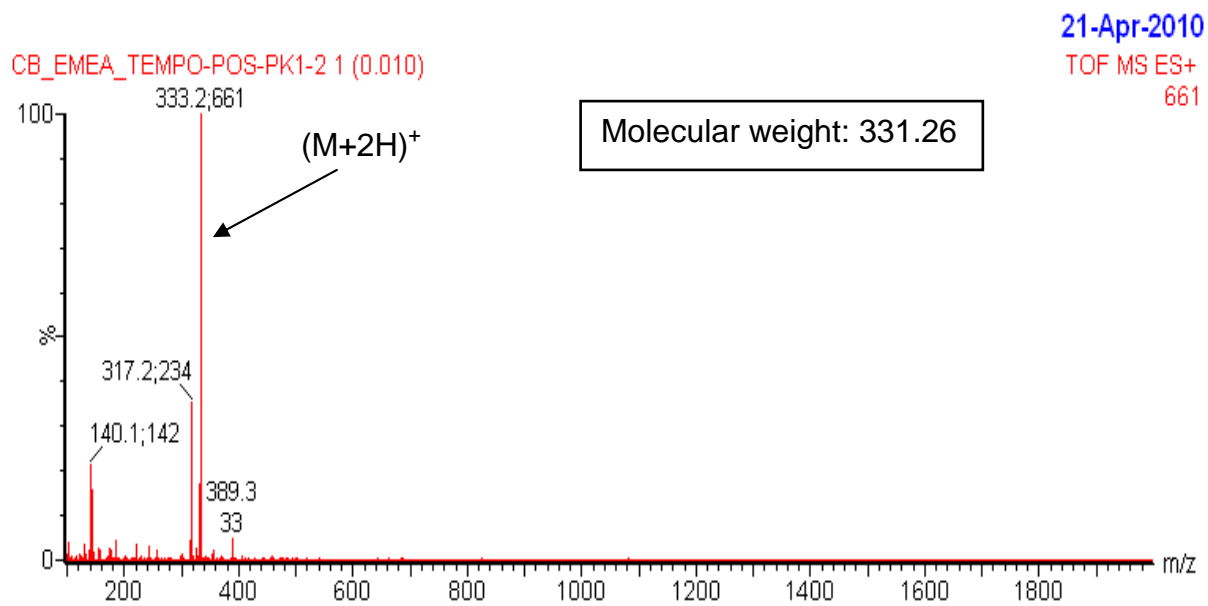


Figure A-1: HPLC spectra of nonanoic acid-TEMPO (NAT).



**Figure A-2:** An ESI-MS spectrum of NAT in methanol. Peak 297 corresponds to the molecule with the loss of oxygen.



**Figure A-3:** Mass spectrum of EMEAT. Peak 317.2 corresponds to the molecule with the loss of oxygen.

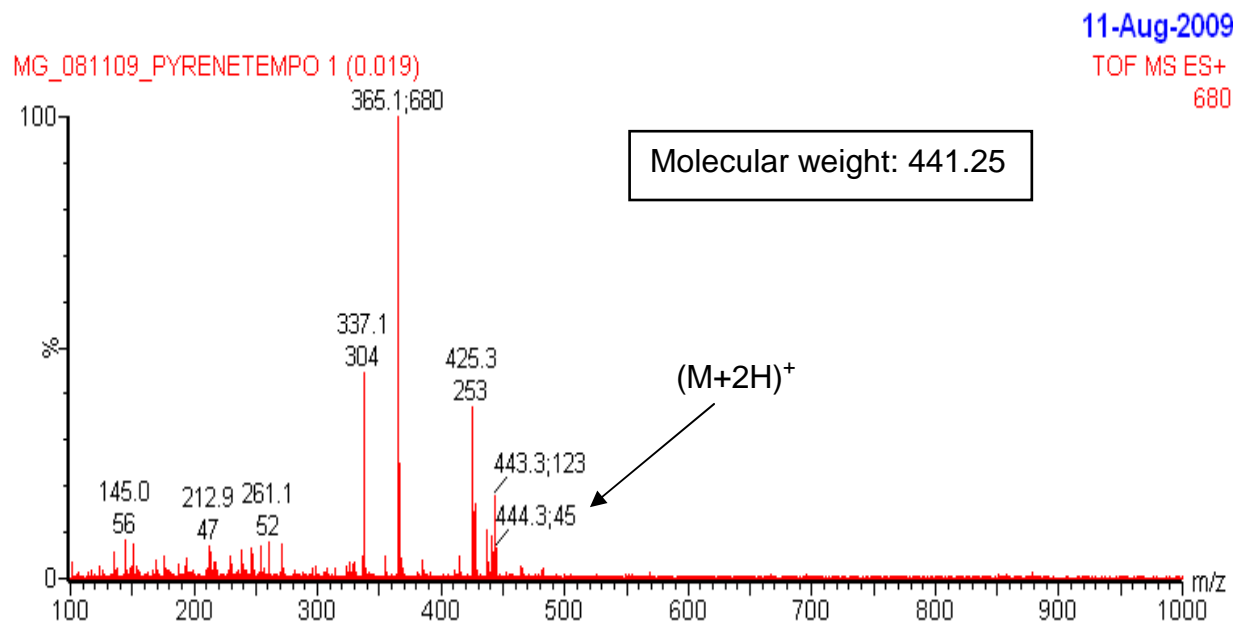


**Figure A-4:** Mass spectrum of PT. The m/z value 425 corresponds to the fragment produced as a result of the water molecule. Some of the other peaks might be from the impurities in the solvent or the compound.

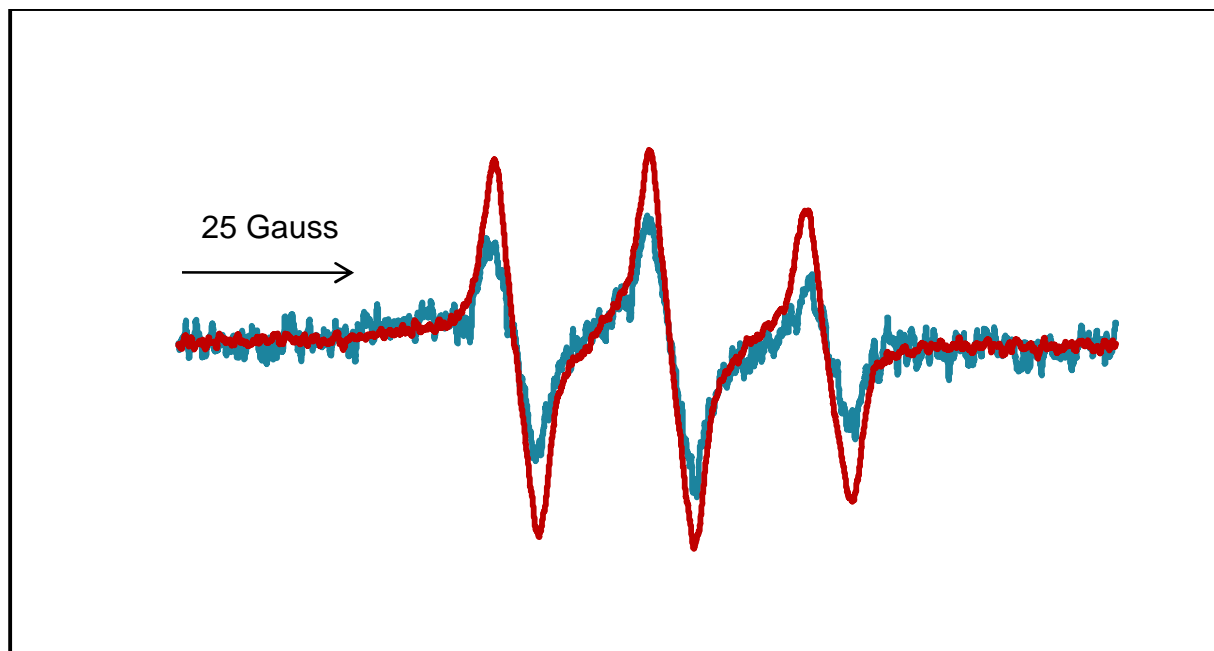


**Figure A-5:** EPR spectra of NAT in the presence (blue) and absence (red) of liposomes.

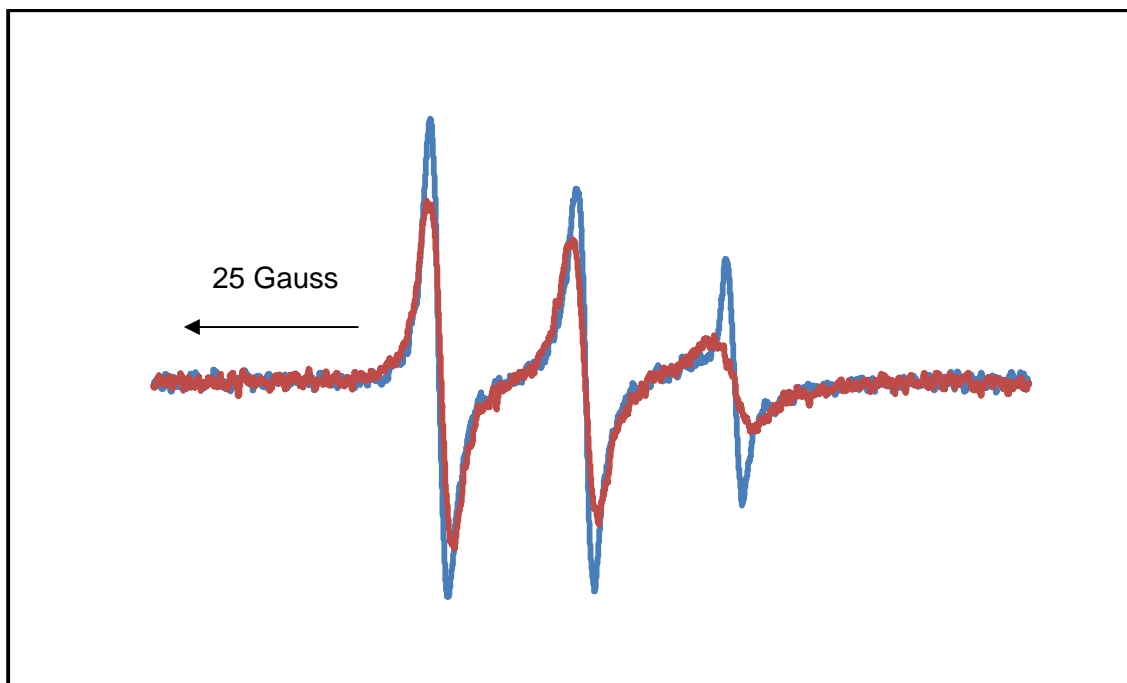


**Figure A-6:** EPR spectra of NAT in liposomes with (red) and without (blue) chromium oxalate.